The Mechanism by which Arabidopsis Vesicle Associated Membrane Proteins Regulate Root Development Under Salt Stress

MICHAEL JAMES LEWIS

The Mechanism by which *Arabidopsis* Vesicle Associated Membrane Proteins Regulate Root Development Under Salt Stress

BY

Michael James Lewis

Of HATFIELD COLLEGE

A Thesis Submitted in Fulfilment of

the Requirements for the Degree of

MASTER OF SCIENCE

SCHOOL OF BIOSCIENCES

DISCIPLINE OF PLANT SCIENCES

UNIVERSITY OF DURHAM

January 2024

Supervisors: Prof. Keith Lindsey and Dr. Jen Topping

Table of Contents

Abbreviations

ABA	Abscisic Acid
ABC	ATP-Binding Cassette
ABI4	ABA-INSENSITIVE 4
ACN	Acetonitrile
ADP	Adenosine Diphosphate
AFB	Auxin Signalling F-Box
Amp	Ampicillin
ANOVA	Analysis of Variance
APX2	Ascorbate peroxidase
ARF	Auxin response factor
NAC2	Highly conserved NAC (for NAM, ATAF1, 2, and CUC2) domain
ATP	Adenosine triphosphate
ATPase	Adenosine triphosphatase
Att	Site-specific attachment site
AttB	Bacterial attachment site
AUX1	AUXIN RESISTANT1
BCA	Bicinchoninic acid
BP	Base pair
BSA	Bovine serum albumin
Cas9	CRISPR-associated proteins
CAT1	Catalase 1
cDNA	Complementary DNA
CDS	Protein coding sequence
cFBPase	cytosolic fructose-1,6-bisphosphatase
CID	Collision induced dissociation
CK	Cytokinin
COPI	Coat protein complex II
COPII	Coat protein complex I
CRISPR	Clustered Regularly Interspaced Short Palindromic Repeats
CTAB	Cetyltrimethylammonium bromide
DAVID	Database for Annotation, Visualisation, and Integrated Discovery
DEGs	Differentially expressed genes

DEPs	Differentially expressed proteins
dH2O	Distilled water
DNA	Deoxyribonucleic Acid
DNase	Enzyme that cleaves DNA
dNTPs	deoxyribonucleoside triphosphates
DR5	highly active auxin response element
ds/m	deciSiemens per metre
DT1-BsF	Template plasmid-BsaI Forward Primer
DT1-F0	Template plasmid-sgRNA Forward Primer
DT1T2	Insert plasmid
DT1T2-PCR	PCR product of DT1T2
DT2-BsR	Template plasmid-BsaI Reverse Primer
DT2-R0	Template plasmid-scRNA Reverse Primer
DTT	Dithiothreitol
EDTA	Ethylenediaminetetraacetic acid
EIF4a	Eukaryotic initiation factor 4a
ePM	enriched Plasma Membrane Fraction
ER	Endoplasmic Reticulum
EXO70	Exocyst subunit 70 family
FA	Formic Acid
FDR	False discovery rate
GA	Gibberellic acid
GA3o	Gibberellic acid hydroxylase gene
GA4	Gibberellic acid active form
GABI-KAT	German plant genomics research program-Kolner Arabidopsis T-DNA
GAPC	Glyceraldehyde-3-phosphate dehydrogenase
gDNA	Genomic DNA
GFP	Green fluorescent protein
GH3	GRETCHEN HAGEN3
GO	Gene Ontology
GPI	Glycosylphosphatidylinositol
GRF7	General regulatory factor 7
gRNA	guide RNA
GSH	Glutathione

GST1	Glutathione S-Transferase 1
GTP	Guanosine triphosphate
GTPase	Guanosine triphosphate hydrolase
GV3101	A strain of Agrobacterium
H^+-ATPase	Proton adenosine-triphosphatase pump
H_2O_2	Hydrogen peroxide
HALT	A protease inhibitor cocktail
HCl	Hydrochloride
HEPES	4-(2-hydroxyethyl)-1-piperazineethanesulfonic acid
HKT1	HIGH-AFFINITY K+ TRANSPORTER 1
IAA	Indole-3-acetic acid
IAA-aa	Indole-3-acetic acid-amino acid conjugate
iTRAQ	Isobaric tags for relative and absolute quantitation
KOH	Potassium Hydroxide
LAX	LIKE AUX1
LAX3	LIKE AUX3
LB	Luria Broth
LC	Liquid Chromatography
LC-MS	Liquid Chromatography-Mass Spectrometry
LP	Gene specific left primer
LR	a recombination reaction between attL and attR sites
LSCM	Laser Scanning Confocal Microscopy
m/z	mass-to-charge ratio
MES	2-Morpholinoethanesulphonic acid
MilliQ	water purified using a Millipore
MMTS	methyl methanethiosulfonate
MOPS	3-(N-morpholino)propanesulfonic acid
mRNA	Messenger RNA
MS	Mass Spectrometry
ms	Milliseconds
NaCl	Sodium Chloride
NAD	Nicotinamide Adenine Dinucleotide
NaOH	Sodium Hydroxide
NASC	The Nottingham Arabidopsis Stock Centre

NEB	New England Biolabs
NHX1	Na+/H+ ANTIPORTER 1
NO	nitric oxide
NPA	N-1-naphthylphthalamic acid
OD	optical density
PBS	phosphate-buffered saline
pCBC-DT1T2	Plasmid containing CRISPR inserts
PCR	Polymerase chain reaction
pDONR	Gateway adapted vector
PFA	Paraformaldehyde
pHEE401	Plasmid that contains gRNA scaffold
PIN	PIN-FORMED
pK_a	$-\log_{10}K_a$ (where K_a is the acid dissociation constant)
PM	Plasma Membrane
ProDR5::GFP	Native Promotor DR5 GFP tag
pTiC58DT	plasmid pmp90
pUCIDT	Golden Gate plasmid
Q-SNAREs	glutamine (Q) soluble N-ethylmaleimide-sensitive factor adaptor protein receptor
QC	Quiescent centre
R-SNARE	Arginine (R) soluble N-ethylmaleimide-sensitive factor adaptor protein receptor
RAB	Ras related protein
RABA1c	RAB GTPase HOMOLOG A1C
RABB1b	RAB GTPase HOMOLOG B1B
RABD2c	RAB GTPase HOMOLOG D2C
RABE1	RAB GTPase HOMOLOG E1
RABE1C	RAB GTPase HOMOLOG E1C
RABG3c	RAB GTPase HOMOLOG G3C
RABG3d	RAB GTPase HOMOLOG G3D
RABG3e	RAB GTPase HOMOLOG G3E
REST	Relative expression software tool
RGA	Repressor of Gibberellin
RGL3	RGA-LIKE3

RNA	Ribonucleic Acid
RNAi	Ribonucleic Acid interference
RNase	Enzyme that cleaves RNA
ROS	reactive oxygen species
ROX	a passive fluorescent dye
RP	Gene specific right primer
RSA	Root system architecture
RT-qPCR	Real-time quantitative PCR
SALK	An institute for T-DNA seeds
SBT1	Subtilisin-like protease
SCF	Skp, Cullin, F-box containing complex
SCN	stem cell niche
SD	Standard Deviation
SDS	Sodium Dodecyl Sulphate
SDS-PAGE	Sodium Dodecyl Sulphate-Polyacrylamide Gel Electrophoresis
SE	Standard Error
SEA	Singular Enrichment Analysis
SEC13	Protein transport protein
SMT1	sterol methyltransferase 1
SNAP	soluble N-ethylmaleimide-sensitive factor adaptor protein
SNARE	soluble N-ethylmaleimide-sensitive factor adaptor protein receptor
SNF1	sucrose non-fermenting 1-related
SOC	super optimal broth with catabolite repression medium
SOD	superoxide dismutase
T-DNA	Transfer DNA insertion
TAE	40 mM Tris-acetate, 1 mM EDTA buffer
TAIR	The Arabidopsis Information Resource
TBS-T	20 mM Tris-HCl pH7.6, 150 mM NaCl, 0.1% [v/v] tween-20
TCEP	Tris (2-carboxyethyl) phosphine
tDNA	transfer DNA
TE	Tris-EDTA
TEAB	Triethylammonium bicarbonate
TIR	Transport Inhibitor Response
TripleTOF	Triple Time of Flight

Tris	tris(hydroxymethyl)aminomethane
UK	United Kingdom
USA	United States of America
UV	Ultraviolet
V-ATPase	epsilon subunit of tonoplast H+ATPase
VAMP71	VESICLE ASSOCIATED MEMBRANE PROTEIN 71 Family
VAMP71C	VESICLE ASSOCIATED MEMBRANE PROTEIN 71 Family
VAMP72	VESICLE ASSOCIATED MEMBRANE PROTEIN 72 Family
VDAC1-5	voltage-dependent anion-selective channel protein 1-5
v/v	Volume per volume or the Volume concentration of a solution
w/v	Weight by Volume
WT	Wild-type *Arabidopsis thaliana*
ZEO	Zeocin antibiotic

Table of Figures

Table of Table

Abstract

When plants are grown in saline soil, they deploy their vesicle trafficking system to alter membrane protein dynamics rapidly. High-salt conditions induce prompt ionic and osmotic stresses, subsequently leading to the generation of reactive oxygen species. In response to salt stress, roots, being the initial affected organs, experience inhibited growth, limiting water and nutrient absorption and, consequently, reducing overall plant biomass and crop yield. In eukaryotic cells, intracellular vesicle trafficking serves vital roles, including membrane trafficking and delivery of cargo proteins to their designated destinations. A major exocytic route in plants is vesicle trafficking to the cell plasma membrane and the vacuole, which plays an essential role in plant salt tolerance. The proposed role for a vesicle-mediated trafficking system which adjusts the localisation and availability of transporters of the plant hormone auxin to facilitate rapid changes in directional root growth was investigated; auxin is known to regulate root development under salt stress. Specifically, the focus of the work described is the family of VESICLE ASSOCIATED MEMBRANE PROTEIN 71 (VAMP71) R-SNAREs in *Arabidopsis thaliana*, which may play a role in auxin transporter function but whose precise role in root development under salt stress has not been explored before. This thesis presents transcriptomic and proteomic evidence that VAMP71 family members are important for the correct regulation of auxin transport and signalling events under salt stress. The results also indicate a high degree of redundancy between the *VAMP71* genes. Quantitative proteomics identified putative VAMP712-dependent targets by analysing differentially expressed proteins between wild-type *Arabidopsis* and *vamp712* loss-of-function mutants exposed to salt stress. Proteins associated with auxin homeostasis and other vesicle-mediated processes associated with the plant cell vacuole were identified by gene ontology analysis. Confocal microscopy also revealed that the loss of function of *vamp712* and *vamp713* disrupted the abundance and distribution of auxin transporters at the root tip. Overall, this study has strengthened the link between *VAMP71* family genes and auxin-mediated processes and highlights the genotype-dependent sensitivity to salt stress and exogenous auxin.

Acknowledgements

First and foremost, I am incredibly grateful to my supervisors Keith and Jen, who have supported me through my undergraduate studies and this master's project. Without them, this project would not have been possible, and I appreciate all the time and resources you have committed to me. As role models, you have had a lasting impact on my life and career as a scientist. I am very grateful for the funding afforded to me by the Department of Biosciences and Keith's lab.

I appreciate the help of Dr. Adrian Brown in the Proteomics facility at Durham University, who helped with the planning of the iTRAQ experiment and his invaluable contribution with the mass spectrometry. The extensive training I have gained in protein biology from Adrian and Dr. Steve Chivasa has motivated me to pursue this discipline of molecular biology during my doctoral training. I'd also like to acknowledge Dr. Wenbin Wei, experimental officer (Bioinformatics) in the Department of Biosciences, for his contribution to genome sequencing data analysis.

Thank you to Julien, Cian and Jialei, who made working in the lab a pleasure and for their friendship and support throughout the past year. Your company will be greatly missed. I especially want to thank Julien for hosting me for a summer internship before starting this MRes, whose guidance helped prepare me for graduate lab work. Dr. Helen Thompson, a former post-doctoral researcher in Keith’s lab, also positively impacted my training as a molecular biologist. I was pleased to spend six weeks of the summer break in 2019 working with her; thank you.

Lastly, thank you to my family and friends for your support and encouragement to achieve the best of my ability. Especially to my partner, Ellie, for standing by me throughout this busy and extraordinary year.

Declaration

This thesis is submitted to Durham University in fulfilment for the degree of Master of Science. All works herein have been composed by myself and have not been submitted in any previous application for a degree.

The findings presented here have been produced by myself unless stated otherwise.

- Michael J Lewis

Chapter 1. Introduction

Soil salinity

Salt stress is a major abiotic stress that is an increasing threat to agriculture. Over 20% of global cultivatable land is affected by increases in soil salinity, and these levels continue to rise due to natural and anthropogenic activities (Arora, 2019). One of the most severe sources of soil salinity affects arid and semi-arid lands, whereby excessive irrigation combined with poor drainage and extreme drought events causes nutrient immobilisation and salt accumulation in soils, making them dry, saline, and non-arable. This phenomenon is termed 'secondary salinisation' in which water evaporation precipitates salts which remain in the soil and is distinct from primary salinisation of seashore salt marshes (Zhu, 2007).

Glycophytes and halophytes

Plants have a range of responses to saline conditions. Plants known as halophytes naturally grow in highly saline soils and are well adapted to grow and reproduce in those conditions. Conversely, plant species in low-sodium ecosystems that cannot withstand the stress effects of saline soil are deemed glycophytes. An investigation into the origins of halophytes revealed widespread occurrence among the various orders of higher plants, indicative of a polyphyletic origin of halophytes (Flowers et al., 1977). Halophytes generally arose through colonisation by pre-adapted individuals rather than by gradual adaptation from glycophytic plants (DiMichele et al., 1987). Today, most plants, including those of significant agricultural importance, are glycophytes and thus very sensitive to salt stress. Humans' domestication/evolution of crop plants had the unintentional consequence of losing tolerance to various stresses and the genetic variability needed to revert this. Therefore, understanding the molecular basis of salt stress responses in glycophytic plants is essential to provide potential avenues for engineering salt-tolerant crops that will offer food security, particularly in countries with limited economic resources and infrastructure. Such efforts will first require the identification of genes that have a role in the salt stress response pathways.

Arabidopsis thaliana is an angiosperm in the Brassicaceae family that has achieved the status of a model organism in plant biology through years of research. While this species is a glycophyte, its small size, short life cycle, self-compatibility, natural variability, and

ability to generate abundant offspring (Meyerowitz, 1989) make it a useful plant for researching many abiotic stress responses, including salt stress. It was the first plant genome to be published (The Arabidopsis Genome, 2000), and its diploid nature has facilitated the development of a wide range of tools for genetic manipulation with remarkable ease (Martinez-Zapater and Salinas, 1998). The whole genome sequence of *Arabidopsis* is publicly available and updated by The *Arabidopsis* Information Resource (TAIR at www.arabidopsis.org). TAIR works alongside the SALK Institute, whose Genome Analysis Library (signal.salk.edu) makes transfer DNA (T-DNA) insertional mutants available, which facilitates a range of research into the function of *Arabidopsis* genes and proteins.

This project investigates the function of genes belonging to the VESICLE ASSOCIATED MEMBRANE PROTEIN 71 (VAMP71) R-SNARE (soluble N-ethylmaleimide-sensitive factor adaptor protein receptor, SNAP receptor) family in the *Arabidopsis thaliana* genome. The VAMP71 family in *Arabidopsis* is comprised of four members with extended homology: VAMP711, VAMP712, VAMP713 and VAMP714. These proteins all share a longin domain, transmembrane domain, and v-SNARE coiled-coil homology. Selective binding of the different VAMP71 members is thought to be linked to the longin domain, which varies in each member of the family (Figure S1) (Zhang et al., 2015).

Prior work has found that one of the VAMP71 family members, VAMP714, is involved in regulating growth at the root tip and has subsequent effects on development across the whole root (Gu et al., 2021). Unlike VAMP714, the role of the other three *VAMP71* genes in root development is poorly understood. VAMP711 and VAMP712 have proposed roles in abiotic stress tolerance, including salt stress (Leshem et al., 2010, Leshem et al., 2006, Xue et al., 2018). Further, salt stress has a substantial effect on root growth and development. This thesis will focus on the role of VAMP711, VAMP712, and VAMP713 in salt-stress-induced developmental changes at the root tip and the whole root.

Arabidopsis thaliana – a model organism

In addition to possessing traits that render *Arabidopsis* a valuable representative for studying molecular genetics and development in flowering plants, *Arabidopsis* roots offer a convenient model for analysis. They have a highly ordered structure and follow predictable developmental steps, presenting an ideal system for studying many biological processes,

including cellular differentiation, patterning, and polarity. *Arabidopsis* roots are easy to visualise when grown on clear agar, which makes for straightforward imaging and trait quantification.

Effect of salt stress on plants

Plants are affected by salt stress at all stages of their life cycle, from the inhibition of seed germination to the reduction in growth and development of mature plants. High salt concentrations affect plant growth and development by reducing the uptake of water and nutrients and increasing the accumulation of toxic sodium ions (Na^+) (Zhao et al., 2021). As a result, the plant experiences ion toxicity, oxidative and osmotic stress, and increased susceptibility to diseases (Hasanuzzaman and Fujita, 2022). High saline conditions can cause plant death by altered soil porosity and hydraulic conductivity that leads to reduced water potential of the soil, therefore causing osmotic stress, cell membrane destabilisation and protein degradation due to the toxic effects of different ions (mainly Na^+) (Hasanuzzaman and Fujita, 2022).

The root system in abiotic stress

As sessile organisms, plants often face multiple environmental stresses, so they have evolved to elicit responses to enhance their survival chances and tolerance to the given stressor. The plant root system architecture (RSA) is highly responsive to many environmental stimuli. The RSA comprises primary roots, which help anchor the system into the soil, and lateral roots, which grow into the soil through environmentally responsive radial growth and determine the overall root system shape and size.

Following germination, the primary root grows downward towards the pull of gravity, a phenomenon termed gravitropism. Soil conditions with high salinity or low moisture dramatically affect RSA and gravitropism. Plants growing in saline soils alter their root growth pattern to find larger domains of soil that are less harmful, a phenomenon called halotropism. This ability to alter root growth and development is facilitated primarily through changes in plant hormone levels (Sun et al., 2007). Auxin is a plant hormone that is vital in regulating cell differentiation and elongation, organogenesis, and shoot and root architecture in response to environmental factors, such as light and gravity (Benjamins and Scheres, 2008).

A high concentration of auxin in the root tip's stem cell niche (SCN) is necessary for the coordination and establishment of root tissue growth (Petersson et al., 2009, Smolko et al., 2021). The SCN contains the quiescent centre (QC) enclosed by four types of stem cells (Figure 1.1). Although the cells of the QC are not very mitotically active, they produce cellular signals that regulate the maintenance of the surrounding stem cells [reviewed in Sozzani and Iyer-Pascuzzi (2014)] (Dolan et al., 1993).

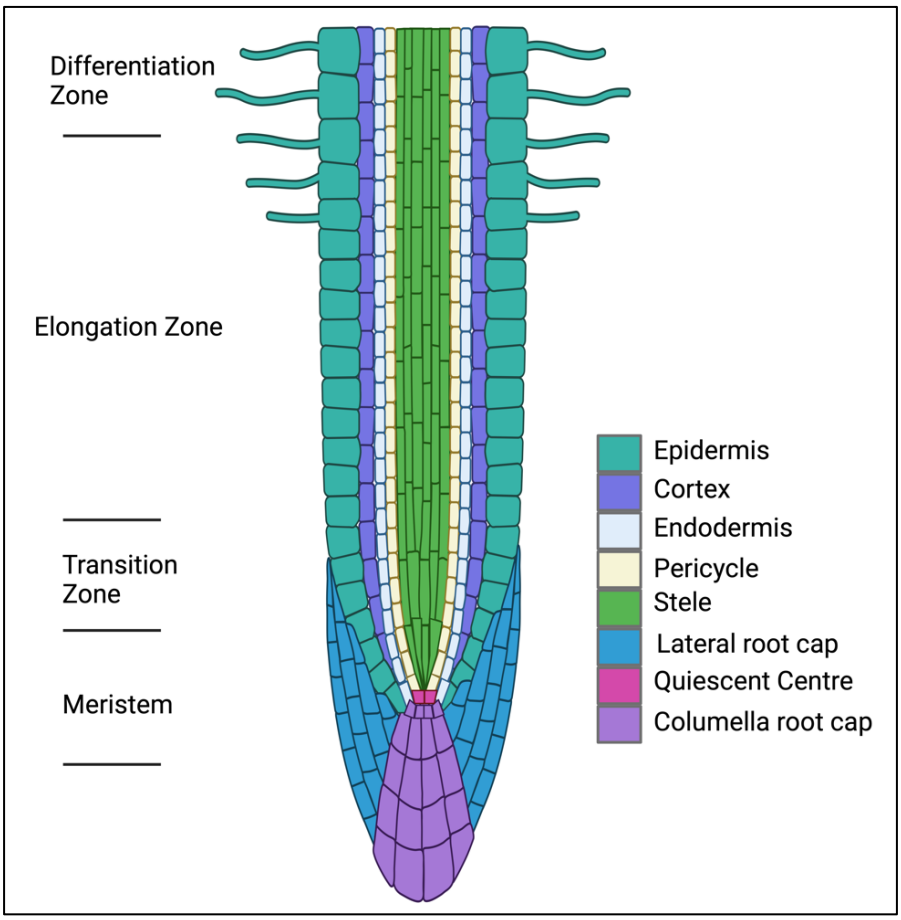

Figure 1.1: *Cellular organisation of an Arabidopsis primary root. The longitudinal section through the root shows different cell types (each differently coloured) arranged in single-cell files that form concentric rings with radial organisation around a central axis. Distinct developmental phases are formed along the root, through which new cells progress following their origin in the root's apical meristematic zone. Cell division rate slows in the basal meristem, and cells start to elongate in the elongation zone. The boundary between the meristematic and elongation zones is indicated as the transition zone. Figure created using BioRender.com.*

In nature, auxins contain an indole and carboxylic acid group, with the most abundant active form being indole-3-acetic acid (IAA). Primarily, auxin is biosynthesised in young, developing tissues such as in the shoot apex and other sites of cell differentiation (Petersson et al., 2009), and shoot-derived auxin is required for root growth (Friml et al.,

2003). Although IAA is transported via the phloem from the shoot to the root system (Swarup et al., 2001), symplastic polar transport is essential for the redistribution of IAA within these organs and throughout the rest of the plant. Therefore, intercellular auxin transport is one process that determines auxin-mediated regulation of root growth and development.

Cellular auxin transport

Cells' uptake and efflux of auxin is mediated by a combination of chemiosmotic forces and adenosine triphosphate (ATP) hydrolysis (Figure 1.2) (Geisler, 2021). The pK_a of IAA is around 4.85, making it a weak acid. Consequently, the apoplast's acidic (pH 5.5) environment means only 17% of IAA molecules are protonated and thus permitted to diffuse passively across the plasma membrane (Rubery and Sheldrake, 1974). The remainder of the auxin pool is unavailable for lipophilic diffusion in its proton-dissociated form (IAA^-). Protein importers are required to meet developmental demands for the active polar transport of auxin. Members of the PIN-FORMED (PIN) family of efflux facilitators accumulate on specific sides of the cell plasma membrane and determine the direction of auxin streams through tissues (Wisniewska et al., 2006).

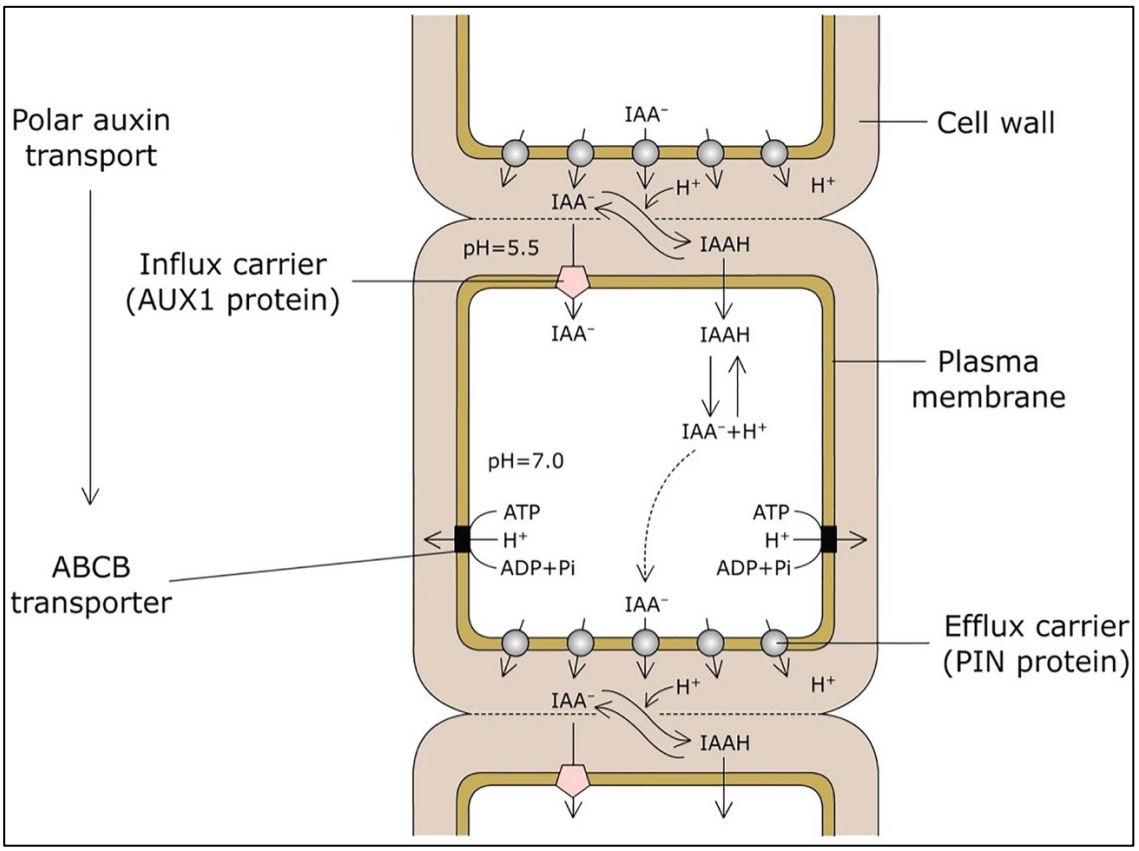

Figure 1.2: *The chemiosmotic model for polar auxin transport through cells by PIN efflux and AUX1 influx carriers at the plasma membrane. The deprotonation of IAA, which occurs to trap auxin within the cell, is illustrated. The plasma membrane H^+-ATPase activity and ABCB transporters maintain the pH of the cell apoplast. Taken from (Bhatla and Lal, 2018).*

There are a total of eight PIN proteins in plants. PIN1, PIN4, and PIN7 maintain the polar auxin streams necessary for organogenesis and development in conjunction with AUXIN RESISTANT1/LIKE AUX1 (AUX1/LAX) influx carriers (Reinhardt et al., 2003). The activity of PIN2 is essential for gravitropism and the return flow of auxin from the root tip (Müller et al., 1998). The relocation of PIN3 to specific sides of the columella cells redirects auxin flux and leads to asymmetric auxin accumulation, which is essential for directional growth (Figure 1.3) (Friml et al., 2002). In contrast to the other PINs, PIN5, PIN6 and PIN8 are referred to as “short” proteins with a reduced or absent central hydrophilic loop (Adamowski and Friml, 2015). These are located in endomembrane structures and have a role in the homeostatic compartmentalisation of auxin (Mravec et al., 2008). Our group previously found that VAMP714 is required for correct PIN1 and PIN2 localisation and auxin transport in the root tip (Gu et al., 2021).

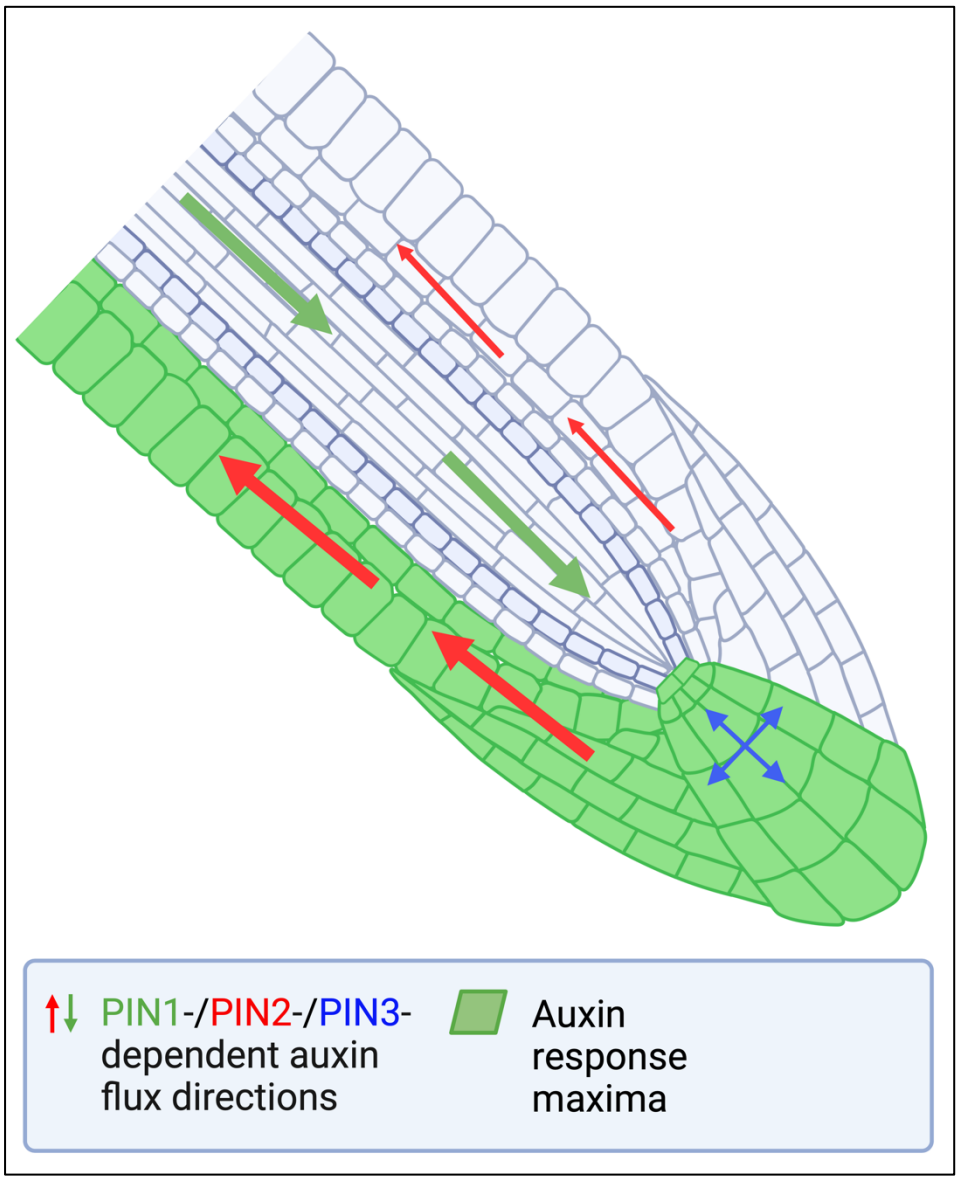

Figure 1.3: *The redistribution of auxin via PIN proteins in response to a gravitropic stimulus. An auxin maximum is created on one side of the root tip. The cells with lower auxin abundance then grow at a higher rate, causing the root to bend. Changes in the direction of polar auxin flow involves PIN relocation along the plasma membrane through vesicle trafficking. Illustration created in BioRender.*

Auxin transport changes during salinity stress

As salt stress conditions alter plant development in many ways, auxin is vital in this process. Various studies report that salt stress decreases auxin levels and reduces auxin transporter expression in plants (Liu et al., 2015, Park et al., 2007, Wang et al., 2009). Furthermore, the decreased auxin levels are associated with impaired auxin transport and distribution along the root (Shen et al., 2010, Sun et al., 2007). Plasma membrane proteins are recycled and sorted to generate polarity for auxin efflux transporters (Löfke et al., 2013). Salt stress has been shown to alter auxin transport and distribution in plants (Fu et

al., 2019, Liu et al., 2015, Wang et al., 2009). Previous reports have shown that PIN1, PIN2, PIN3, and PIN7 are negatively regulated under salt stress conditions (Fu et al., 2019, Liu et al., 2015). This response impacts PIN protein abundance, auxin transport, and, therefore, auxin signalling. Salt-dependent transcriptional regulation of these PIN genes is partially mediated by an increase in reactive oxygen species (ROS) and nitric oxide (NO) in the roots, which decreases PIN1, PIN3, and PIN7 expression (Fu et al., 2019, Liu et al., 2015). In addition to this transcriptional response, it has been shown that the PIN1 endocytosis rate increases under osmotic stress, and its recycling to the plasma membrane is repressed (Nakayama et al., 2012). Moreover, salt stress triggers clathrin-mediated endocytosis of PIN2, which was not shown under osmotic stress (Galvan-Ampudia et al., 2013). These changes to auxin efflux transporters are necessary to facilitate a halotropic response of root growth, that is, the ability of plant roots to deviate their growth direction away from salt. This halotropism has been shown to be dominant over gravitropism (Sun et al., 2007). The regulation of auxin transporters is critical to producing the asymmetric distribution of auxin and consequently altered root growth away from the salt-affected soil area (Galvan-Ampudia et al., 2013).

Also essential for proper root development is auxin influx, which has been linked to salt stress responses (Wang et al., 2009). The salt-stress response of *Arabidopsis* mutants defective in auxin influx (*aux1-7*) showed enhanced sensitivity in primary root growth compared with the wild-type control (Wang et al., 2009). Additionally, the auxin influx carrier LIKE AUX3 (LAX3) has been linked to the plant salt stress response by modulating the conjugation of auxin to amino acids via a feedback loop with GRETCHEN HAGEN3 (GH3), which may protect auxin homeostasis (Mellor et al., 2016, Vaseva et al., 2021). GH3 is an essential component in the auxin-degradation pathway, necessary because, at high concentrations, intracellular auxin can be toxic (Bhatla and Lal, 2018). Therefore, homeostatic control of auxin through conjugation and degradation is an important addition to the regulatory mechanisms of its biosynthesis and intercellular transport.

For future biotechnological applications, fine-tuning auxin levels will be crucial for adjusting biosynthesis, transport, perception, or signalling as a strategy for salt-resistant crop creation. This is because changes in cellular auxin levels also alter many downstream signalling events that determine a plant's response to salt stress.

Auxin signalling

An auxin maximum triggers a signalling cascade which begins with auxin binding to the TRANSPORT INHIBITOR RESPONSE 1/AUXIN SIGNALLING F-BOX (TIR1/AFB) receptor (Salehin et al., 2015). TIR1/AFB is part of the E3 ubiquitin ligase complex SCF (Skp, Cullin, F-box containing complex), and the binding of Aux/IAA repressor proteins leads to their ubiquitination and subsequent degradation via the 26S proteasome (Maraschin Fdos et al., 2009). The consequent absence of Aux/IAA results in the activation of auxin response factor (ARF)-mediated transcriptional responses (Ulmasov et al., 1997). Thus, DNA-binding ARFs regulate freely the expression of many genes and are important indicators of auxin-mediated growth and developmental responses in plants (Verma et al., 2022).

Perception of auxin signals:

The role of auxin receptors in stress responses, including salt stress, has been extensively studied (Bouzroud et al., 2018, Ha et al., 2013, Liu et al., 2015, Song et al., 2019, Verma et al., 2022). The regulation of TIR/AFB receptors occurs at multiple levels, including transcriptionally, post-transcriptionally via microRNAs (miRNAs), and through auxin receptor Aux/IAA affinity, which is different among receptors (Calderón Villalobos et al., 2012, Du et al., 2022, Parry et al., 2009, Parry and Estelle, 2006, Prigge et al., 2020). The TIR/AFB receptors have been shown to play a crucial role in the salt stress tolerance of *Arabidopsis*. The salt-induced expression of *AtNAC2* (for NAM, ATAF1, 2, and CUC2) has been shown to be unresponsive to salt stress in *tir1-1* loss of function mutants of *Arabidopsis* (He et al., 2005). Moreover, the *tir1afb2* double mutant exhibits increased salt stress tolerance over wild-type *Arabidopsis* regarding improved germination rate, root elongation and chlorophyll content (Iglesias et al., 2010). The role of auxin receptors and miRNA-dependent transcript degradation has also been demonstrated to be involved in salt stress responses through transgenic lines resistant to specific miRNAs. For instance, overexpression of a miR393-resistant *TIR1* gene (*mTIR1*) in *Arabidopsis* demonstrated enhanced resistance to salt stress conditions with an increased germination rate, more primary root growth, delayed senescence, and less water loss (Chen et al., 2015, Iglesias et al., 2014). These reports are evidence of the importance of auxin perception in mediating the level of salt stress resistance in plants.

Aux/IAA proteins:

The Aux/IAA repressor proteins are vital regulators of the auxin signalling pathway. Relative to the other auxin signalling components, the role of Aux/IAAs under salt stress is not well studied. Salt-induced overaccumulation of NO and overexpression of *IAA17* have been shown to downregulate the gibberellic acid (GA) hydroxylase gene *GA3ox* required for GA biosynthesis, resulting in lower concentrations of bioavailable auxin and GA_4 (Shi et al., 2017). A decrease in these hormones stabilises Aux/IAA17 via a direct interaction with RGA-LIKE3 (RGL3), thereby inhibiting the IAA17-TIR1 interaction and subsequent degradation (Shi et al., 2017). Further, overexpression of *IAA17* and *RGL3* partially alleviated the inhibitory effect of NO deficiency on salt resistance, providing increased survivability when grown in 180 mM or 220 mM NaCl (Shi et al., 2017).

Clearly, auxin perception, transport and signalling are deeply involved in mediating the salt stress response. Transcriptomic analysis of *Arabidopsis* treated with salt stress and osmotic stress found salt-specific genes were enriched in the gene ontology term "response to auxin", suggesting auxin is one of the dominant phytohormones involved in salt-specific adaptations to salinity stress (Cackett et al., 2022). Previous work has provided evidence that VAMP714 mediates the delivery of PIN-carrying vesicles to the plasma membrane, and that this forms part of a positive regulatory loop in which auxin activates a VAMP714-dependent PIN/auxin transport system to control development (Gu et al., 2021). It is possible that other SNARE proteins are involved in mediating auxin transport and signalling responses during salinity stress.

Vesicle trafficking

The plasma membrane represents the primary interface between the cell and its extracellular environment, which controls the movement of materials into and out of the cell. Proteins with transmembrane domains are synthesised in the endoplasmic reticulum and trafficked via the Golgi apparatus to the plasma membrane. Many membrane proteins play an important role in helping plants overcome salt stress by regulating the movement of ions across the plasma membrane (reviewed by Banik and Dutta (2023)). This involves different types of membrane proteins, such as ion channels, transporters, and pumps. In eukaryotes, the regulation of membranes and associated proteins depends on the protein trafficking system. Membrane-bound transport vesicles carry cargo proteins to and from

compartments and deposit their cargo into a target compartment by fusing with the target membrane.

In plant cells, membrane trafficking is accomplished through four sequential steps, namely vesicle budding, movement, tethering and membrane fusion (Figure 1.4). In the budding stage, dynamin-related guanosine triphosphate hydrolases (GTPases) and coat protein complexes, such as COPI and COPII, form a vesicle from donor organelles and deform the local membrane until a vesicle is freed by scission. The movement phase occurs when the freed vesicle associates with cytoskeletal motors and other molecular motors, such as kinesin and myosin, as it moves towards the acceptor compartment (Matanis et al., 2002, Shorter et al., 2002). Next, tethering of vesicles to the target membrane is accomplished through RAB GTPases and SNARE proteins. Lastly, fusion with the target membrane or organelle is mediated through SNARE proteins (Ebine and Ueda, 2009, Gu et al., 2020).

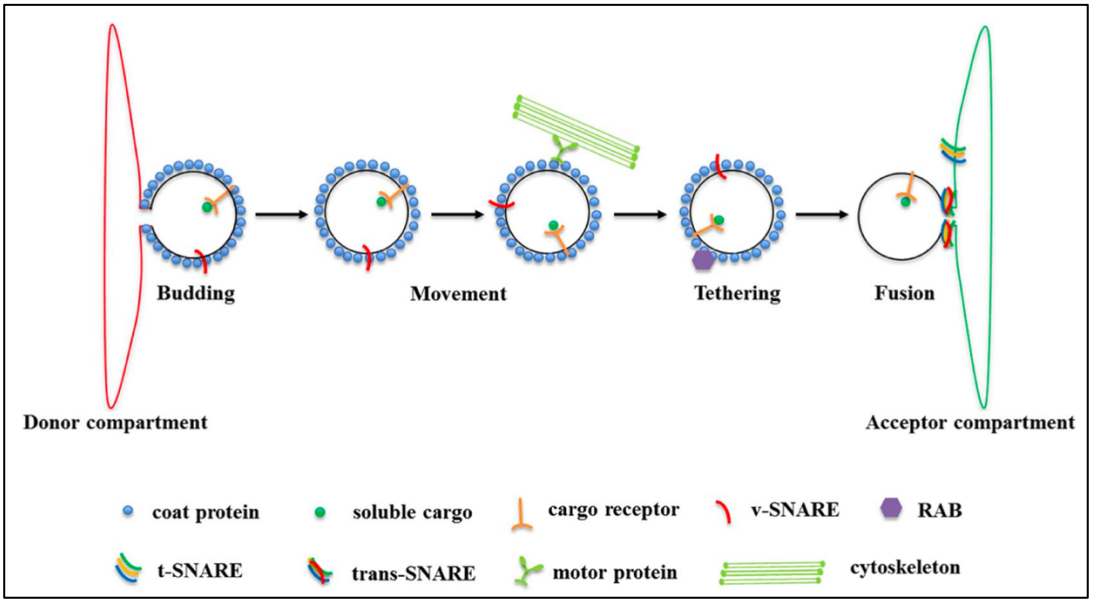

Figure 1.4: *The vesicle trafficking pathway. Taken from Gu et al. (2020).*

SNARE Proteins

Typically, SNAREs are small proteins comprising between 100 and 300 amino acids (Jahn and Scheller, 2006). They contain a highly conserved SNARE motif of approximately 60 to 70 amino acid residues, which consists of the heptad repeat forming a coiled-coil structure (Rehman and Di Sansebastiano, 2014). SNAREs also contain a transmembrane domain in the C-terminus that anchors the protein to the membrane and a variable N-terminal domain (Gu et al., 2020). SNAREs are classed on a functional basis as vesicle-

associated (v-SNAREs) and target membrane-associated SNAREs (t-SNAREs) (Söllner et al., 1993). The SNAREs are also structurally reclassified as either Q-SNAREs or R-SNAREs according to the occurrence of either a conserved glutamine (Q) or arginine (R) residue in the SNARE domain (Fasshauer et al., 1998). There are two gene families of VAMP7-like R-SNAREs in Arabidopsis; four VAMP71 group protein members mediate vesicle trafficking and regulate protein delivery and recycling at the plasma membrane (Uemura et al., 2004), while eight VAMP72 group proteins represent R-SNARE components involved in secretion (Zhang et al., 2015). Broadly, t-SNAREs correspond to Q-SNAREs and v-SNAREs to R-SNAREs. Many R-SNAREs localise to trafficking vesicles and are attached via the C-terminal transmembrane domain (Gu et al., 2020).

The R-SNAREs VAMP711 and VAMP712 have been implicated in the abiotic stress tolerance of *Arabidopsis*. The R-SNARE *AtVAMP711* has been shown to have an important role in stomatal functioning during drought stress and salt stress tolerance (Leshem et al., 2010, Leshem et al., 2006). These studies manipulated the expression of the *AtVAMP711* gene in *Arabidopsis* with sense and antisense constructs. They found decreased stomatal closure during drought stress or following treatment with abscisic acid (ABA) in the antisense plants, which resulted in premature leaf senescence. However, overexpression lines of *AtVAMP711* showed no improvement in drought tolerance, indicating a potential stoichiometry or expression threshold is required for correct VAMP711 functioning (Leshem et al., 2010). The authors also showed that when treated with ABA, ROS production was induced in the guard cells of wild-type and antisense plants, suggesting that correct sensing of ABA and other plant hormones is maintained. In the antisense lines, ABA treatment significantly increased vacuole size and the proportion of ROS-containing vacuoles. It is possible that the localisation of ROS within the alternatively sized vacuoles could have different impacts on downstream signalling. Therefore, the authors concluded that VAMP71 group proteins are necessary for properly localising ROS and regulating stomatal closure by ABA. Similarly, Xue and co-workers (2018) found that VAMP711 has a role in the ABA-mediated inhibition of plasma membrane (PM) H^+-ATPase activity. The authors show that ABA treatment decreased PM H^+-ATPase activity in the *vamp711* mutant. However, the decrease was not as significant as in the wild-type; this implies that VAMP711 might have functional redundancy with VAMP711 homologous proteins.

Considering the recent evidence of a VAMP714-dependent pathway of PIN trafficking (Gu et al., 2021) and that related *AtVAMP71* genes are induced by auxin, it is hypothesised that VAMP711, VAMP712 and VAMP713 are also involved in regulating auxin transport and signalling. Given the known changes to auxin transport during salinity stress, another hypothesis is that these VAMP71s are necessary for mediating auxin-dependent salt stress responses. Thus far, the possible connection between VAMP71, auxin transport and developmental changes to the root system under salt stress has not been explored.

Aims and Objectives

The main aim of this study concerned investigating a possible role for three VAMP71 proteins in the salt stress-induced developmental response of plant roots. With the dominant role of auxin in regulating root growth and development and in the salt stress response, the work reported here has focussed on this link. By comprehensively understanding the molecular and physiological aspects of auxin-mediated root responses to salt stress, this research aims to contribute to the body of knowledge in plant biology and provide potential avenues for engineering salt-tolerant crops.

The project aims were addressed through three experimental objectives: 1) the phenotypic characterisation of *VAMP71* family mutants under standard growth and salt stress conditions; 2) an analysis of signalling events mediated by *VAMP71* family genes under salt stress; and 3) an analysis of the salt-induced proteome in the *vamp712* mutant.

Ultimately, the findings hold significant implications for sustainable agriculture, as they could pave the way for the development of crops that can resist saline environments, ensuring food security and agricultural productivity in regions affected by soil salinisation.

Chapter 2: Methods

2.1 Plant materials

Arabidopsis line

This research used the wild-type plant *Arabidopsis thaliana* of the ecotype Columbia-0 (Col-0), and the seeds were obtained from lab stocks.

Reporter lines

The reporter lines *ProVAMP712::VAMP712—GFP* and *ProVAMP713::VAMP713—GFP* were generated as part of this research by Gateway cloning in a Col-0 background. See the section on cloning (Methods 2.2). The reporter lines containing a highly active auxin response gene (*ProDR5::GFP)* were utilised, which contains a synthetic auxin-inducible promoter for confocal microscopy visualisation in wild-type Col-0 background, *vamp712,* and *vamp713* T-DNA insertional mutant backgrounds.

Mutant lines

Two homozygous mutants with T-DNA insertions in *VAMP712* (AT2G25340, GABI-Kat_054H03) (Rosso et al., 2003) and *VAMP713* (AT5G11150, SALK_121609) (Alonso et al., 2003) were obtained from The Nottingham Arabidopsis Stock Centre (NASC; http://arabidopsis.info/). The gene knockout mutants of *AtVAMP711* were made using the CRISPR-Cas9 technology. See the section on cloning (Methods 2.2).

Seed sterilisation

Seeds were sterilised before sowing to minimise the possibility of surface contamination when germinating and propagating *Arabidopsis* in tissue culture. Seeds in 1.5 mL microcentrifuge tubes were treated with a solution containing 5% (v/v) sodium hypochlorite and 0.02 % (v/v) Tween-20 for 15 minutes on a tube revolver (Fisher Brand) at 40 rpm. The seeds were then washed up to four times with sterile MilliQ water in a laminar flow cabinet. As much water as possible was removed, and the seeds were resuspended in 1 mL sterile 0.1% agar solution before sowing.

Plant growth conditions and stress treatments

For tissue culture experiments, seeds were sown on sterilised half-strength Murashige and Skoog medium (½ MS) (MS Salt mixture 2.2 g/L) (Merck, Dorset, United Kingdom) with 1% (w/v) sucrose and 1% (w/v) agar (Sigma A6686) (Merck, Dorset, United Kingdom), adjusted to pH 5.9 with 0.1 M potassium hydroxide (KOH). All growth media were autoclaved at 121°C for 20 minutes to sterilise. A growth medium was made as before for salt stress treatments with the addition of 150 mM NaCl. For control and stress treatments, 75 mL of medium was serologically pipetted in 100 x 100 mm square plates (Thermo Scientific) in the laminar flow cabinet and allowed to set. The relevant sterilised seeds suspended in 0.1% agar were sown on solid medium by taking up 100 µl seeds in a P1000 pipette tip, which was then removed from the pipette. One seed was dispensed from the tip, held horizontally, by lightly touching the agar surface, holding the plate at a 45° angle. The plates were left open to dry for up to 30 minutes, sealed with Micropore™ tape and placed in the dark at 4°C for at least 48 hours for stratification to synchronise germination. After stratification, the tissue culture plates were placed vertically at 22 °C (c. 3000 lux) in a Versatile Environmental Test Chamber (model MLR-351; Sanyo Electric Co. Ltd.) set to long-day conditions (16 hours light, 8 hours dark photoperiod). To select mutant and transgenic lines, seeds were sown on ½ MS agar medium supplemented with the relevant antibiotic, according to Table 2.1.1.

Table 2.1.1: *Antibiotics used for screening of mutant and transgenic seedlings.*

Genotype	Antibiotic	Final Concentration
vamp711 (*DT1T2*)	Hygromycin	50 µg/µL
vamp712 (GABI-KAT)	Sulfadiazine	7.5 µg/µl
vamp713 (SALK)	Kanamycin	50 µg/µL
ProVAMP712::VAMP712:GFP	Hygromycin	50 µg/µL
ProVAMP713::VAMP713:GFP	Hygromycin	50 µg/µL

Root length measurements

Vertical agar plates were scanned using an Epson Expression 1680 Pro flatbed scanner (Epson) at 600 dpi resolution. Primary root length, lateral root length, and number of lateral roots were quantified from these images using the software ImageJ (Schneider *et al.*, 2012; https://imagej.net/). ImageJ data were transferred to Microsoft™ Excel to visualise with graphs.

Statistical analyses

Analysis of primary root lengths was carried out in Microsoft™ Excel with a one-way ANOVA and Tukey-Kramer post-hoc test and, in some cases, a pairwise *t-test*. All statistical analyses used a *P-value* < 0.05 as the significance threshold.

2.2 Cloning

Gateway cloning

The Gateway® Technology (Invitrogen) is a cloning method that allows DNA fragments to be transferred between different cloning vectors via the site-specific recombination properties of bacteriophage lambda (Landy, 1989). This Lambda-based recombination technique is achieved by integrating site-specific *att*achment (*att*) sites into the gene cassette by polymerase chain reaction (PCR), *att*B, that then recombines with the *att*P attachment sites of the donor vectors to produce the entry clones. All the primers were designed by ApE™ software, and sequences are provided in Appendix II (Table S2). The pDONR/ZEO vector was used for all the BP reactions.

Isolation of promoter and coding sequences

Native promoter sequences of VAMP712 and VAMP713 were isolated from leaf genomic DNA of Col-0 plants using PCR to produce a 1 kb and 1.5 kb amplicon, respectively. For this, forward primers were designed to incorporate the 25 bp *attB1* site followed by 24 bp of template-specific sequence. The reverse primers contained a 25 bp reverse complement overlap with the start of the protein coding sequence (CDS), followed by 25 bp of the promoter template-specific sequence.

Isolation of the *VAMP713* CDS was conducted by PCR using the cDNA from wild-type Col-0 plants as the template. In this case, four guanine (G) residues at the 5′ end followed by the 25 bp *attB2* were included in the reverse primer and 21 bp CDS template-specific sequence excluding the stop codon. For both the promoter and CDS PCR products, primer length was designed to ensure the gene reading frame was correct for the expression.

After several unsuccessful troubleshooting attempts to amplify the CDS of *VAMP712*, the gene sequence with the relevant *AttB2* site was synthesised by Integrated DNA

Technologies (Brussels, Belgium) in a pUCIDT (Amp) vector. From this, the CDS was amplified by PCR.

The promoter and CDS PCR fragments were analysed by gel electrophoresis and sequenced by the Genomics Facility at Durham University. In some cases, the PCR yielded non-specific DNA bands and required gel extraction using the GeneJET Gel Extraction Kit (Thermo Fisher Scientific, Horsham, UK) following the manufacturer's instructions. Where there was only one PCR amplicon, the DNA was purified using the Monarch® PCR & DNA Cleanup Kit (5 μg) (NEB, Hitchin, UK) according to the manufacturer's protocol. The concentration of DNA was measured using the NanoDrop ND-1000 Spectrophotometer (Thermo Fisher Scientific, Horsham, UK).

DNA assembly of promoter and CDS

The isolated promoter and CDS were fused together using the Gibson Assembly® Master Mix (NEB, Hitchin, UK). The number of pmols of each promoter and CDS fragment was calculated using equation (1):

(1) pmols = (weight in ng) x 1,000 / (base pairs x 650 daltons)

Subsequently, 0.4 pmols of each fragment were combined with the Gibson Assembly reaction mix in a 0.2 mL PCR tube and incubated in a thermocycler at 25°C for 60 minutes.

BP reaction

The assembled *ProVAMP712:CDSVAMP712* and *ProVAMP712:CDSVAMP712* sequences were then cloned into the entry clone Gateway™ pDONR™/ZEO vector using the Gateway™ BP Clonase™ II Enzyme mix (Thermo Fisher Scientific, Horsham, UK). The reaction was set up according to Table 2.2.1 in a 0.2 mL PCR tube and incubated in a thermocycler at 25°C for up to three hours.

Table 2.2.1: *Components mixture for BP reaction*

Component	Volume
pDONR/ZEO vector (150ng)	1 µl
attb-PCR Fragment (150ng)	1 µl
BP Clonase™ II Reaction Mix	2 µl
TE Buffer, pH 8.0	6 µl

The entire BP reaction product was used to transform NEB® 5-alpha Competent *Escherichia coli* (*E. coli*) (High Efficiency) cells (NEB, Hitchin, UK).

E. coli transformation

NEB® 5-alpha Competent *E. coli* cells were thawed on ice, and a 50 µl aliquot was combined with the BP reaction product and incubated on ice for 30 minutes. The transformed cells were outgrown in 950 µl super optimal broth with catabolite repression (SOC) media for one hour at 37°C in the dark and on a shaker set at 225rpm, then spread on Petri dishes containing 30 mL low salt Luria Broth (LB) agar and 50µg/mL zeocin antibiotic. These plates were grown in the dark for up to 16 hours at 37°C. Colonies of positive transformants were picked under a blue flame with a sterile pipette tip and transferred to a 15 mL Falcon tube containing 5 mL liquid low salt LB and 50 µg/mL zeocin, then grown in the dark for up to 16 hours at 37°C. The pDONR/ZEO plasmid containing our gene of interest was then extracted using the GeneJET Plasmid Miniprep Kit (Thermo Scientific™) following the manufacturer's protocol and analysed by DNA gel electrophoresis and sequencing.

LR reaction

The pDONR/ZEO entry clone was then cloned into the destination clone Gateway™ pmdc107 vector using the Gateway™ LR Clonase™ II Enzyme mix (Thermo Fisher Scientific, Horsham, UK). The reaction mix was set up according to Table 2.2.2 and incubated at 25°C for four hours. Proteinase K (2 µl) was added to the completed LR reaction mix and incubated at 37°C for 10 minutes to stop the reaction. Then, the whole mixture was used to transform *E. coli* competent cells as previously described. Positive transformants containing the cloned pmdc107 plasmid were selected on LB agar plates supplemented with 50 µg/mL kanamycin. Again, liquid cultures were made, and the

plasmids extracted. The pmdc107 plasmid extract was analysed by DNA gel electrophoresis and sequenced to check for the gene insertion.

Table 2.2.2: *Components mixture for LR reaction*

Component	Volume
pDONR/ZEO entry clone (150ng)	1 µl
Pmdc107 destination vector (150ng)	1 µl
LR Clonase™ II Reaction Mix	2 µl
TE Buffer, pH 8.0	6 µl

Agrobacterium transformation

GV3101 Agrobacterium

Chemically competent *Agrobacterium tumefaciens* are highly effective for Agrobacterium-mediated transformation of several dicots, such as *Arabidopsis thaliana* and tobacco. The GV3101 strain contains the C58 chromosomal backbone conferring rifampicin resistance and the Ti plasmid pmp90 (pTiC58DT-DNA), providing resistance to gentamicin. This strain has the innate T-DNA region removed from the Ti plasmid and has instead a binary vector containing the missing T-DNA region, making the transfer of T-DNA into the plant genome possible. *Agrobacterium* GV3101 was obtained from lab stocks.

Preparing chemically competent cells

A. tumefaciens GV3101 cells were made chemically competent following an adaptation of the protocol described by Jyothishwaran et al., (2007). An overnight culture of an existing aliquot of cells was prepared and used to inoculate 500 ml of LB medium containing gentamycin and rifampicin. This was incubated under constant agitation at 30°C until an optical density (OD) of 0.6 was reached. Cells were pelleted by centrifugation at 4000 rpm, 4 °C for 30 min. The cells were resuspended in 5 mL of cold 150 mM NaCl and left on ice for 15 minutes. The centrifugation step was repeated, and the pellet was resuspended in 5 mL of cold 20 mM NaCl. Glycerol was added to a final volume of 20%, and 100 µl aliquots were snap-frozen in liquid nitrogen and then stored at -80°C.

Transformation

The transformation of *Agrobacterium* was conducted using an adaptation of the freeze-thaw method described by Hofgen and Willmitzer (1988). The volume required for 1µg of purified plasmid was mixed with 100 µl competent *Agrobacterium* cells and incubated in an ice bath for 5 minutes, followed by 5 minutes of incubation in liquid nitrogen, and at 37°C for 5 minutes or until the mixture has fully thawed. Under the blue flame of a Bunsen burner, 200 µl of sterile LB medium was added to the tube and then kept at 30°C for two hours. The entire tube contents were spread on LB agar plates supplemented with 50 µg/ml rifampicin, 30 µg/ml gentamicin, and 30 µg/ml kanamycin.

Arabidopsis transformation: Floral dip method

The transformation of *Arabidopsis thaliana* plants followed the floral dipping procedure detailed by Clough & Bent (1998). An *Agrobacterium* culture carrying the gene of interest was grown in 500 mL of selective LB medium until an OD600 of between 0.7 and 1.0 was reached. The culture was split into 50 mL aliquots and centrifuged at 3200 x *g* for 30 minutes. The pelleted cells were resuspended in 100 mL of 5% sucrose (w/v) and 0.05% Silwet L-77 (v/v) (Lehle Seeds, Texas, USA) per pellet. Between 400-500 mL of resuspended cells were collected in a container. Healthy wild-type (Columbia-0) plants with abundant flowers were held in the solution for 45-60 seconds. These plants were then covered with a propagation lid to ensure high humidity and placed in the dark overnight. Plants were grown in a greenhouse for an additional 2-4 weeks until dry enough to collect seeds. Seeds were selected by germination on ½ MS Agar (1%) plated with appropriate antibiotics.

Generation of CRISPR-Cas9 *vamp711* mutants

To generate the *vamp711* mutants, CRISPR-Cas9 technology was used. Here, two guide RNA (gRNA) spacer sequences on the negative strand were designed as targets for Cas9 cleavage: target 1 (5’ – GGGTTGCTGTCGTTGTCTCC -3’) and target 2 (5’ – ATAGGATTAATCGTATTAA -3’). A four-primer mixture with DT1-F0/DT2-R0 and DT1-BsF/DT2-BsR (Table S2) was used for PCR amplification to assemble the two gRNAs from the pCBC-DT1T2 template as described by Xing et al. (2014). The amplified PCR product DT1T2-PCR (626 bp) was purified with Monarch PCR and DNA clean-up kit (NEB) and assembled into pHEE401 by Golden Gate cloning method, using *Bsa*I and T4

Ligase (NEB). The reaction was incubated for 5 hours at 37°C, 5 minutes at 50°C and 10 minutes at 80°C, thus producing a gene expression module for two *VAMP711* gRNAs accompanied by a U6-26tail for the target 1 gRNA and a U6-29promoter for target 2 gRNA (Figure. 2.2.1).

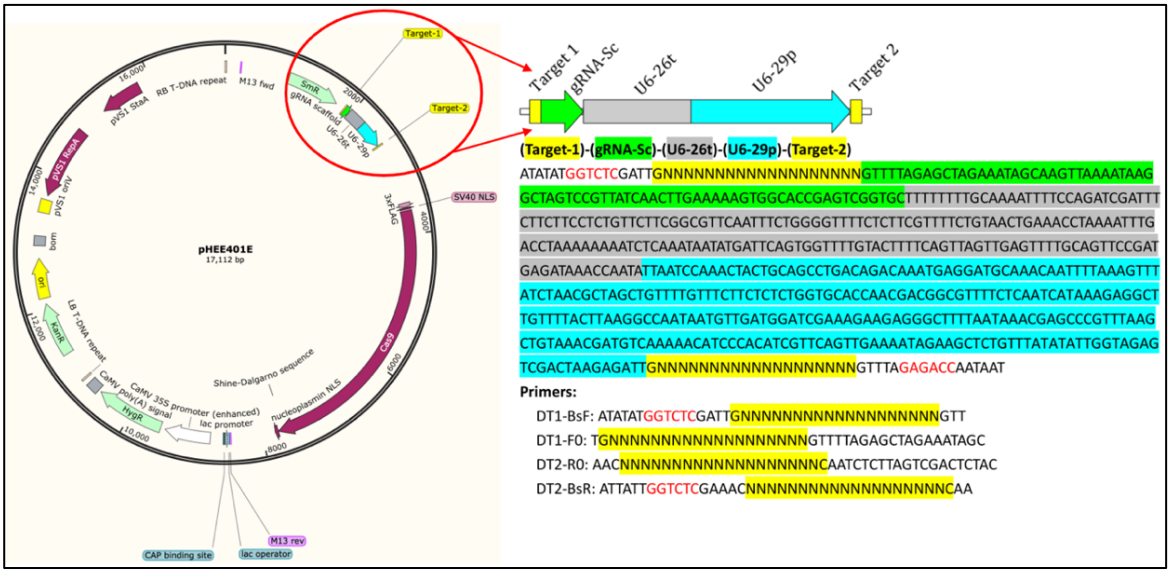

Figure 2.2.1: *The plasmid construct pHEE401E containing the gRNA and two target sites. The primers include a spacer sequence to alter the gap between the restriction-enzyme-recognition site and the cleavage site. The primer name 'DT' is used to denote the template plasmid, and the following number indicates which gRNA target is included in the primer. Forward and reverse primers are indicated with capital F and R, and the required restriction enzymes are denoted as Bs for BsaI. The pHEE401E plasmid map was generated using SnapGene™ software.*

This plasmid product was purified, *E. coli* competent cells were transformed, positive recombinants selected and verified with DNA sequencing. Finally, the CRISPR-Cas9 construct was transformed into *Agrobacterium tumefaciens* strain GV3101 and used to transfect Col-0 *Arabidopsis* plants using the previously described methods. Positively transformed offspring were screened using antibiotic selection.

2.3 Molecular biology techniques

RNA extraction

Total RNA was extracted from approximately 100 mg of tissue powder ground in liquid nitrogen using a pre-cooled pestle and mortar. The GeneJET™ Plant RNA Purification Mini Kit (Thermo Fisher Scientific, Horsham, United Kingdom) was used according to the manufacturer's instructions with one modification to extract total RNA. Following the first wash step, the On-column DNase I Digestion Set (Merck, Dorset, United Kingdom) was used according to the manufacturer's instructions. The DNase I was removed by repeating the first wash step of the GeneJET™ Plant RNA Purification Mini Kit. Quality control was conducted on all RNA extractions by gel electrophoresis in 1x MOPs buffer (4.18% w/v MOPS, 20 mM sodium acetate, 10 mM ethylenediaminetetraacetic acid (EDTA), pH adjusted to 7 with 2 M NaOH). Volumes estimated to contain 300 ng of RNA samples were incubated in 5 µL RNA Loading Dye (64% v/v formamide, 8%v/v formaldehyde, 130mM MOPS, 0.1 % (w/v) orange G, 0.013% w/v ethidium bromide) for 15 minutes at 55°C to allow the ethidium bromide to bind RNA before loading samples in a 1.2% agarose gel with 1x MOPS. Samples were separated by electrophoresis using a gel tank cleaned with 2% SDS. The gel was run at 50 volts for around 1 hour before being visualised using a UV transilluminator. The concentration of RNA was determined by measuring the optical density at 260 and 280 nm using a NanoDrop ND-1000 spectrophotometer (Thermo Fisher Scientific, Horsham, United Kingdom).

cDNA synthesis

Total RNA samples to be used in real-time quantitative PCR (RT-qPCR) had their concentrations normalised to give 600 ng final amount. To produce complementary DNA (cDNA) from the total RNA extraction, the qPCRBIO cDNA Synthesis Kit (PCRBIO, London, UK) was used following the manufacturer's instructions. Oligo dt and random primers were included in the kit and used as instructed by the manufacturer.

DNA amplification

The amplification of specific target sequences was done by PCR using the HS VeriFi™ Mix (PCRBIO, London, UK) in sterile 0.2 ml PCR Tubes (Starlab) according to the manufacturer's reaction protocol for a 50 µL reaction. A thermocycler was used with a Hot Start PCR programme: 95 °C for 60s, followed by 37 cycles of 95 °C (15s), 55-65 °C*

(20s), 72 °C for a time determined by the amplicon length (30 s/kb), followed by a final of extension 10 minutes at 72°C. PCR products or DNA samples were analysed by gel electrophoresis. Depending on the expected size of the DNA fragment, either 3.5% or 0.8% molecular grade agarose (Bioline, Tennessee, USA) was melted in 1x TAE buffer (40 mM tris(hydroxymethyl)aminomethane (Tris)-acetate, 1 mM EDTA). Once cool to the touch, ethidium bromide was added (0.5 μg/mL), and the gel was cast.

*Annealing temperatures were determined using the New England Biolabs (NEB) T_m calculator. Where further optimisation was needed, a gradient PCR was conducted at ± 5°C of the calculated T_m estimate.

Quantitative RT-PCR analyses

In every case, three replicates of samples pooled from up to approximately 40 individual seedlings from independent tissue culture plates were used for RT-qPCR analysis. The qPCRBIO SyGreen Mix Separate-ROX (PCRBIO) was used to quantify gene expression at half the concentrations given in the manufacturer's protocol. In these reactions, no ROX was added. The genes *ACTIN-2* (*ACT2*) and *EUKARYOTIC INITIATION FACTOR 4a* (*EIF4a*) were used as constitutive reference controls whose expression does not change in response to salinity stress. Gene expression fold-change was calculated using *REST 2009* software (Pfaffl et al., 2002) of the take-off and amplification data. The list of primers used in the RT-qPCR experiments is given in Table S1 Appendix II.

Genomic DNA extraction

Genomic DNA (gDNA) was isolated from Arabidopsis leaf tissue in two ways. For gDNA used in downstream cloning applications, the Edward's Prep extraction was performed based on the method described by Edwards et al. (1991). Briefly, frozen ground tissue was homogenised in a microcentrifuge tube by pipetting in 400 μl of DNA extraction buffer (200 mM Tris-HCl (pH 7.5), 250 mM NaCl, 25 mM EDTA, 0.5% SDS). Samples were centrifuged for 1 minute at 17,000 x *g* to pellet the debris. Then, up to 300 μl of the supernatant was transferred into a new microcentrifuge tube. An equal volume of isopropanol was added and mixed by inverting. After two minutes of incubation at room temperature, DNA was pelleted by five minutes of microcentrifugation, and the

supernatant was discarded. The pelleted DNA was resuspended in 50 µl sterile MilliQ water or TE Buffer (10mM Tris-HCl, 0.1mM EDTA, pH 8.0).

For gDNA extraction to be used in whole genome sequence analysis, the method described by Healey et. al (2014) was followed with some modifications. Here, 100 mg of ground leaf tissue was homogenised in 1 mL of cetyltrimethylammonium bromide (CTAB) DNA extraction buffer (100 mM Tris-HCl (pH 7.5), 25 mM EDTA, 1.5 M NaCl, 2% (w/v) CTAB, 0.3% (v/v) β-mercaptoethanol) and incubated at 65°C for 30 minutes. Debris was removed by centrifugation, and in a clean microcentrifuge tube, one volume of 24:1 chloroform:isoamyl alcohol was added to the supernatant. After thorough mixing and centrifugation for 10 minutes, the upper aqueous phase was carefully transferred to a new tube and treated with 50 µg RNase A (20 mg/mL RNase A stock in 50 mM Tris-HCl, pH 8.0, 10 mM EDTA) for 15 minutes at 37°C before being removed with chloroform:isoamyl alcohol precipitation again. Finally, one-half volume of 5 M NaCl and three volumes of cold >95% (v/v) ethanol were added and placed at -20°C for 60 minutes. DNA was pelleted by centrifugation and washed with 70% ethanol before being resuspended in 50 µl of TE buffer (pH 8.0). In both cases, the quality of DNA was tested by gel electrophoresis and the concentration was measured by reading the optical density at 260 and 280 nm using a NanoDrop ND-1000 spectrophotometer (Thermo Fisher Scientific, Horsham, UK).

Purification of DNA fragments from agarose gel

PCR products of interest were visualised on an ultraviolet transilluminator (model UVT 400-M; International Biotechnologies Inc.) and excised using a sterile scalpel blade, collected in a 1.5 ml microcentrifuge tube, and then recovered according to QIAquick Gel Extraction Kit (Qiagen) manual.

Purification of DNA from PCR samples

To isolate high-quality DNA following PCR reactions, the Monarch PCR and DNA Cleanup Kit was used following the manufacturer's protocol. This process minimised the potential disruptive effects of the remaining PCR reaction components, such as polymerases, primers, deoxyribonucleoside triphosphates (dNTPs), or plasmids. The final concentrated DNA products were then used in subsequent cloning experiments.

Plasmid purification

Plasmid DNA was extracted from recombinant *E. coli* cells using the GeneJET Plasmid Miniprep Kit (Thermo Scientific™) following the manufacturer's protocol. These extracted plasmids were used for sequencing, further cloning experiments and bacterial transformation.

2.4 Microscopy

Laser scanning confocal microscopy (LSCM)

Seedlings were removed from plates and fixed using paraformaldehyde (PFA), and then the ClearSee method was applied. ClearSee is used to clear plant tissues of chlorophyll autofluorescence while retaining the fluorescence of GFP-tagged proteins (Kurihara et al., 2015) and is compatible with several fluorescent dyes (Ursache et al., 2018). After sufficient clearing, all seedlings were stained with Calcofluor White (Merck™, Dorset, United Kingdom), a fluorescent blue dye commonly used to visualise plant cell walls (Herth and Schnepf, 1980). Microscopy imaging in this project focused predominantly on the root tip, where auxin accumulation and distribution at the root apical meristem controls root growth and significantly impacts plant development (Perilli et al., 2012).

Seedlings were imaged with a Zeiss LSCM 800 confocal scanning laser microscope (https://www.zeiss.com/-microscopy/int/home.html). Roots and leaves were imaged using an x40 oil immersion objective lens. Gain, line averaging, detection frequencies and other microscope settings were altered between fluorescent marker lines to optimise image quality. Excitation of fluorophores was performed as follows in Table 2.4.1 unless otherwise stated.

Table 2.4.1: *Excitation of fluorophores and dyes for LSCM.*

Fluorophore/Dye	Excitation/Laser Line
Calcofluor White	405 nm
Green Fluorescent Protein (GFP)	488 nm (Argon laser)

Preparation of 4% PFA and the fixation procedure

In a fume cupboard, 2 g of paraformaldehyde (PFA) powder was mixed in 50 mL of 1x phosphate-buffered saline (PBS) solution using a magnetic stirrer and warmed to 60°C to yield a 4% PFA solution. A few drops of 1 M KOH were added to aid the dissolution of

PFA powder, and then 1 M HCl was added to lower the pH to approximately 6.9, approximated using pH strips. The PFA solution was allowed to cool before use and made fresh each time. Whole seedlings were transferred to the 4% PFA solution for 30 minutes under vacuum treatment to facilitate infiltration. Finally, the fixed seedlings were washed with PBS twice before proceeding with the ClearSee clearing procedure.

Preparation of ClearSee and clearing procedure

ClearSee solution was made according to Table 2.4.2. and stored for up to two months.

Table 2.4.2: *ClearSee solution used for clearing plant tissues*

Chemical	Final w/v
Xylitol	10%
Na-Deoxycholate	15%
Urea	25%
Water	To the final volume

Fixed and washed seedlings were kept in ClearSee solution at room temperature for at least a week. The clearing solution was changed every 2-3 days. After clearing, seedlings were used for staining and imaging.

Calcoflour White Staining

Fixed and cleared seedlings were submerged in a 0.1% solution of Calcofluor White in ClearSee for 30-60 minutes. Stained seedlings were removed from the Calcofluor White solution and washed with ClearSee solution for at least 30 minutes before imaging. Seedlings were mounted on slides with ClearSee solution for imaging using LSCM.

Analysis of confocal images

Images were exported in Tiff format and opened in ImageJ2™ (version: 2.14.0/1.54f) for analysis (https://imagej.net/ij/). Images were taken from at least three individual roots for each analysis.

2.5 Proteomics

Protein extraction

The roots of approximately 750 Arabidopsis seedlings were harvested 9 days-post-germination (dpg) per biological replicate and ground into a powder using a mortar and pestle in liquid nitrogen. For stress treatment analysis, 7-dpg seedlings were transferred to ½ MS Agar plates containing 150 mM NaCl and grown for a further 48 hours before being harvested. As illustrated in Figure 2.5.1, the ground tissue was thawed on ice before being suspended in 1.5 mL homogenisation buffer containing 50 mM HEPES-KOH (pH 7.5), 5% (v/v) glycerol, 10 mM EDTA (pH 8.0), 3 mM dithiothreitol (DTT) and 1x HALT protease inhibitor cocktail (Thermo Fisher Scientific, Horsham, UK). Samples were centrifuged at 800 x g, 4°C for 10 minutes to remove plant debris. The supernatant was transferred to a new microcentrifuge tube and centrifuged for 15 minutes at 8000 × *g*, 4°C. For SDS-PAGE and immunoblot analysis of the total protein fraction, 30 µl supernatant was retained. The remainder of the supernatant was transferred to an ultracentrifuge tube and used for ultracentrifugation at 150,000 x *g*, 4°C for 60 minutes. The supernatant was retained for SDS-PAGE and immunoblot analysis of the soluble protein fraction. The pellet was homogenised in 100 µl resuspension buffer (0.1 M triethylammonium bicarbonate (TEAB), 5% SDS) using a cut P100 micropipette tip and incubated on ice for 15 minutes. This represents the microsomal fraction highly enriched with solubilised membrane proteins, which were transferred to a clean 1.5 mL microcentrifuge tube and stored at -20°C until required.

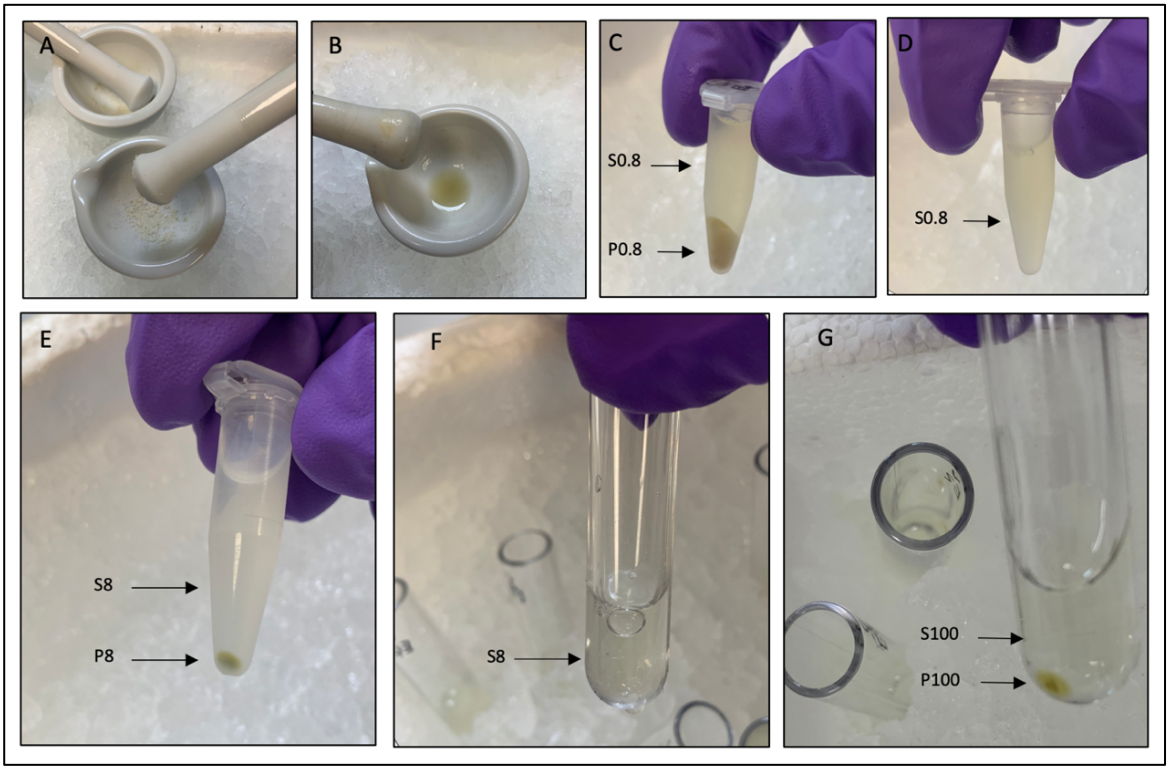

Figure 2.5.1: *Workflow of protein extraction method by differential centrifugation. (A) Harvested root tissue was snap-frozen and ground in liquid N_2 using a mortar and pestle. (B) Ground tissue was kept on ice to defrost. Homogenisation buffer was added and grinding continued for two minutes. (C) Homogenate was centrifuged at 800 x g, 4°C. (D) The supernatant (S0.8) was transferred to a clean microcentrifuge tube. (E) This was centrifuged at 8000 x g, 4°C. (F) Supernatant S8 was transferred to an ultracentrifuge tube, and samples were balanced using additional buffer. (G) Ultracentrifugation at 150,000 x g, 4°C yields an S100 supernatant containing soluble/cytosolic proteins and a P100 pellet containing microsomal proteins.*

Protein quantification

Protein concentrations of each fraction were estimated using the Pierce™ BCA Protein Assay Kit (Thermo Scientific) according to the manufacturer's instructions regarding the micro-tire plate protocol. Absorbance values were read using the BioTek™ ELx800 microplate reader (Agilent, California, USA). Bovine serum albumin (BSA) was used as a protein standard, by which sample concentrations were determined from the equation of the standard curve (Figure 2.5.2).

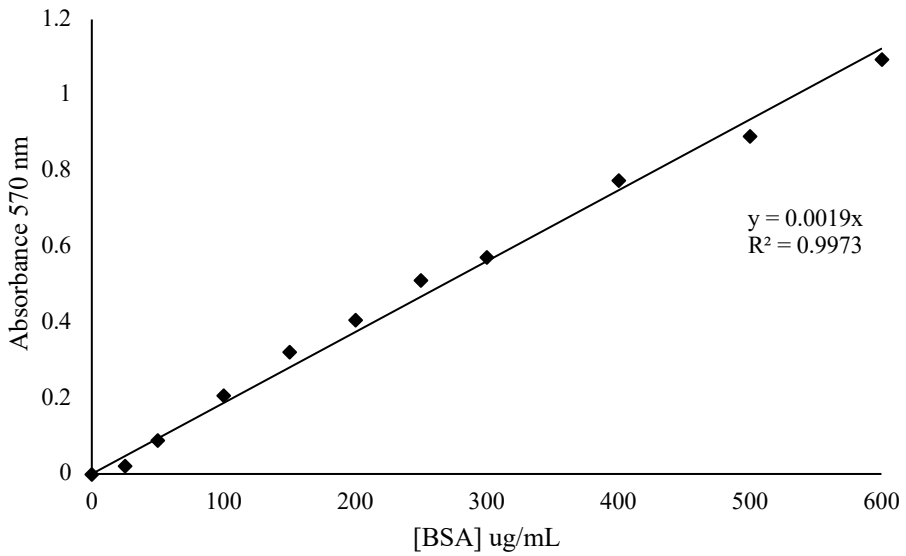

Figure 2.5.2: *BCA protein assay calibration curve of Bovine Serum Albumin (BSA). The line of best fit provides an R^2 value of 0.9973 and the coefficient of the slope is 0.0019.*

SDS-PAGE

Casting and running protein gels was conducted according to the standard Laemmli method (Laemmli, 1970) using BioRad's Miniprotean II with the following separating and stacking gel mixtures:

Separating gel:
12% [v/v] bis/acrylamide, 0.375 M Tris (pH 8.8), 0.08% [w/v] N',N',N',N'-tetramethyl-ethylenediamine and 0.8% [w/v] ammonium persulfate.

Stacking gel:
3.75% [v/v] bis/acrylamide, 0.125 M Tris (pH6.8), 0.08% [w/v] N',N',N',N'-tetramethyl-ethylenediamine and 0.8% [w/v] ammonium persulfate.

Electrophoresis and activity staining

Protein extract aliquots were thawed on ice and mixed with an equal volume of 2x sample buffer (0.125 M Tris-HCl (pH 6.8), 20% glycerol [v/v], 4% SDS [w/v], 0.02% bromophenol [w/v]) and then denatured at 95°C for 5 minutes. The stacking and separating gel were first run at 90 V for about 25 minutes and then 180 V in 1x running buffer (50 mM MES, 50 mM Tris, 0.5 M EDTA and 0.1% [w/v] SDS).

Coomassie blue staining

Protein samples resolved on acrylamide gels by SDS-PAGE were prefixed in fixation solution (50% methanol [v/v] and 10% acetic acid [v/v]) for 30 minutes. After removing the fixation solution, the gel was stained with 0.1% Coomassie Blue R-250 [w/v] dissolved in the fixation solution for 2-4 hours or until the gel was no longer visible in the dye solution. The gel was destained for 1-2 hours or until bands became visible in 5% methanol [v/v] and 7.5% acetic acid [v/v].

Western blot

After resolving protein samples by one-dimensional SDS-PAGE, the proteins were transferred onto a nitrocellulose membrane (BIO-RAD) using a wet BIO-RAD mini-PROTEAN® blotting system (BIO-RAD). The transfer system was filled with 1x transfer buffer (25 mM Tris-HCl, 190 mM glycine, 20% methanol). The transfer was carried out overnight at a constant 100 V. Successful transfer of proteins was determined by Ponceau red staining. The membranes were rinsed with dH_2O and blocked for one hour with 5% non-fat milk in 1x TBS-T (20 mM Tris-HCl pH 7.6, 150 mM NaCl, 0.1% [v/v] tween-20). Primary antibodies were diluted in 5% non-fat milk + TBS-T according to the manufacturer's specification (Agrisera, Sweden). The hybridisation of primary antibodies was conducted for each antibody by incubating the membrane at 4°C with gentle shaking for 5 hours. The membrane was then washed four times with 1x TBS-T with 4 minutes of gentle rocking per wash repetition. Then, the membrane was incubated for 1 hour at room temperature with an anti-rabbit secondary antibody suspended in 5% non-fat milk and TBS-T, and the wash step was repeated as before. The membrane was then treated with Clarify™ Western ECL Substrate (BIO-RAD) according to the manufacturer's instructions. Membranes were exposed in an iBright™ CL1500 Imaging System (Invitrogen).

Isobaric tags for relative and absolute quantification (iTRAQ)

The mass spectrometry-based proteomics technique iTRAQ is a valuable way of comparing protein abundance across different samples in a quantitative manner, making it particularly useful in comparative proteomics studies. In iTRAQ labelling, isobaric tags are used to label peptides from different samples, allowing their simultaneous identification and quantification in a single mass spectrometry experiment.

Trypsin digestion

The volume required for 12.5 µg of each sample was made up to 100 µl with 75 mM Tris (pH8.8), then precipitated in 80% acetone overnight at -20°C. Protein was pelleted by centrifugation, the supernatant discarded, the pellet resuspended in 5 µl of 2% SDS [w/v] and then incubated at 60°C for one hour. The volume was made up to 100 µl with the addition of dissolution buffer (500 mM TEAB) and vortexed for one hour at room temperature. After a 10-second centrifugation spin, 2 µl of reducing agent (tris-(2-carboxyethyl) phosphine (TCEP) (50 mM)) was added and incubated at 60°C for one hour. Next, 1 µl of blocking agent (methyl methanethiosulfonate (MMTS), 200 mM) was added and left for 10 minutes at room temperature. Overnight protein digestion was carried out at 37°C by adding 2 µg of trypsin gold.

iTRAQ labelling

Digested samples were freeze-dried and reconstituted in 55 µl of TEAB (50 mM), and pH strips were used to ensure a pH of 7.5-8.0. Next, 20 µl of diluted tag was added to label every protein sample. After two hours at room temperature, the 8 labelled samples per experimental line were combined and freeze-dried.

Mass spectrometry

Liquid chromatography tandem mass spectrometry (LC-MS/MS) was performed using a TripleTOF 6600 mass spectrometer (Sciex) linked to an Eksigent 425 LC system via a Sciex Nanospray III source. Each LC-MS run used peptides from 5 µg protein, and chromatographic separations used a 'trap and elute' method. Samples were loaded and washed on a Triart C18 guard column 1/32", 5 µm, 5 x 0.5 mm (YMC) acting as a trap, and online separation of peptides was performed over 87 minutes on a TriArt C18 1/32", 3 µm, 150 x 0.3 mm column (YMC) at a flow rate of 5 µL/min.

Buffers A and B were made using 0.1% formic acid (FA) in water and acetonitrile (ACN), respectively. Sequential linear gradients of 3 – 5% buffer B over two minutes, 5 – 30% over 66 minutes, 30 – 35% over 5 minutes and 35 – 80% over two minutes were followed by a column wash in 80% buffer B for three minutes. Return to 3% buffer B was over one minute before column re-equilibration for 8 minutes. The MS-MS acquisition, employing a data-dependent top-30 approach, commenced immediately with the initiation of the

gradient, and continued for a duration of 85 minutes. Collision energy was adjusted specifically for iTRAQ-labelled peptides.

During this timeframe, precursor-ion scans (400 to 1600 m/z) of 250 ms facilitated the selection of a maximum of 30 multiply-charged ions (>500 cps) for collision-induced dissociation (CID) fragmentation. MS/MS spectrum acquisition occurred in the m/z range of 100-1500 for 50 ms. The cycle time was set at 1.8 seconds, and a rolling precursor exclusion of 15 seconds was implemented to prevent multiple fragmentations of the same peptide. Spectrometer data acquisition was carried out using the Analyst TF 1.7.1 instrument control and data processing software from AB Sciex.

Mass spectra data analysis

Protein identification and relative quantification involved processing the raw .wiff data-files against relevant databases using ProteinPilotTM 5.0.1 version 4895 software, which incorporates the ParagonTM Algorithm 5.0.1.0.4874 (AB Sciex). A Paragon method for iTRAQ 8-plex (peptide-labelled) samples, focusing on tryptic peptides with iodoacetamide cys-modification, was employed, and the data were acquired on a TripleTOF 6600 spectrometer. This method included label bias-correction, activation of 'Thorough ID,' selection of 'Run False Discovery Rate Analysis' options, and setting the Detected Protein Threshold at 0.05 (10%) [Unused ProtScore (conf)]. Subsequently, peptide and protein tables were exported from ProteinPilot for further manual data-handling and filtering. This data analysis was conducted using a combination of Microsoft Excel^{TM} and R-Studio programming language.

2.6 Bioinformatics

Protein families of the identified salt stress responsive proteins were retrieved from the InterPro (http://www.ebi.ac.uk/interpro/) and SupFam (www.supfam.org) databases. Singular Enrichment Analysis (SEA) of Gene Ontology (GO) terms for biological processes, cellular compartments, and molecular function was carried out using the DAVID (Database for Annotation, Visualisation, and Integrated Discovery) web servers (https://david.ncifcrf.gov) (Huang et al., 2009).

Protein sequence alignments of the VAMP71 family were conducted using ClutalOmega and ClustalW web tools as described previously (Larkin et al., 2007). The respective

sequences used as inputs were retrieved from the TAIR (https://www.arabidopsis.org) and UniProt (https://www.uniprot.org) databases.

For analysis of whole genome sequencing data, the following was conducted by the in-house bioinformatics chief experimental officer Dr. Wenbin Wei. Adapter sequence in the sequence reads were removed using fastp (https://github.com/OpenGene/fastp). The sequence reads were aligned to Arabidopsis thaliana TAIR10 genome using bwa-mem2 (https://github.com/bwa-mem2/bwa-mem2). Duplicated reads were remove using sambamba (https://lomereiter.github.io/sambamba/). Mutations were identified using Strelka2 (https://github.com/Illumina/strelka) and annotated using snpEff (http://pcingola.github.io/SnpEff/). Sequence alignment was viewed using IGV (https://www.igv.org/).

Chapter 3: Genotypic and Phenotypic Characterisation of the VAMP71 Family Genes

VAMP71s are R-SNAREs which typically localise to trafficking vesicles and are attached via the C-terminal transmembrane domain. Recently, a role for a vesicle-associated VAMP714-dependent pathway of PIN trafficking was characterised (Gu et al., 2021), and related VAMP71 family proteins (Gu et al., 2020) were shown to be auxin-regulated. These are VAMP711, VAMP712 and VAMP713, whose function is not well researched. Previously, VAMP711 and VAMP712 have proposed roles in abiotic stress tolerance (Leshem et al., 2010, Leshem et al., 2006, Xue et al., 2018). It is well known that auxin signalling pathways and polar auxin transport are both highly regulated in plants exposed to salt stress (Liu et al., 2015, Park et al., 2007). Specifically, salt stress impairs auxin transport and distribution along the root (Shen et al., 2010, Sun et al., 2007), resulting in decreased growth.

Presently, the role of VAMP71 family proteins in plant auxin-mediated salt stress responses remains unknown. The main aim of this project was to investigate the possible link between VAMP71 protein family members and the salt stress response of plants via changes in auxin abundance, transport, and signalling. This work focussed on the salt-induced root growth phenotypes of individual knockout mutants of the *VAMP711*, *VAMP712*, and *VAMP713* genes.

Genotyping

Genomic DNA extracted from leaf tissue of five-week-old wild-type and mutant *Arabidopsis* plants was used for genotyping. Gel electrophoresis using PCR products amplified with genotyping primers confirmed if the individuals tested were homozygous for the T-DNA insertion (an example of genotyping on *vamp712* and *vamp713* mutants is shown in Figure 3.1). Seeds were harvested from confirmed homozygous knockout mutants and used in further analyses.

Whole genome sequencing of *vamp711* mutants was analysed using bioinformatics. A mutation in *AtVAMP711* (chr4: 15527001 A->AT insertion, p.Ile130fs, frameshift) was found in 3 out of 7 reads (Figure S2, appendix 2). This confirms that the CRISPR

experiment was successful; however, plants that are homozygous for the mutation need to be acquired in future work. Therefore, the work presented here has been conducted on heterozygotes.

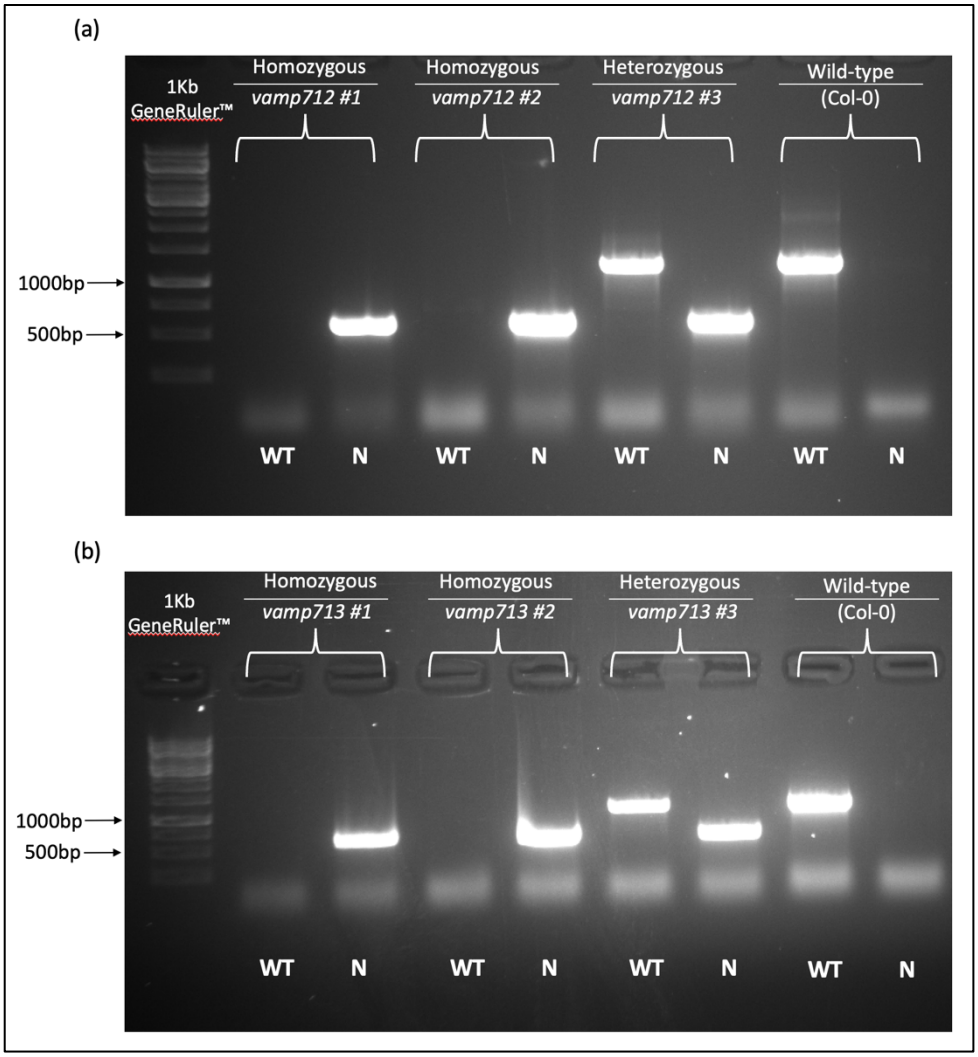

Figure 3.1: *Verification of vamp712 GABi-KAT T-DNA insertion mutant and vamp713 SALK T-DNA insertion mutant. (a) Representative tests of genomic DNA extracted from three individual transgenic plants (#1-3) and one wild-type (Col-0) as a control. Individuals #1 and #2 were found to be homozygous for the T-DNA insertion since amplification was only seen with the insertion-specific primers (N), o8474 + 054H03, with a band in the expected size range (600bp). No band was present when the gene-specific primers (attb1 + attb2) were used, showing no amplification of the WT VAMP712 gene. Individual #3 was found to have amplification with both wild-type and insertion primers, indicating this sample was heterozygous for the T-DNA insertion. The wild-type control showed an absence of the insertion band, confirming the primers' specificity for the mutant. (b) Three vamp713 transgenic mutant plants were tested; #1 and #2 were homozygous for the T-DNA insert, as only the insertion-specific primers, LB + RP, were amplified. Again, #3 was heterozygous with wild-type (LP + RP), and insert primers gave bands. All PCR products were separated by gel electrophoresis on a 0.8% Agarose gel. GeneRuler™ (Thermo Scientific) was used as the DNA size marker in lane 1.*

Phenotyping – Primary root length

Under controlled optimal growing conditions, the primary root lengths five days post-germination were compared between wild-type Col-0 seedlings and the *vamp71* mutants. A total of 35 seedlings, split across seven square plates, were measured for each genotype. On average, *vamp713* seedlings had the slowest primary root growth compared with the other three, whilst the *vamp711* CRISPR knockout mutants grew the longest and were significantly different to wild-type *Arabidopsis* according to the Tukey-Kramer statistical test ($P<0.05$) (Figure 3.2a). The *vamp712* plants were not significantly different from wild-type or *vamp711* (Figure 3.2a). Despite statistically significant differences between some transgenic lines and wild-type, there was a high degree of variation, as the box-and-whisker plot demonstrates (Figure 3.2a). Phenotypically, *vamp712* roots appeared to grow in a 'wavey' or 'zig-zag' manner, which was also observed in *vamp711* and *vamp713,* though less frequently (Figure 3.2b). The observed phenotypes for the heterozygous *vamp711* mutants suggest the gene acts in a semi-dominant way, and therefore, half the gene dosage still has an effect on phenotype.

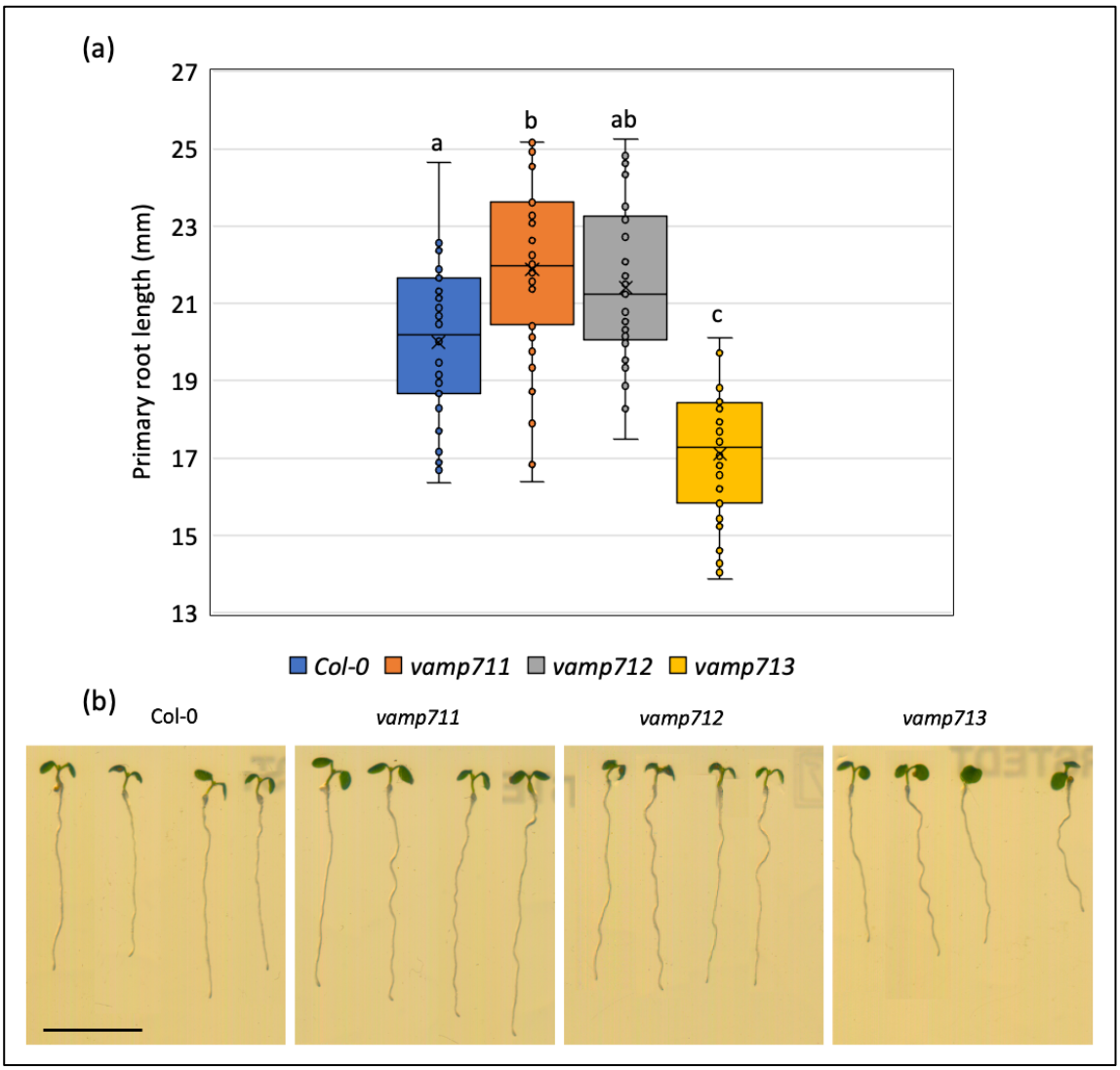

Figure 3.2: *Comparison of primary root growth five days post germination. (a) Whisker and box plot of primary root lengths. The line represents the median average and cross the mean average. Data was analysed with a one-way ANOVA and Tukey-Kramer post-hoc test. Plots with the same letter have no statistically significant difference at P<0.05, n=35. (b) Images of seedlings showing phenotypic differences. Images were modified to move seedlings closer together whilst their size and scale were not altered. Scale bar equals 10mm and is an applicable scale for each image.*

Salinity stress modifies Arabidopsis root system architecture.

To screen for which salt stress level led to the most significant difference in root growth of wild-type and *vamp71* mutant Arabidopsis seedlings, six-day-old seedlings were treated with different concentrations of salt stress for four days. The *vamp711* plants had significantly less primary root growth after four days without salt stress than the wild-type and *vamp713* mutant plants (Figure 3.3a). Root growth was inhibited by all salt treatments in a concentration dependent manner. 30mM NaCl had a significantly greater inhibitory effect on the root growth of the three *vamp71* mutants compared with the wild type. There

was no significant difference in root growth between the wild type and *vamp711* mutants at other concentrations (Figures 3.3a and 3.3b). For comparison, the relative primary root length was calculated using the mean root length change divided by the root growth without salt stress treatment (Figure 3.3b). This calculation aimed to assess any difference in basal root growth rates that might contribute to the salt-mediated growth differences. Since the relative root growth follows a similar trend to the actual root growth length comparisons, it is concluded that the growth rates were not a confounding factor.

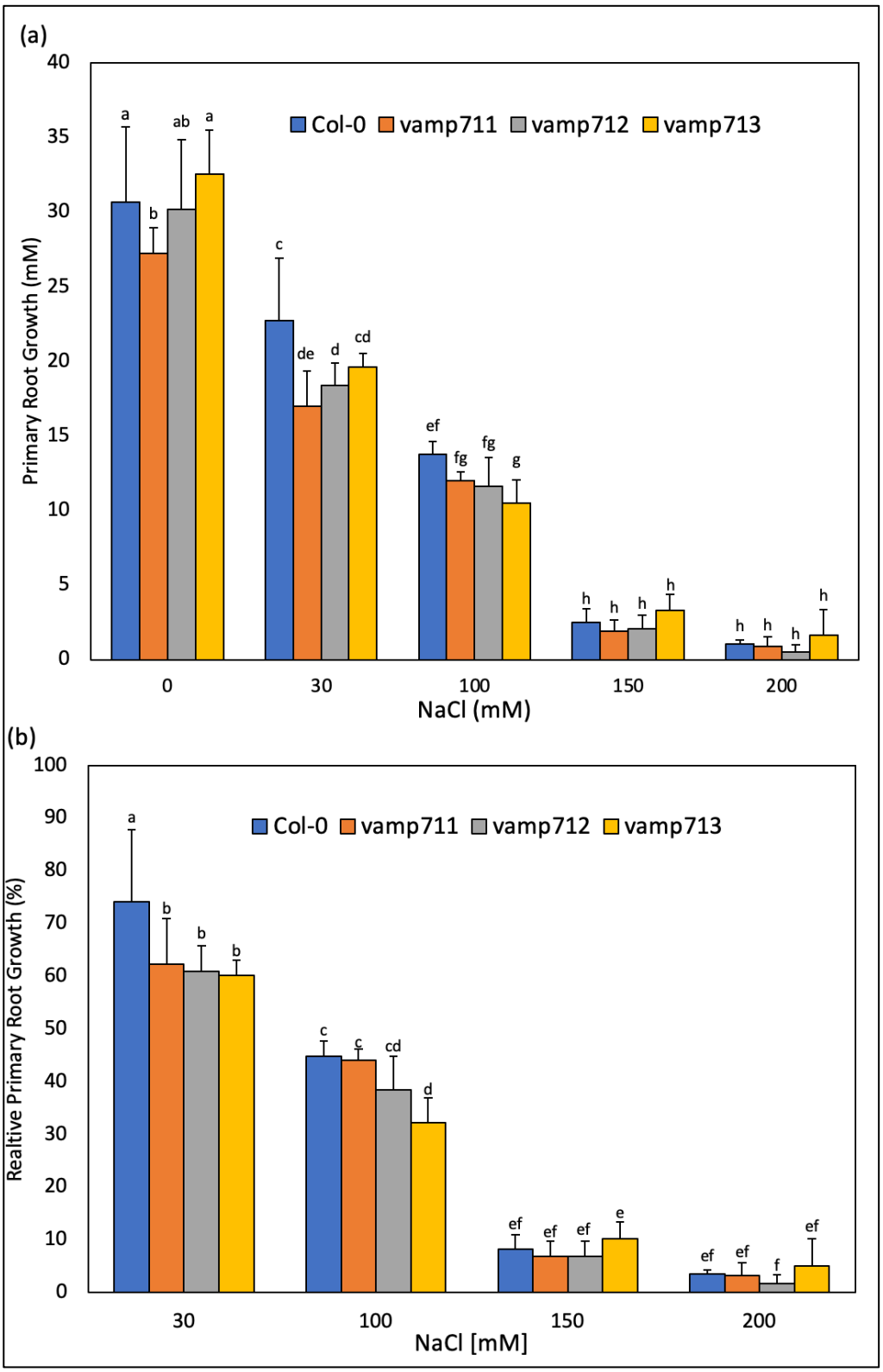

Figure 3.3: *Primary root length growth of six-day-old wild-type Col-0 and vamp711, vamp712, and vamp713 mutants transferred to different concentrations of NaCl for four days. (a) Measured new root growth using ImageJ. Bars are mean averages, and error bars represent standard deviation. (b) Relative root growth was calculated using the mean root length change divided by the root growth without salt stress treatment. Bars represent percentage root growth. A two-way ANOVA was conducted for statistical analysis, followed by Tukey-Kramer HSD post hoc to find statistical differences at $P<0.05$, $n= 20$.*

In addition to determining an appropriate concentration of salt stress for further experimental analysis, how root growth changed over time when exposed to salt stress was assayed. After two days, a significant difference in new primary root growth was observed between the four plant genotypes according to ANOVA analysis (Figure 3.4). Interestingly, despite *vamp713* having the shortest primary root lengths five days after germination in normal growth conditions, their roots were inhibited the least by 150mM NaCl of all the genotypes, indicating reduced salt sensitivity of this mutant. The primary root growth of *vamp711* and *vamp712* was inhibited the most from day two onwards, suggesting these genes are involved in maintaining root growth under salt stress. After day four, the variation between individuals of each group was substantial as some seedlings in each group ceased to grow their primary roots. Therefore, day four was selected as a good time point to report other salt-dependent physiological measurements and analysis, representing a good trade-off between mean differences and within-group individual variation.

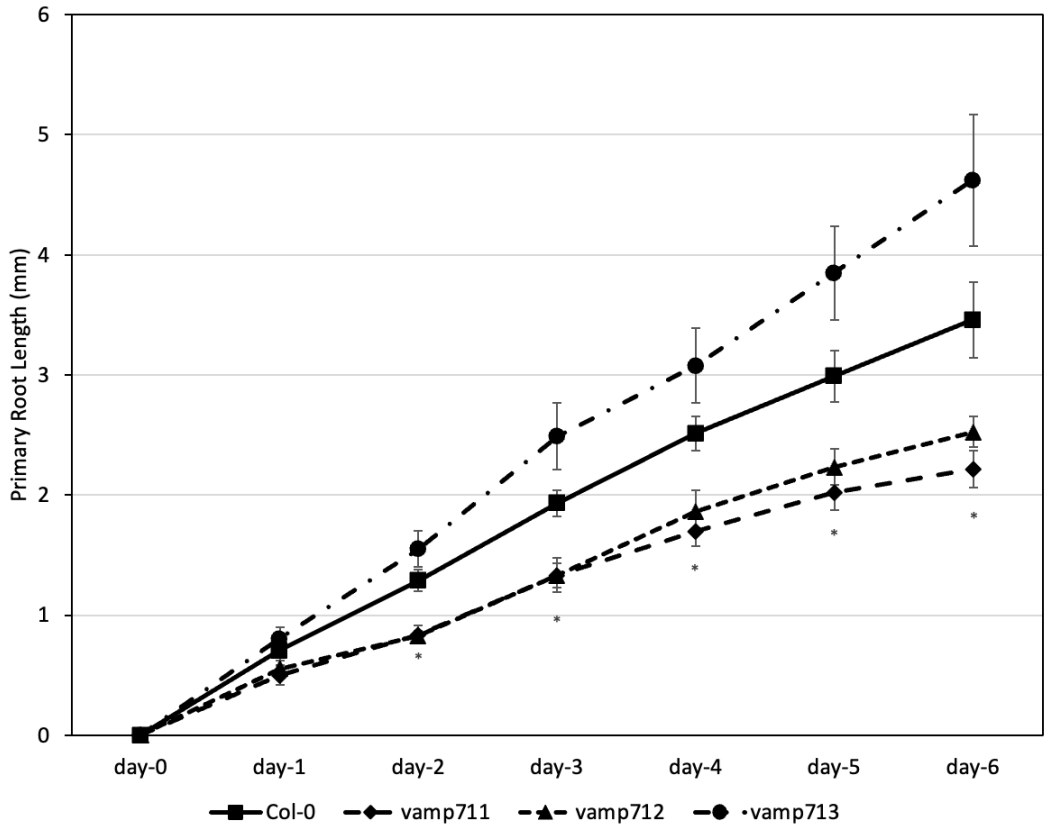

Figure 3.4: *Time course of primary root growth of six-day-old wild-type Arabidopsis (Col-0) and vamp71 mutant lines transferred to media supplemented with 150mM NaCl. Mean ± SE root length change (mm) was measured daily for six days. Asterisks show significant differences between the groups according to single-factor ANOVAs, p values <0.05, n=12 in each group.*

Lateral root growth under salt stress

When the lateral root growth was compared for all three mutants and wild-type grown in media treated with 150mM NaCl, *vamp713* mutants were found to have significantly decreased lateral root length and lower lateral root count according to Pairwise *t-test* (*P<0.05)* (Figure 3.5).

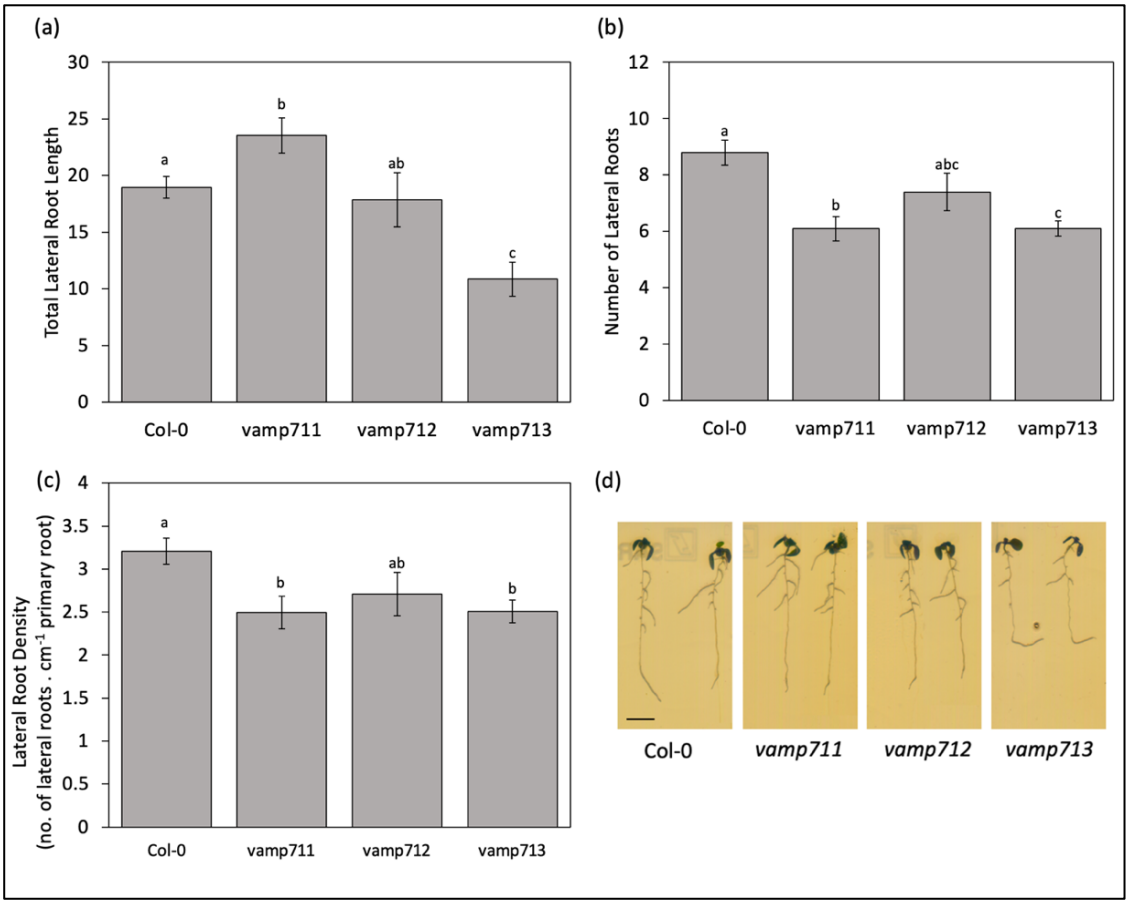

Figure 3.5: *Lateral root growth after four days of 150 mM salt stress. Seedlings were transferred to salt-stress media six days after germination. (a) Bars show mean ± SE total lateral root length (mm), (b) total number of lateral roots, (c) lateral root density calculated by dividing the number of lateral roots by primary root length, (d) a representation of the seedlings after four-days of salt stress, scale bar = 0.5cm (d). Different letters show significant differences between the groups according to single-factor ANOVAs with Pairwise t-test follow-up, P-values <0.05, n=10 in each plant group.*

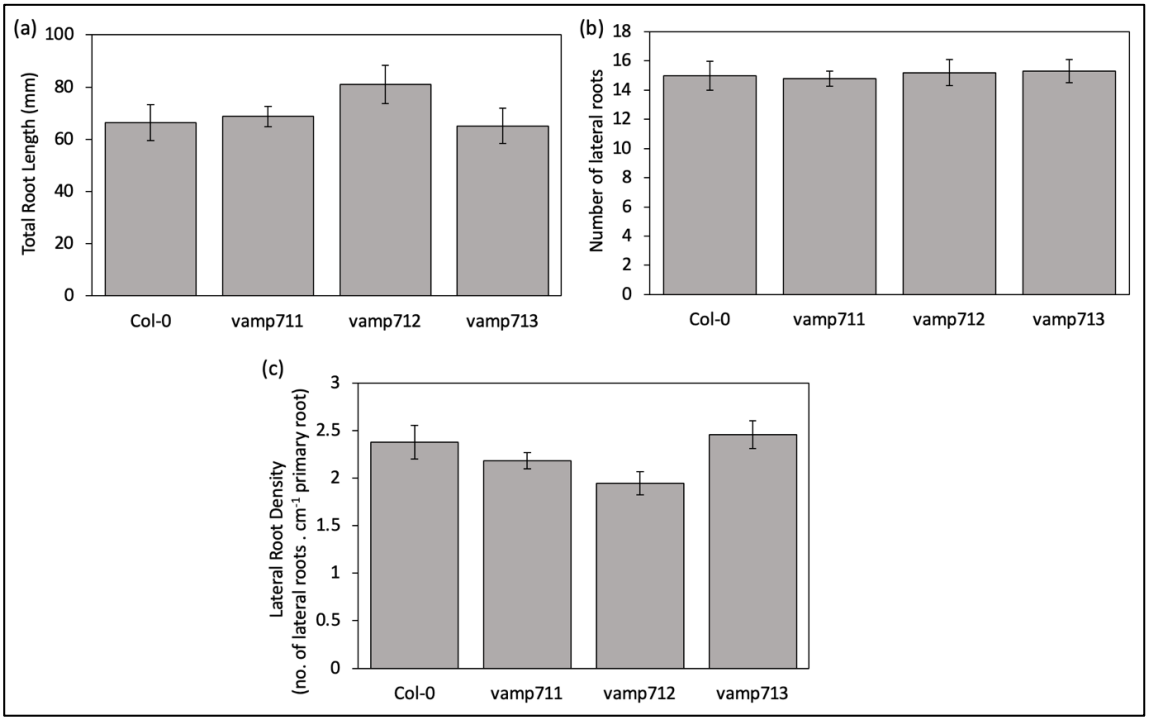

Figure 3.6: *Lateral root measurements following the same experimental conditions without salt stress treatment. (a) Bars show mean ± SE total lateral root length (mm), (b) total number of lateral roots, and (c) lateral root density calculated by dividing the number of lateral roots by primary root length. No significant differences were found using a one-way ANOVA test.*

Gene expression of VAMP71 family members is modulated by salt stress.

Given that the *vamp71* mutants showed altered root system architecture (RSA) following salt stress treatment, the subsequent analysis sought to assess the salt-induced regulation of *VAMP71* gene expression. In wild-type Arabidopsis plants exposed to 150 mM of NaCl for up to 24 hours, all four *VAMP71* genes showed trends of increased expression, though *VAMP712* did not show statistical significance (Figure 3.7). The expression change peaked at 5 hours of salt stress for all but one. Interestingly, despite the *vamp713* mutants not having a different salt-induced RSA phenotype, *VAMP713* was upregulated most of the *VAMP71* gene family (Figure 3.7c).

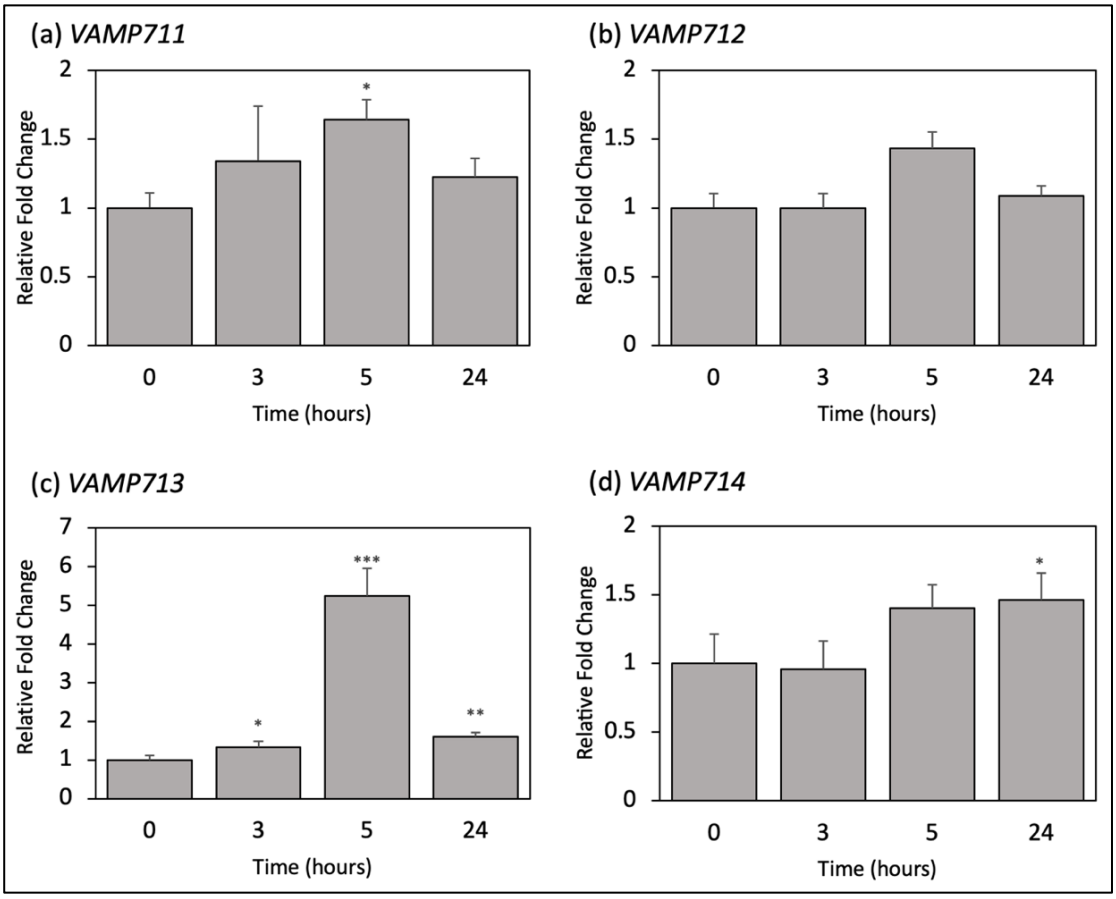

Figure 3.7: *Time-course of salt stress induced expression of VAMP71 family genes. Wild-type Arabidopsis (Col-0) seedlings were grown for 6dpg on ½ MS Agar + 1% sucrose growth medium, then transferred to media treated with 150 mM NaCl. RT-qPCR analysis of mRNA abundance was conducted for VAMP711 (a), VAMP712 (b), VAMP713 (c), and VAMP714 (d). All fold changes are relative to time point 0-hour without NaCl. Bars represent mean ± SD (n=3). One, two or three asterisks show significant differences between treated and control at * P<0.05, ** P<0.01, or *** P<0.001 according to Student's t-test.*

The salt-induced expression of *VAMP71* family genes in the various mutant backgrounds was tested to ascertain the possible level of redundancy between the gene family members (Figure 3.8). The *VAMP711* and *VAMP712* genes are upregulated following 5 hours of 150 mM NaCl treatment in the *vamp712* and *vamp713* backgrounds to a similar extent to wild-type plants (Figure 3.8a,b). Uniquely, the *vamp711* mutants did not show induced expression of *VAMP713* and *VAMP714*, and only a modest increase in *VAMP712* expression (Figure 3.8b,c,d). These results indicate that *VAMP711* is required for the salt-induced expression of *VAMP713* and *VAMP714*, and to some extent, *VAMP712*.

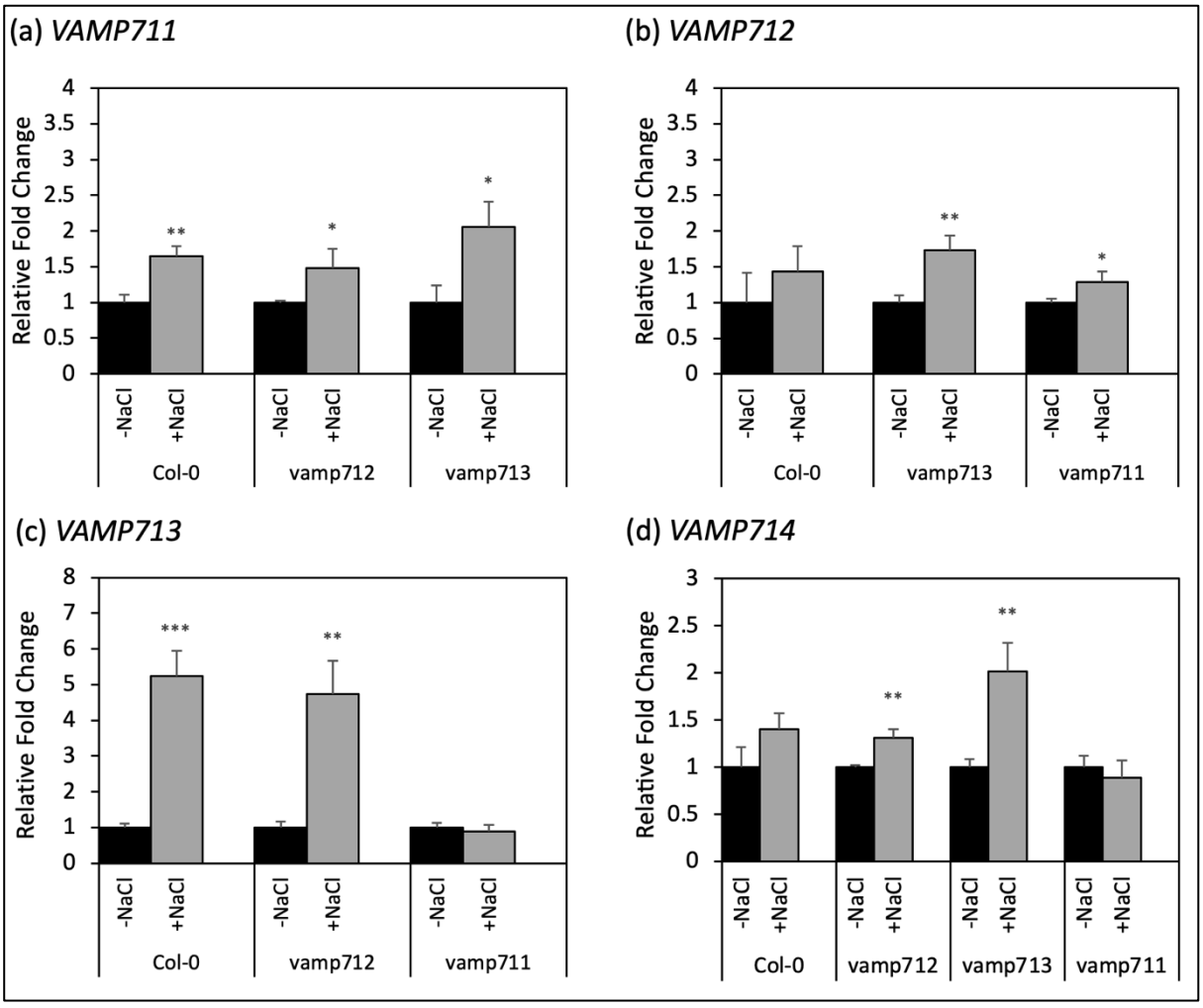

Figure 3.8: *VAMP71 gene expression is induced by salt stress in vamp71 loss of function mutants and wild-type. Wild-type (Col-0) and vamp711, vamp712, and vamp713 seedlings were grown for 6dpg on ½ MS Agar + 1% sucrose growth medium, then transferred to media treated with 150 mM NaCl for 5 hours. RT-qPCR analysis was conducted for VAMP711 (a), VAMP712 (b), VAMP713 (c), and VAMP714 (d). All fold changes are relative to the 0-hour timepoint without NaCl of the same genotype. Bars represent mean ± SD (n=3). One, two or three asterisks show significant differences between treated and control at * P<0.05, ** P<0.01, or *** P<0.001 according to Student's t-test.*

Chapter Summary:

- This research delved into the genotypic and phenotypic characteristics of *Arabidopsis* plants under salt stress conditions, focusing on the role of VAMP71 family members in root system architecture modifications.
- **Genotyping and Mutant Analysis**: Genotyping confirmed homozygous T-DNA insertion mutants for *VAMP712* and *VAMP713*, and a frameshift mutation in *VAMP711* was identified. Phenotyping showed significant differences in root growth among mutants under both normal and salt stress conditions.
- **Primary Root Growth**: Under normal conditions, *vamp713* mutants had the shortest primary roots, while *vamp711* mutants had the longest. Salt stress further inhibited root growth, with *vamp711* and *vamp712* mutants showing the largest reductions. Therefore, the absence of *VAMP71* was found to significantly impact the root system architecture of *Arabidopsis* plants, shedding light on the importance of vesicle trafficking in plant responses to salt stress.
- **Gene Expression Modulation**: Salt stress increased the expression of all *VAMP71* family genes, with *VAMP713* showing the highest upregulation. The expression of *VAMP71* genes in mutant backgrounds indicated potential redundancy and regulatory interactions among the family members.

Chapter 4: Signalling Events Mediated by *VAMP71* Family Genes Under Salt Stress

The VAMP71 family is required for the correct expression of auxin-regulated genes under salt stress conditions.

It is well-established that the phytohormone auxin is crucial for normal growth and development, especially for root growth and RSA, both under optimal and stressed conditions (Korver et al., 2018, Smolko et al., 2021). At high salt concentrations, major changes to the distribution and abundance of auxin occur, associated with disruption to auxin transporters (Shen et al., 2010, Sun et al., 2007). Therefore, we investigated the changes in gene expression of the auxin efflux carrier genes *PIN1* and *PIN2* following salt stress exposure. It was found that the expression of *PIN1* and *PIN2* was at the same level in the presence and absence of salt stress (Figure 4.1a,b). However, others have shown that these two genes are downregulated under salt stress conditions, each with slightly different experimental settings to those used in this project (Fu et al., 2019, Liu et al., 2015, Sun et al., 2007). In contrast, the *vamp712* seedlings showed significant upregulation of *PIN1* and *PIN2* following salt stress treatment, with 7.8-fold and 2.1-fold higher transcript abundance levels, respectively (Figure 4.1a,b). The *vamp711* mutants showed significant downregulation of both *PIN1* and *PIN2* as well as the auxin-induced genes *IAA1* and *IAA2* (encoding Indole-3-acetic acid-induced protein 1 and 2, respectively) under salt stress conditions (Figure 4.2a,b).

As for the other Arabidopsis genotypes, *IAA1* and *IAA2* expression showed mixed results. In *Arabidopsis thaliana*, the genes *IAA1* and *IAA2* encode Aux/IAA transcriptional repressor proteins, which are part of the auxin signalling pathway (Tiwari et al., 2004). Under normal growth conditions, these IAA proteins negatively regulate auxin-responsive gene expression by forming a complex with auxin response factors (ARFs), preventing their transcriptional activity (Luo et al., 2018). However, under salt stress conditions, the expression of *IAA1* and *IAA2* can be significantly altered. Because their expression is induced by auxin, the abundance of mRNA transcripts was measured over a time course of 24 hours following 150 mM NaCl treatment. The expression of *IAA1* was downregulated at

every time-point for wild-type and *vamp711* knockout mutants (Figure 4.2a). Conversely, expression of *IAA1* showed no statistically significant change in expression in *vamp712* mutants exposed to salt stress and *vamp713* knockout mutants have an acute significant upregulation effect after at 3 hours, then returned to untreated levels (Figure 4.2).

The expression of *IAA2* shows a rapid and transient increase *vamp713* mutants, whilst *vamp711* plants significantly repressed *IAA2* similarly to *IAA1* (Figure 4.2b). It was also observed that the expression level of *IAA2* in *vamp712* mutants was not affected by salt stress over the 24-hour period (Figure 4.2b). Although wild-type plants did not exhibit a statistically significant increase in *IAA2* expression, there was a marginal increase. These findings suggest that VAMP712 and VAMP713 are required to suppress *IAA1* and *IAA2* expression, while VAMP711 induces expression, and so modulates auxin responses, under salt stress. Therefore, the initial upregulation of *PIN* and *IAA* genes might be part of the plant's rapid response to stress and reprogramming of its growth and developmental processes.

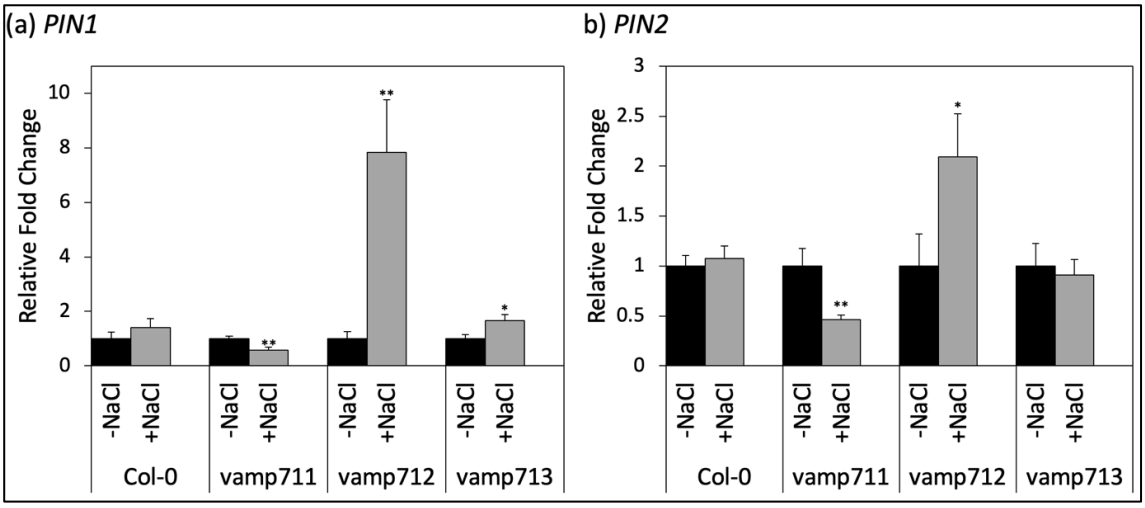

Figure 4.1: *Auxin-efflux carrier genes are differentially regulated in vamp71 mutants treated with NaCl. Wild-type (Col-0) and vamp711, vamp712, and vamp713 seedlings were grown for 6-dpg on ½ MS Agar + 1% sucrose growth medium, then transferred to media treated with 150 mM NaCl for 5 hours. RT-qPCR analysis was conducted for PIN1 (a) and PIN2 (b). All fold changes are relative to the 0-hour timepoint without NaCl of the same genotype. Bars represent mean ± SD (n=3). One, two or three asterisks show significant differences between treated and control at * P<0.05, ** P<0.01, or *** P<0.001 according to Student's t-test.*

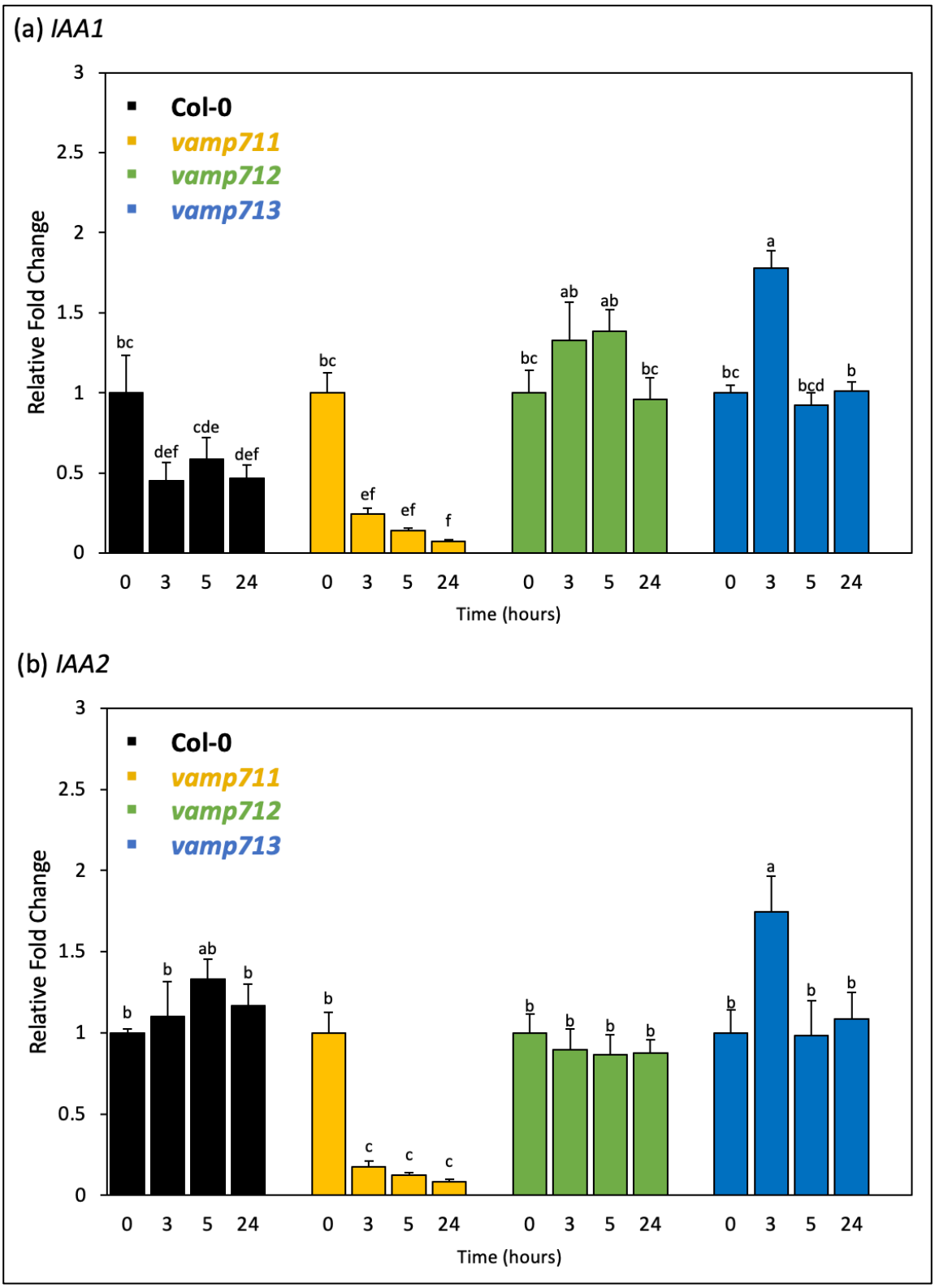

Figure 4.2: *Auxin-induced IAA genes are differentially regulated in vamp71 mutants treated with NaCl. Wild-type (Col-0) (black) and vamp711 (yellow), vamp712 (green), and vamp713 (blue) seedlings were grown for 6-dpg on ½ MS agar + 1% sucrose growth medium, then transferred to media treated with 150 mM NaCl for 3-, 5- and 24-hours. RT-qPCR analysis was conducted for IAA1 (a) and IAA2 (b). All fold changes are relative to the 0-hour timepoint without NaCl of the same genotype. Bars represent mean ± SD (n=3). Bars with the same letter represents no statistically significant difference according to two-way ANOVA with Tukey-HSD test.*

The expression of *PIN* and *IAA* genes is affected by the expression of VAMP71 proteins in 6-day-old seedlings grown in unstressed conditions. The *vamp711* mutants have the most considerable disruption, with the transcript levels of *PIN1, IAA1* and *IAA2* significantly increasing over Col-0 wild-type plants and the other *vamp71* mutants (Figure 4.3a,c,d), indicative of a suppressive role for VAMP711 on the expression of these genes. Conversely, *vamp712* and *vamp713* insertional mutants did not show significantly different abundances of these gene transcripts compared to the wild type, suggesting no role in promoting expression. However, *PIN2* expression was significantly decreased in *vamp711* and *vamp712* mutants compared to wild type plants indicating they are required for its normal expression level (Figure 4.3b).

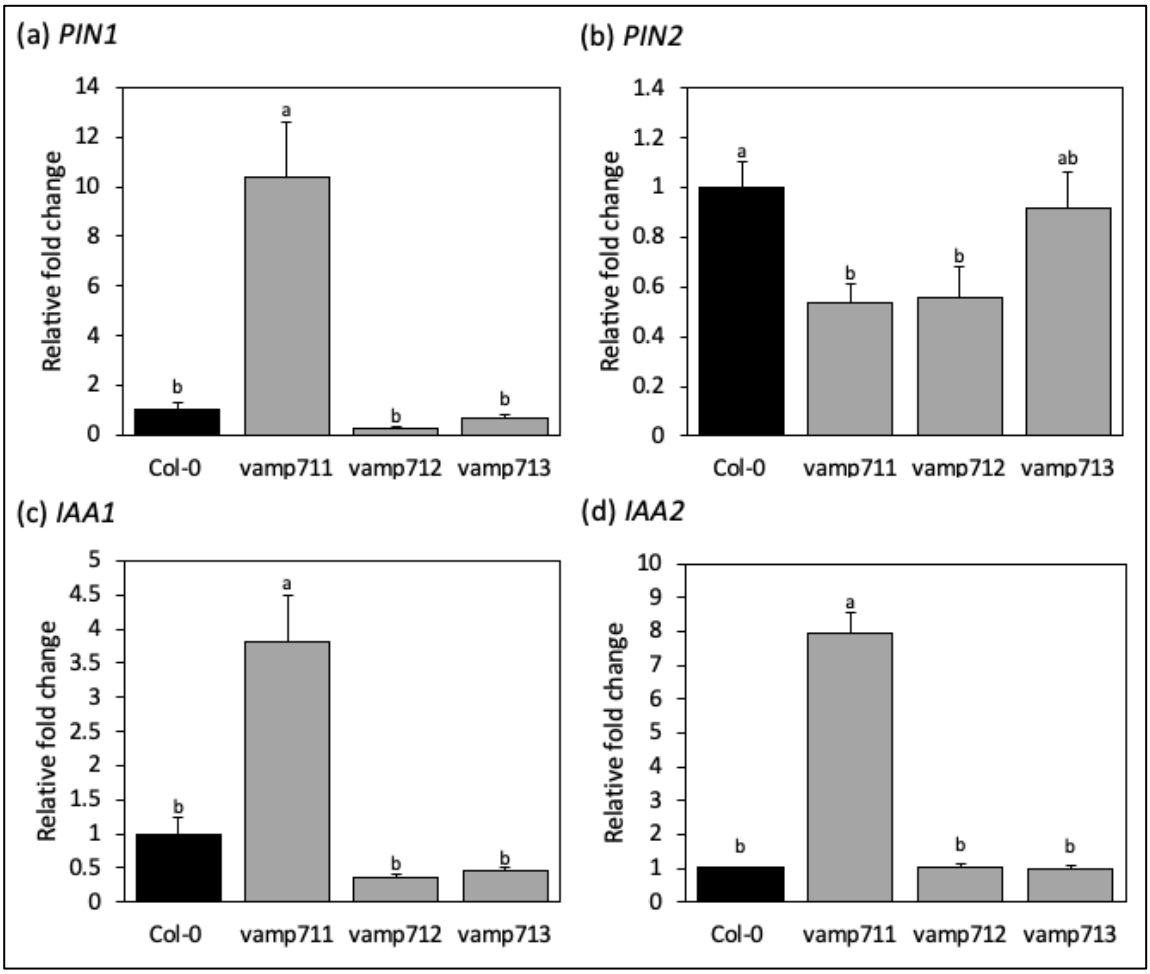

Figure 4.3: *PIN and IAA genes are differentially regulated in vamp71 mutants under optimal conditions. Wild-type (Col-0) and vamp711, vamp712, vamp713 seedlings were grown for 6dpg on ½ MS agar + 1% sucrose growth medium. RT-qPCR analysis was conducted for PIN1 (a), PIN2 (b), IAA1 (c) and IAA2 (d). Fold changes are relative to Col-0. Bars represent mean ± SD (n=3). Bars with the same letter represents no statistically significant difference according to one-way ANOVA with Tukey-HSD test.*

Genes involved in the auxin degradation pathway show VAMP71-dependent expression patterns

The conjugation of auxin via members of the GH3 protein family is an essential component in the auxin-degradation pathway. Group II GH3 enzymes (GH3.1-6, GH3.9, and GH3.17) dynamically adjust IAA concentrations by catalysing the conjugation of IAA to various amino acids, forming indole-3-acetic acid-amino acid conjugate (IAA-aa) which is an inactive form of IAA (Staswick et al., 2005, Chen et al., 2010). It is known that auxin upregulates the expression of *GH3* genes, resulting in a negative feedback loop on intracellular auxin levels; thus, the GH3s have been hypothesised to have a role in auxin homeostasis (Mellor et al., 2016). As negative regulators of auxin signalling, we investigated the dynamic response of these genes following salt stress using the same time course as before. Wild-type and each of the transgenic lines showed a rapid increase in the expression of *GH3.1* and *GH3.3* to various degrees (Figure 4.4). The *vamp712* and *vamp713* knockout mutants significantly upregulate the *GH3* genes and stay upregulated for 5-hours. In comparison, the wild-type plants exhibit a transient increase in expression for *GH3.1* (Figure 4.4b). The *vamp711* mutants only marginally increased transcript abundance of these genes which was not statistically significant over the zero-hour control (Figure 4.4).

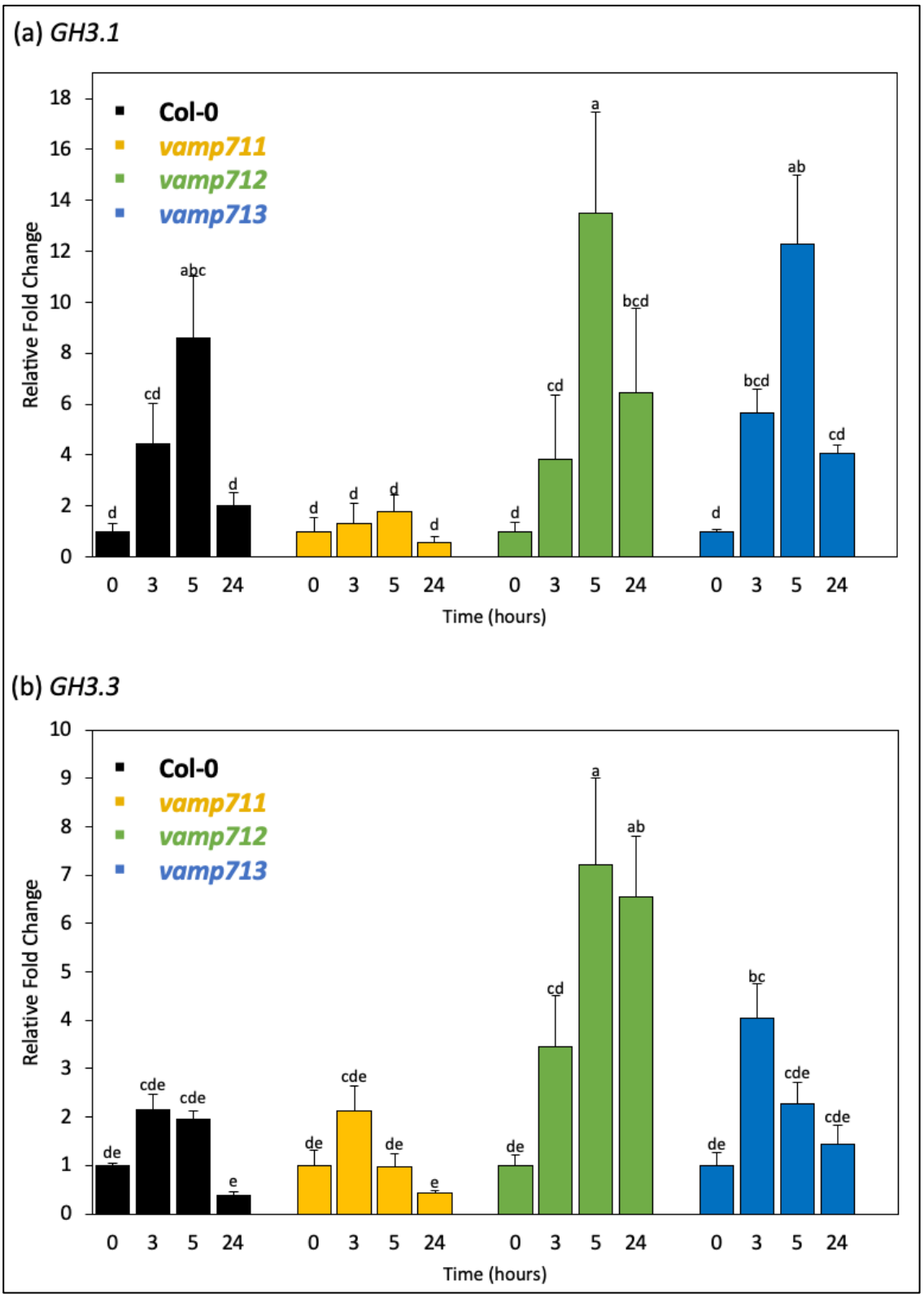

Figure 4.4: *Auxin-induced* GH3 *genes are differentially regulated in* vamp71 *mutants treated with NaCl. Wild-type (Col-0) (black) and vamp711 (yellow), vamp712 (green), and vamp713 (blue) seedlings were grown for 6 dpg on ½ MS agar + 1% sucrose growth medium, then transferred to media treated with 150 mM NaCl for 3, 5 and 24 hours. RT-qPCR analysis was conducted for GH3.1 (a) and GH3.3 (b). All fold changes are relative to the 0-hour timepoint without NaCl of the same genotype. Bars represent mean ± SD (n=3). Bars with the same letter represents no statistically significant difference according to two-way ANOVA with Tukey-HSD test.*

The *vamp712* and *vamp713* insertional mutants grown under optimal growth conditions have a significantly reduced abundance of transcripts for both *GH3* genes compared to Col-0 plants (Figure 4.5). Combined with evidence for the lower expression of *IAA1* in these two transgenic lines, we can hypothesise that these mutants have a lower basal level of auxin than wild-type and the *vamp711* plants. This lower basal expression level might also explain the significant upregulation of these genes observed under salt stress conditions (Figure 4.4).

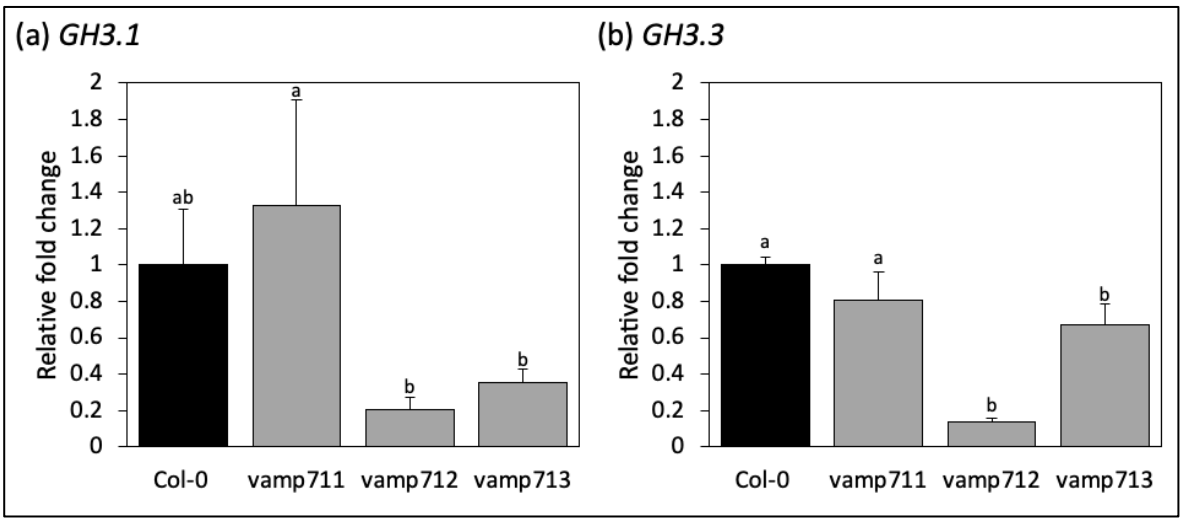

Figure 4.5*: Auxin-induced GH3 genes are differentially regulated in vamp71. Wild-type (Col-0), vamp711, vamp712, and vamp713 seedlings were grown for 6 dpg on ½ MS agar + 1% sucrose growth medium. RT-qPCR analysis was conducted for GH3.1 (a) and GH3.3 (b). Fold changes are relative to Col-0. Bars represent mean ± SD (n=3). Bars with the same letter represents no statistically significant difference according to one-way ANOVA with Tukey-HSD test.*

Root measurements of seedlings treated with IAA and NPA

The gene expression analysis presented so far has provided evidence pointing to the role of specific *VAMP71* family genes in regulating auxin-related genes under salt stress. These changes are expected to contribute to the observed differences in RSA between the *vamp71* knockout plants and wild-type plants exposed to prolonged salt stress. Therefore, we set out to investigate root growth changes in these plants exposed to exogenous application of indole-3-acetic acid (IAA) and the polar auxin transport inhibitor *N*-1-naphthylphthalamic acid (NPA).

Without salt stress, the presence of IAA did not significantly inhibit primary root growth of the *vamp71* mutants compared to wild type, though the mean primary root length was

lower in *vamp711* and *vamp712* mutants (Figure 4.6a). With the combined treatment of IAA and salt stress, *vamp711* seedlings had significantly less primary root growth than Col-0 and *vamp712* transgenic lines (Figure 4.6b).

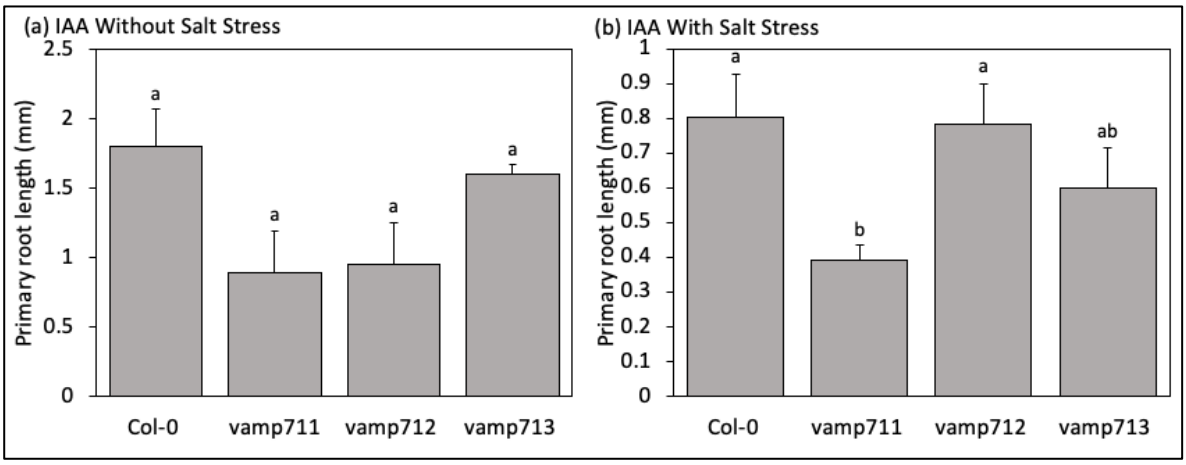

Figure 4.6: *Primary root length growth after four days of exposure to 0.5μM IAA, with and without 150 mM NaCl. Seedlings were germinated on normal ½ MS agar medium and transferred six days after gemination to media containing 0.5 μM IAA with and without salt stress. (a) Bars show mean ± SE primary root growth (mm) without salt stress. (b) Bars show mean ± SE primary root growth (mm) with salt stress. Data was analysed using a one-way ANOVA with Tukey-HSD post-hoc test. Bars with the same letter represents no statistically significant difference.*

In contrast, there was no statistically significant difference between the plant genotypes grown under non-stress conditions with the supplementation of 1μM NPA (Figure 4.7a). In the presence of NPA plus salt stress, all three *vamp71* transgenic lines had decreased primary root growth compared with wild-type Col-0 plants, though no statistical significance was shown between the genotypes (Figure 4.7b).

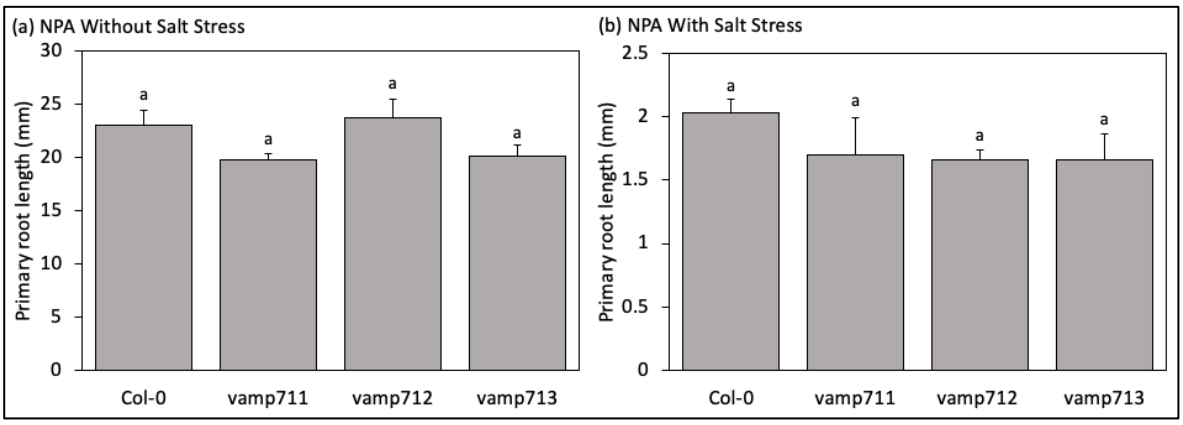

Figure 4.7: *Primary root length growth after four days of exposure to 1 μM NPA, with and without 150 mM NaCl. Seedlings were germinated on normal ½ MS agar medium and transferred six days after gemination to media containing 1 μM NPA with and without salt stress. (a) Bars show mean ± SE primary root growth (mm) without salt stress. (b) Bars show mean ± SE primary root growth (mm) with salt stress. Data was analysed using a one-way ANOVA followed by pairwise t-test. Asterisk represents a significant difference between indicated genotypes at P<0.05, n=6 for each genotype.*

Also investigated were the effects of exogenous application of IAA on the development of lateral roots with and without the presence of salt stress. When exposed to IAA treatment on its own, there were more statistically significant differences than when salt stress was also present (Figure 4.8). The total lateral root length was greatest in wild-type plants, which was significantly different to *vamp711* and *vamp713* knockout plants according to one-way ANOVA and Tukey-HSD test (Figure 4.8a). Salt stress and IAA treatment dissipated these differences (Figure 4.8b). This probably reflects the dominant inhibitory effect that a high level of salt stress has on root growth. This was also the case for the number of observed lateral roots. With IAA alone, all three *vamp71* transgenic plants had significantly fewer lateral roots than wild-type plants, whereas the combination of IAA and salt stress showed no significant differences (Figure 4.8c,d).

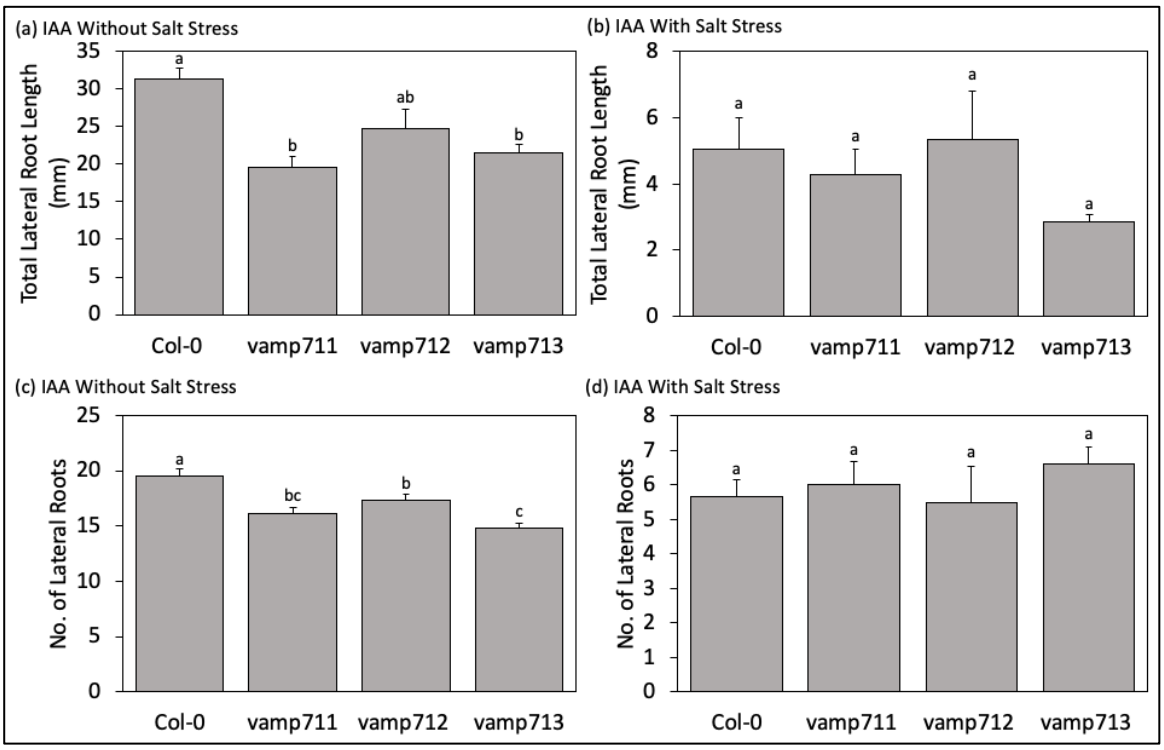

Figure 4.8: *Total lateral root length growth and frequency of lateral roots grown in seedlings following four days of exposure to 0.5 μM IAA, with and without 150 mM NaCl treatment. Seedlings were germinated on normal ½ MS agar medium and grown for six days before transfer to media containing 0.5 μM IAA with and without salt stress. (a) Sum of lateral root lengths without salt stress, bars show mean ± SE (mm). (b) Likewise, with the additional presence of salt stress. (c) Number of lateral roots without salt stress, bars show mean ± SE. (d) Same measurements of plants grown under salt stress conditions. In each case, statistically significant differences were determined using a one-way ANOVA and Tukey-HSD post-hoc test, n=6. Bars with same letter are not statistically different.*

The exogenous application of NPA on wild-type and *vamp71* knockout mutant plants with and without salt stress revealed a significant effect on lateral root development. First, it was observed that NPA treatment alone did not significantly alter the total lateral root length between Col-0, *vamp711* or *vamp713* (Figure 4.9a). However, *vamp712* plants had, on average, 2.7-fold increased lateral root length than wild-type plants and was significantly greater than all other plant genotypes according to one-way ANOVA and Tukey-HSD test (Figure 4.9a). Furthermore, significantly more lateral roots were counted in *vamp712* and *vamp713* than in Col-0 and *vamp711* plants (Figure 4.9c). This data suggests that *vamp712* and, to a lesser extent, *vamp713* seedlings are less sensitive to the auxin transport inhibitory effects of NPA. Therefore, these mutant lines were expected to have more lateral root growth and frequency than Col-0 under the same parameters with the added presence of salt stress. However, the opposite trend was observed. Wild-type Col-0 plants exposed to the combination of NPA and salt stress tended to have

significantly greater lateral root length and number than *vamp712* and *vamp713* seedlings (Figure 4.9b,d). Here, *vamp711* plants also had fewer lateral roots and shorter lengths than Col-0, though not statistically significant.

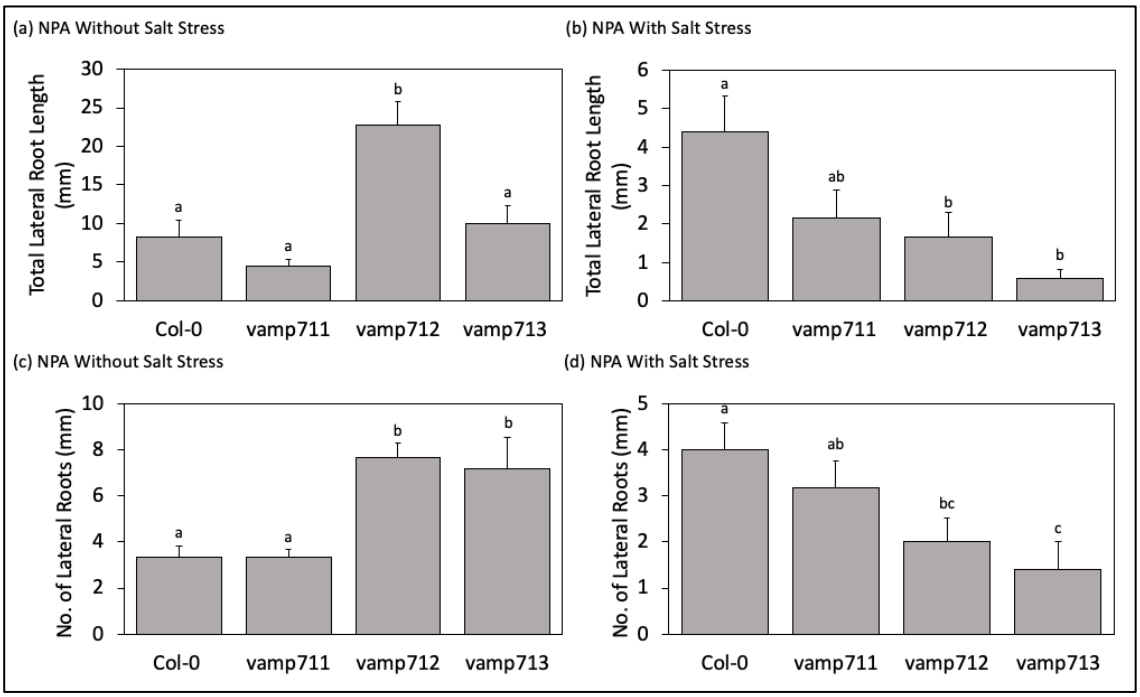

Figure 4.9: *Total lateral root length growth and number of lateral roots grown in seedlings following four days of exposure to 1 μM NPA, with and without 150 mM NaCl treatment. Seedlings were germinated on normal ½ MS agar medium and grown for six days before transfer to media containing 1 μM NPA with and without salt stress. (a) Sum of lateral root lengths without salt stress, bars show mean ± SE (mm). (b) Likewise, with the additional presence of salt stress. (c) Number of lateral roots without salt stress, bars show mean ± SE. (d) Same measurements of plants grown under salt stress conditions. In each case, statistically significant differences were determined using a one-way ANOVA and Tukey-HSD post-hoc test, n=6. Bars with same letter are not statistically different.*

Expression of ion transporter genes involved in the salt stress response.

To withstand the effects of high salinity on plants, it is also important to investigate the mechanisms plants use to modulate the disturbed Na^+ and K^+ homeostasis at cellular and molecular levels. Upon plant exposure to NaCl, Na^+ ions taken up by the roots are translocated to the transpiring leaves, where they can accumulate to toxic levels. In the leaves, Na^+ builds up in cell walls and cytoplasm, eventually leading to cell death since these two compartments are of limited volume (Munns, 1993).

To delay the time at which Na^+ reaches toxic levels in these compartments, and therefore improve salt stress tolerance, is dependent on ion transporters that can either sequester excess Na^+ in vacuoles or efficiently recirculate Na^+ from shoots to the roots via the

phloem sap (Kong et al., 2011, Berthomieu et al., 2003, Munns, 2002). This recirculation has been hypothesised because leaf vacuolar Na^+ sequestration ability is poor and is probably the primary mechanism involved in preventing Na^+ delivery to leaf cells in most salt-sensitive plants (Berthomieu et al., 2003).

Members of the VAMP71 family may be involved in the vesicle trafficking and localisation of certain ion transporters. *HKT1* (*HIGH-AFFINITY K^+ TRANSPORTER 1*) is a gene that encodes a sodium (Na^+)-specific ion transporter in plants. Its role in salt stress is primarily associated with regulating the transport of sodium ions within plant tissues, especially in the roots (Berthomieu et al., 2003). Similarly, *NHX1* (*Na^+/H^+ ANTIPORTER 1*) is a gene that encodes a protein known as a Na^+/H^+ antiporter in plants. The role of NHX1 in salt stress is to help plants maintain ion homeostasis and regulate the balance of Na^+ and protons (H^+) within cells by sequestering Na^+ into vacuoles (Shi and Zhu, 2002). The expression of *HKT1* and *NHX1* is, therefore, an important component of the plant salt stress response needed to maintain ion homeostasis and reduce the ion toxicity effects caused by salt conditions.

First, the basal transcript abundance of these genes in the *vamp71* knockout mutants with wild-type Col-0 plants grown in optimal (no salt stress) conditions was compared. Interestingly, the transcript abundance of *HKT1* in *vamp712* and *vamp713* was significantly lower than in wild-type, suggesting VAMP712 and VAMP713 are required for the expression of these transporter genes; and in *vamp711* mutants, the expression of *NHX1* was significantly increased over the other genotypes, suggesting a role for VAMP711 in suppressing *NHX1* (Figure 4.10a,b).

In response to salt stress (150 mM), *HKT1* is downregulated similarly across all the plant lines, though not until 5 hours for *vamp712* and *vamp713* (Figure 4.10c). This delay may be explained by the lower basal transcript abundance in these two transgenic lines. In contrast, the expression of *NHX1* was initially upregulated in all four plant lines, with *vamp713* exhibiting the most intense increase at 3 hours after exposure to salt stress (Figure 4.10d).

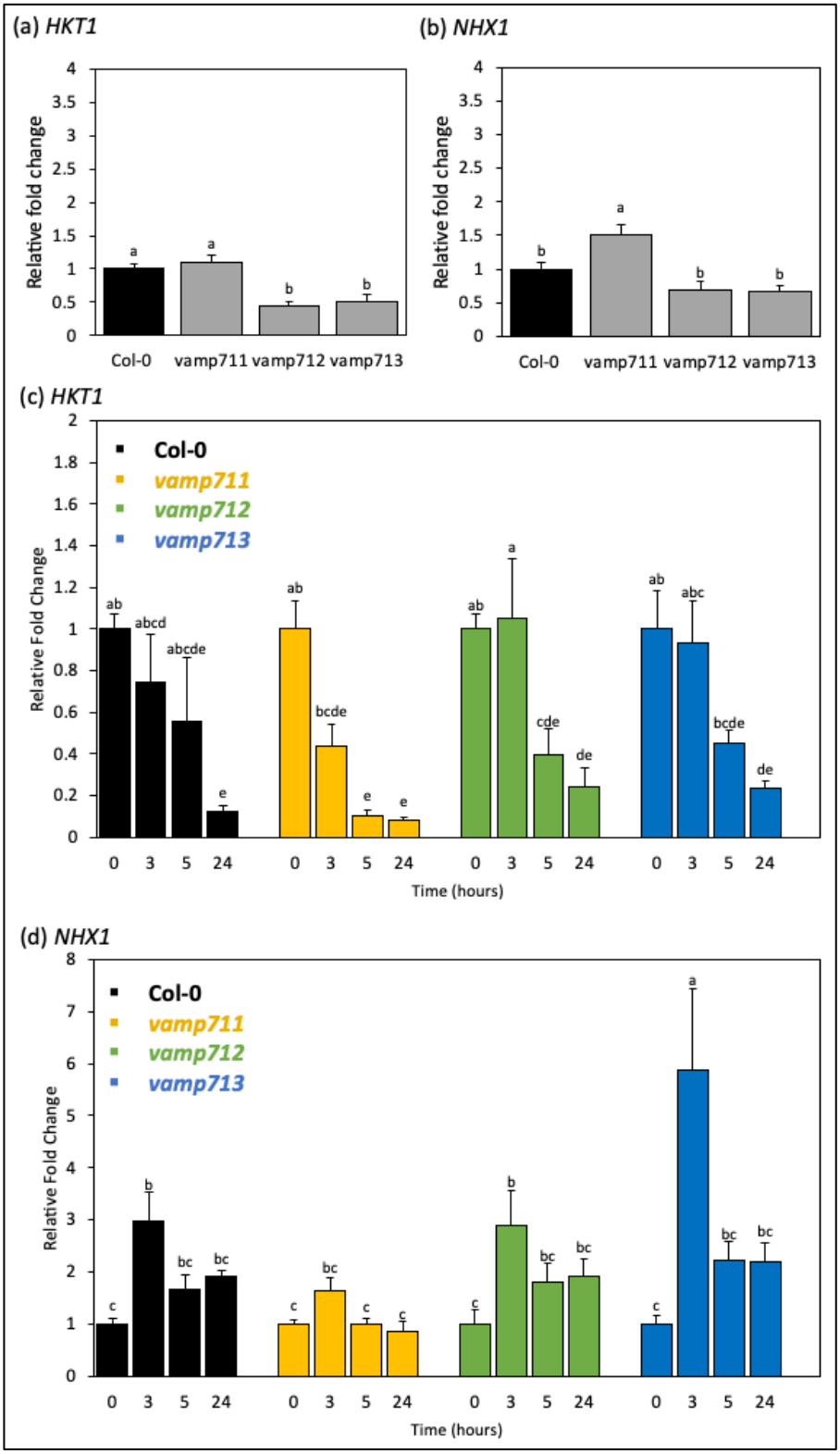

Figure 4.10: *Ion transporter expression in response to salt stress. Wild-type (Col-0), vamp711, vamp712, and vamp713 seedlings were grown for 6 dpg on normal growth medium, then analysed using RT-qPCR for HKT1 (a) and NHX1 (b). Fold-changes are relative to the expression in Col-0. Seedlngs were transferred to media containing 150 mM NaCl for 3, 5 and 24 hours. RT-qPCR analysis was conducted for HKT1 (c) and NHX1 (d). Here, fold changes are relative to the 0h timepoint for each genotype. Bars represent mean ± SD (n=3). Those with the same letter represents no statistically significant difference according to two-way ANOVA with Tukey-HSD test.*

Genes associated with ROS are differentially regulated under salt stress in *vamp71* mutant plants.

To assess whether the *vamp71* mutants exhibit changes in genes associated with ROS generation, gene expression analysis was used to investigate three such genes. The first of these genes encodes the enzyme ASCORBATE PEROXIDASE 2 (APX2), which has a crucial role in detoxifying ROS that accumulates during various stress conditions (Raja et al., 2017). Under salt stress, plants often experience an increase in ROS production, leading to oxidative stress. APX2 catalyses the conversion of hydrogen peroxide (H_2O_2) to water, using ascorbic acid as a specific electron donor (Hong et al., 2018). The gene expression of *APX2* following exposure to 150 mM of salt stress showed increased expression in all plant genotypes, with a peak at 3-hours (Figure 4.11). Although the same pattern of expression was observed, there was no significant difference in expression over time for Col-0 plants (Figure 4.11). The fold-change in the *vamp71* mutants was exponentially higher, particularly for *vamp712* and *vamp713*, which increased over 20-fold compared to the zero-hour control (Figure 4.11).

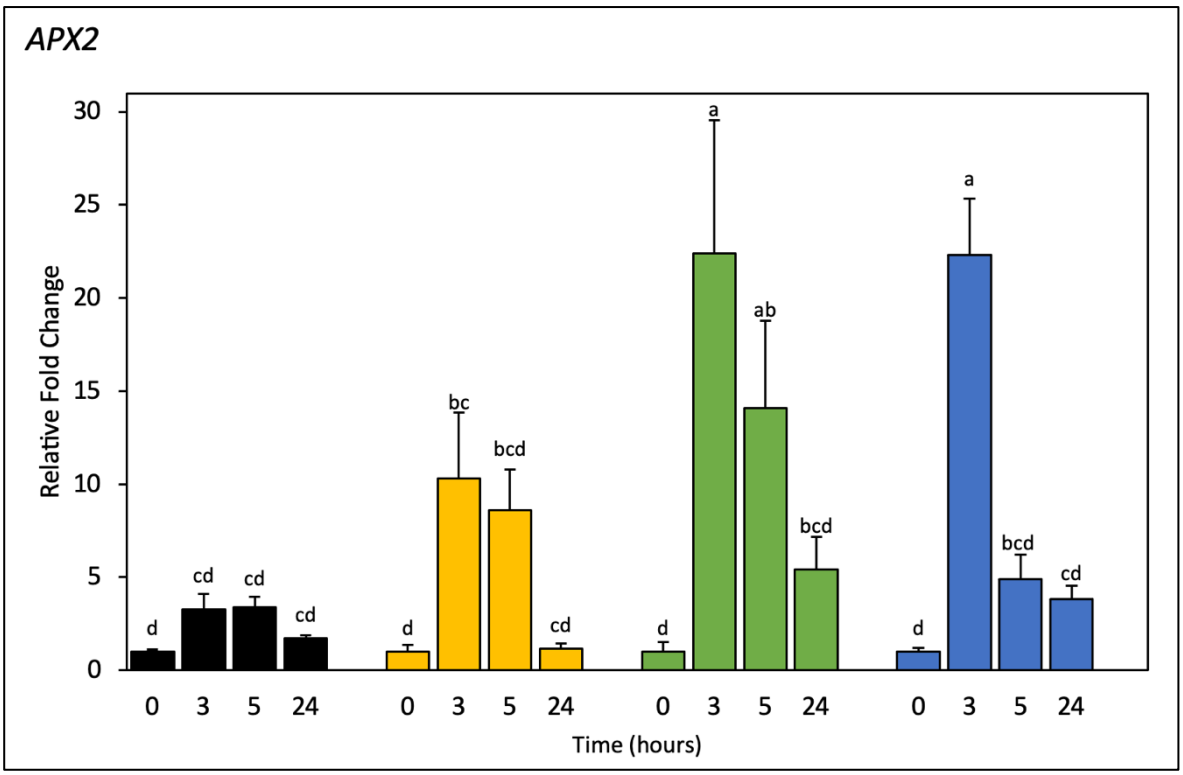

Figure 4.11: *ROS detoxification gene APX2 in response to salt stress. Wild-type (Col-0) (black), vamp711 (yellow), vamp712 (green), and vamp713 (blue) seedlings were grown for 6 dpg on ½ MS agar + 1% sucrose growth medium, then transferred to medium containing 150 mM NaCl for 3, 5 and 24 hours. RT-qPCR analysis was conducted for the APX2 gene. All fold changes are relative to the 0-hour timepoint without NaCl of the same genotype. Bars represent mean ± SD (n=3). Those with the same letter represents no statistically significant difference according to two-way ANOVA with Tukey-HSD test.*

Another critical antioxidant enzyme involved in the detoxification of H_2O_2 is CATALASE1 (CAT1). The role of CAT1 in salt stress is primarily associated with its function in protecting plant cells from oxidative damage caused by the accumulation of hydrogen peroxide under high salinity conditions. Different to *APX2* expression under salt stress, wild-type *Arabidopsis* seedlings showed no significant change in relative transcript abundance of *CAT1* following salt stress, and even showed a slight decrease (Figure 4.12). Similarly, *vamp711* mutants showed a decrease at 3-hours and 24-hours following treatment, whilst the *vamp712* and *vamp713* mutants showed a general increase in expression (Figure 4.12). The two-way ANOVA statistical analysis revealed no within genotype differences in expression, though significant differences were found between genotypes. The upregulation of both *APX2* and *CAT1* suggests ROS accumulation is higher in these plants, which may reflect either enhanced sensitivity to prolonged salt stress or alternatively, prime them for improved resilience to salt stress. Measurement of ROS levels may allow discrimination between these opposing possibilities.

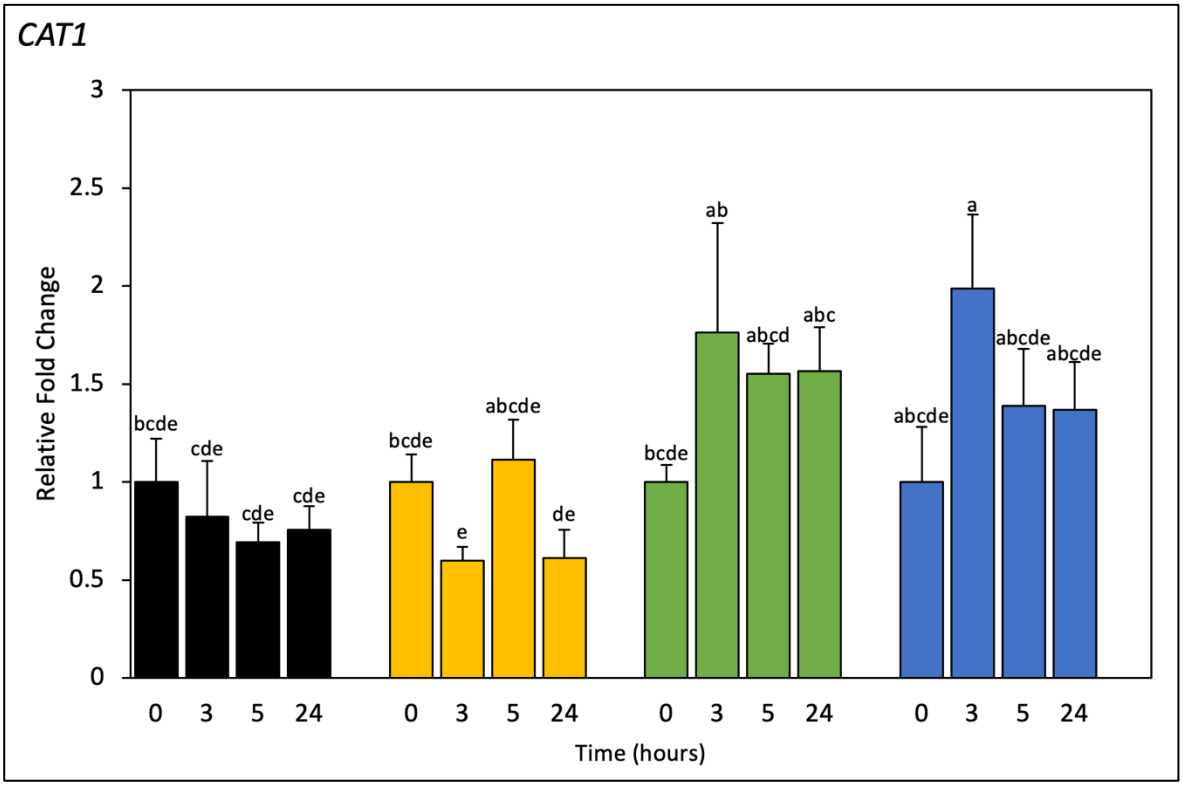

Figure 4.12: *ROS detoxification gene CAT1 in response to salt stress. Wild-type (Col-0) (black), vamp711 (yellow), vamp712 (green), and vamp713 (blue) seedlings were grown for 6 dpg on ½ MS Agar + 1% sucrose growth medium, then transferred to medium containing 150 mM NaCl for 3, 5 and 24 hours. RT-qPCR analysis was conducted for the CAT1 gene. All fold changes are relative to the 0-hour timepoint without NaCl of the same genotype. Bars represent mean ± SD (n=3). Those with the same letter represents no statistically significant difference according to two-way ANOVA with Tukey-HSD test.*

Lastly, the *GLUTATHIONE S-TRANSFERASE 1* (*GST1*) gene was analysed for its role in neutralizing ROS by catalysing the conjugation of glutathione to ROS and other oxidised molecules. The expression of this gene was significantly increased following salt stress exposure in all genotypes after 24 hours, which showed similar time-dependent trends (Figure 4.13). The upregulation of *GST1* expression is a typical response observed in plants exposed to salt stress (Dinler et al., 2014). Unlike the other two ROS detoxifying enzymes, the regulation of *GST1* expression does not appear to depend on the expression of the three individual *VAMP71* genes during salt stress.

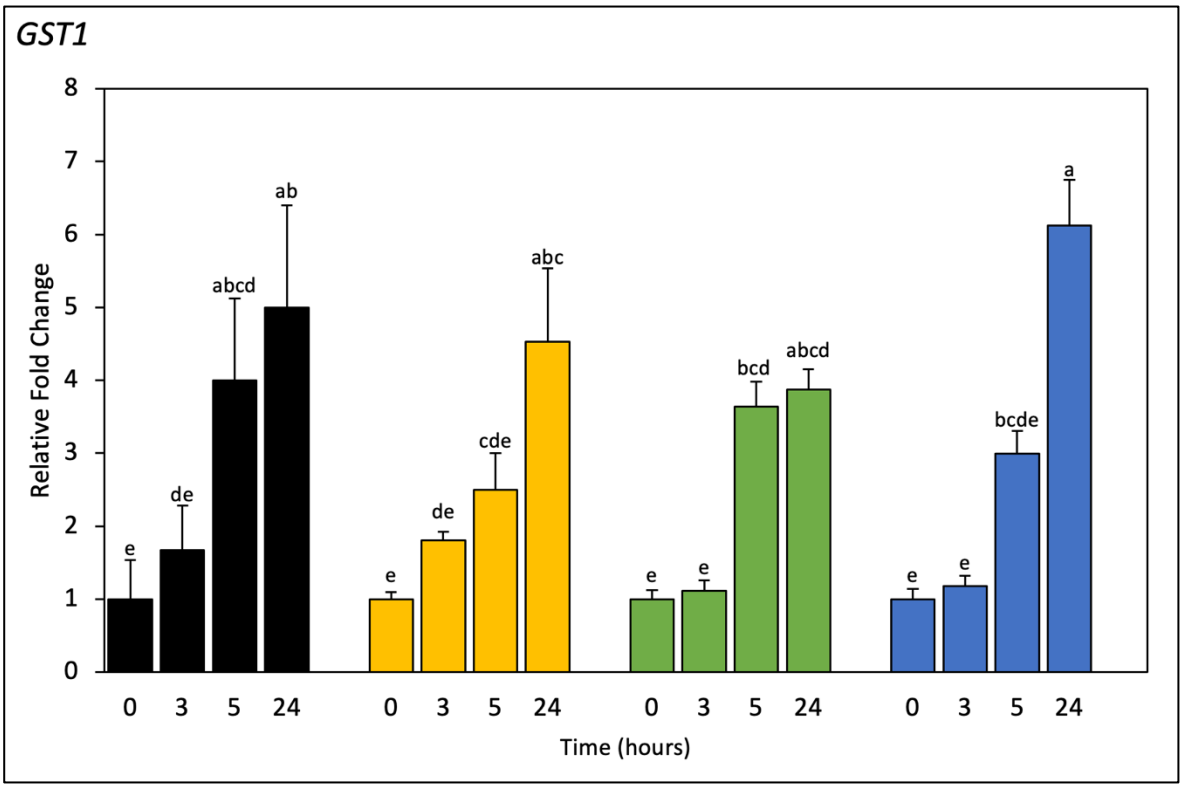

Figure 4.13: *Gene expression analysis of GST1 following salt stress treatment. Wild-type (Col-0) (black), vamp711 (yellow), vamp712 (green), and vamp713 (blue) seedlings were grown for 6 dpg on ½ MS Agar + 1% sucrose growth medium, then transferred to medium containing 150 mM NaCl for 3, 5 and 24 hours. RT-qPCR analysis was conducted for the GST1 gene. All fold changes are relative to the 0-hour timepoint without NaCl of the same genotype. Bars represent mean ± SD (n=3). Those with the same letter represents no statistically significant difference according to two-way ANOVA with Tukey-HSD test.*

Confocal imaging of *ProDR5::GFP* reveals changes in auxin levels at the root tip in response salt stress

The data presented thus far has shown that root growth is inhibited by salt stress and that knocking out the expression of *VAMP71* family members exacerbates this inhibition, except for *vamp713*. The data also established that genes involved in auxin biosynthesis, transport and signalling show differential expression patterns in response to salt stress with

a high degree of variability across the *vamp71* single knockout mutants and in comparison with wild-type Col-0 plants. The upregulation of key genes involved in the ROS antioxidant system also indicated that the oxidative effects of salt stress had affected the plants after 24 hours of salt exposure. Therefore, confocal imaging techniques were used to ascertain further a role for VAMP712 and VAMP713 in auxin response pathways with and without salt stress. The reporter line *ProDR5::GFP* allowed us to qualitatively examine changes in auxin at the root tip following exposure to salt stress (100mM and 150mM) for 48 hours. The DR5 promoter is auxin-responsive and fused to a green fluorescent protein (GFP), making it an effective method for visualising auxin distribution with confocal microscopy (Sabatini et al., 1999). Seedlings were removed from plates, stained with PFA, cleared with ClearSee, treated with Calcofluor-White, and washed with ClearSee before imaging (See Methods 2.4). The *ProDR5::GFP* in Col-0 background revealed that the fluorescence intensity visually decreased with increasing levels of salt stress (Figure 4.14). It was also restricted to the QC and columella root cap, whereas without salt, the GFP signal is fluorescent in the stele cells (Figure 4.14).

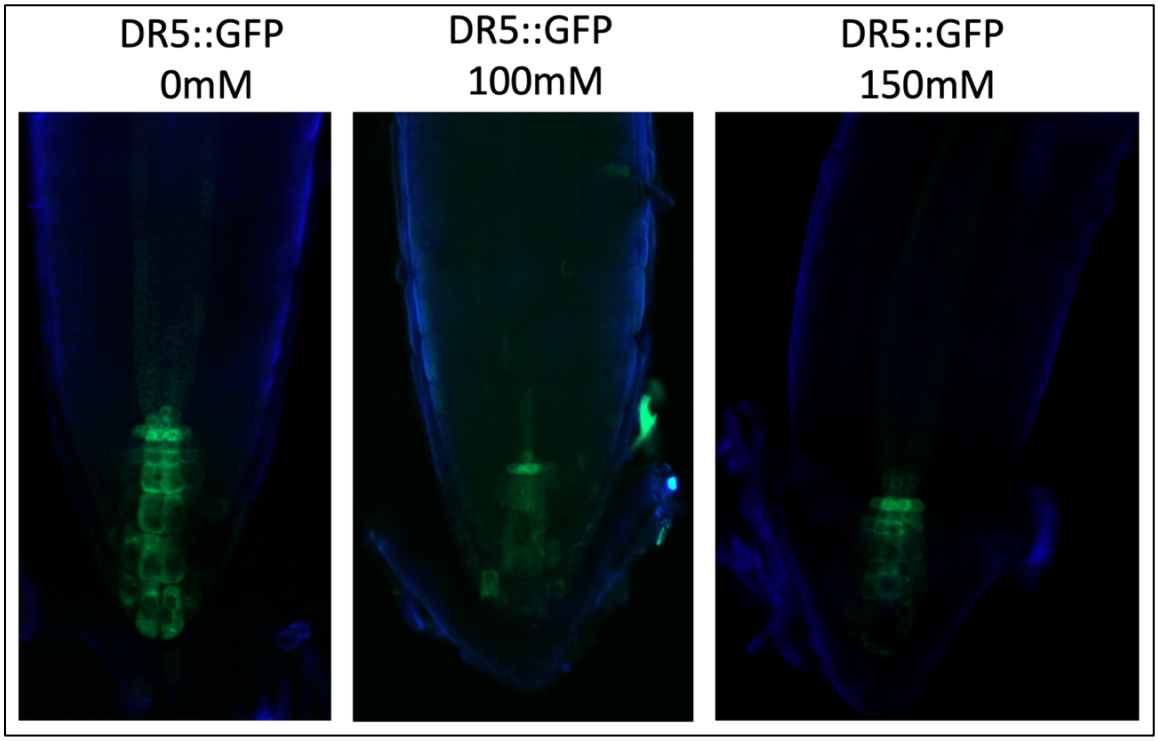

Figure 4.14: *Laser scanning confocal imaging of DR5::GFP. Seedlings were germinated on ½ MS agar, transferred to salt-treated media 5 days after germination, and grown for a further 48 hours. For comparison, control seedlings were transferred to plates not containing salt. Root tips were imaged with a Zeiss LSCM 800.*

Confocal imaging was also conducted with DR5::GFP crossed into the *vamp712* and *vamp713* mutant backgrounds, respectively. These lines allow us to visualise what changes to auxin abundance and distribution occur in the loss of function of these two VAMP71 protein family members, with and without salt stress. In untreated *vamp712* x DR5::GFP plants, the fluorescence pattern was asymmetrically observed in the lateral root cap and not apparent in the stele cells (Figure 4.15). This accumulation of auxin on one side of the root tip was shown in two of the three replicates for this transgenic line and was not specific to a particular side. This might explain the 'zig-zag' root growth phenotype observed in young *vamp712* seedlings (Figure 3.5). Following salt stress treatment, the fluorescent cells become restricted to the QC in a similar way to DR5::GFP in Col-0 background, though they have an apparent increase in fluorescence signal intensity. Under control conditions, DR5::GFP in the *vamp713* background shows a more restricted fluorescence pattern than DR5::GFP in the Col-0 background and increased in intensity after treatment with 100 mM NaCl, which was not the case in the other two lines (Figure 4.15). At 150 mM NaCl concentration, the fluorescence is like that in the Col-0 background, though a stronger signal appears in the QC (Figure 4.15).

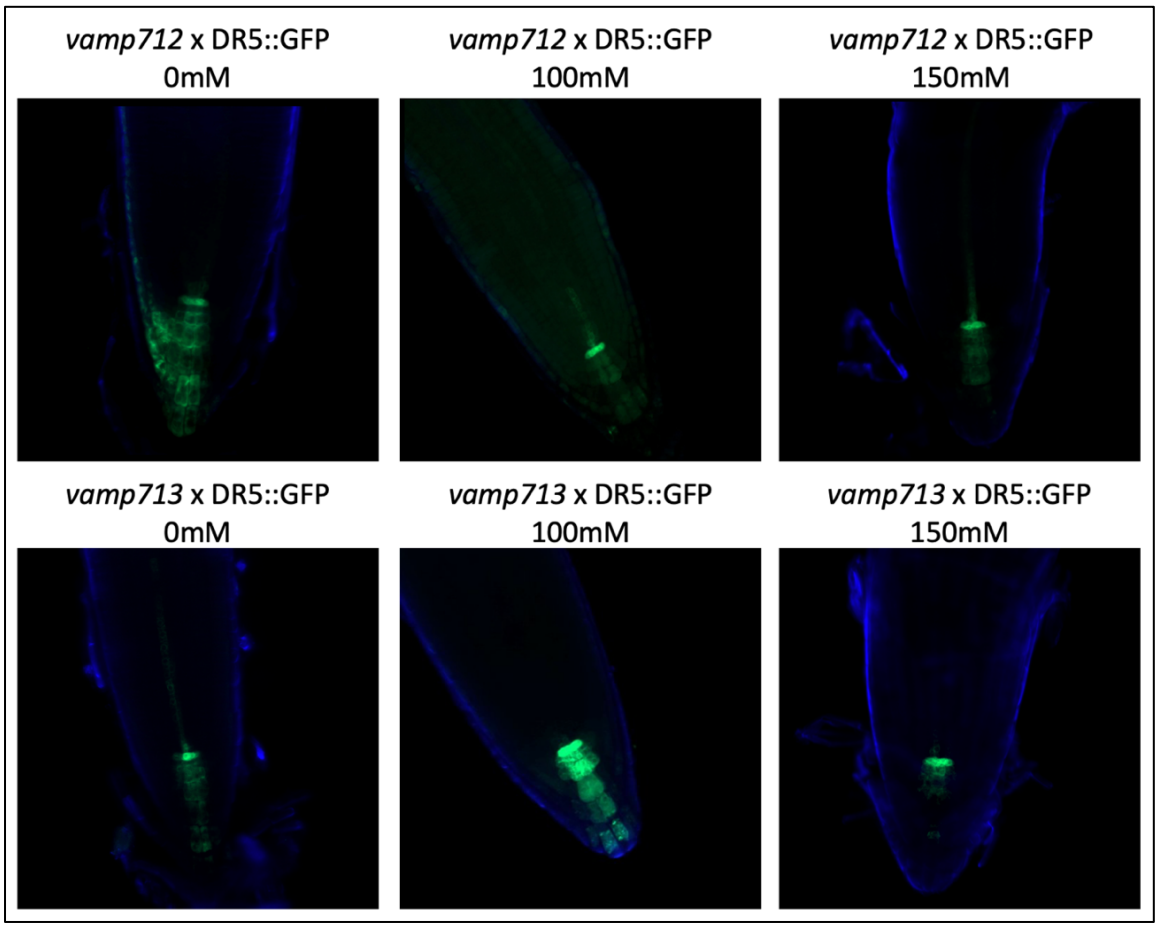

Figure 4.15: *Laser scanning confocal imaging of DR5::GFP in vamp712 mutant (top) and vamp713 mutant (bottom) backgrounds. Seedlings were germinated on ½ MS agar, transferred to salt-containing medium 5 days after germination, and grown for a further 48 hours. For comparison, control seedlings were transferred to plates not containing salt. Root tips were imaged with a Zeiss LSCM 800.*

Confocal imaging was also used to investigate the expression of VAMP713 protein in the root with and without salt stress treatment. The novel T-DNA insertion, *ProVAMP713::VAMP713:GFP*, was transferred 5 days after germination to a medium supplemented with NaCl (100mM and 150mM) and grown for a further 48 hours. At the root tip, the basal expression of VAMP713:GFP was barely detectable but was induced following salt stress and unexpectedly found in the QC (Figure 4.16).

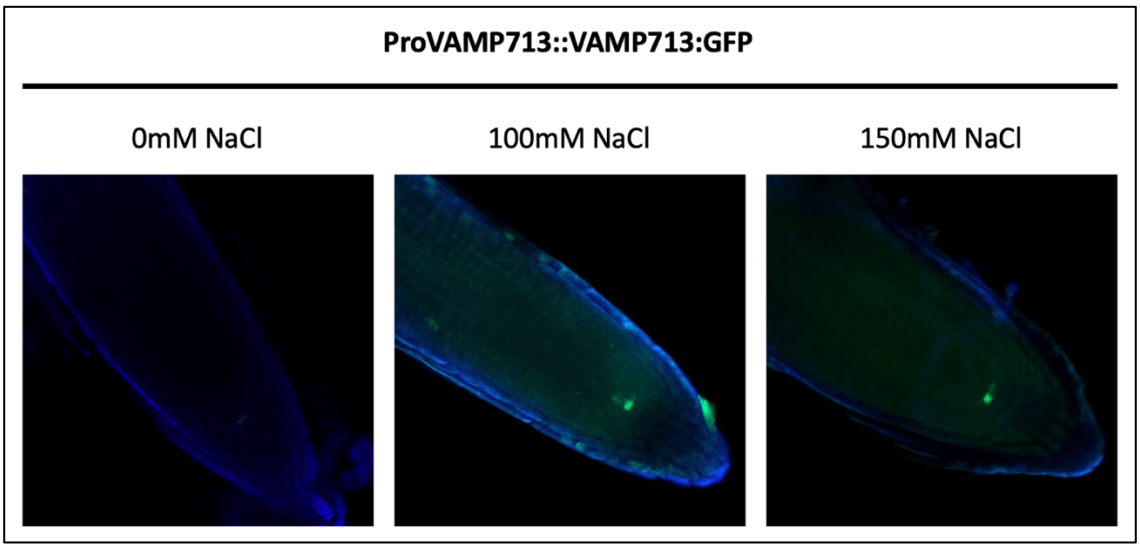

Figure 4.16: *Abundance of VAMP713:GFP at the root tip is induced by exposure to salt stress. Transgenic seedlings expressing ProVAMP713::VAMP713:GFP were grown on ½ MS agar plates for 5-days after germination, then transferred to media containing 0 mM, 100 mM or 150 mM NaCl for 48 hours. Root tips were imaged with a Zeiss LSCM 800.*

When the *ProVAMP713::VAMP713:GFP* seedlings were imaged further up from the root tip adjacent to the meristematic zone, fluorescence was observed at the plasma membranes of the endodermis and pericycle cells (Figure 4.17). The signal became more apparent after salt stress treatment and extended to the stele cells (Figure 4.17).

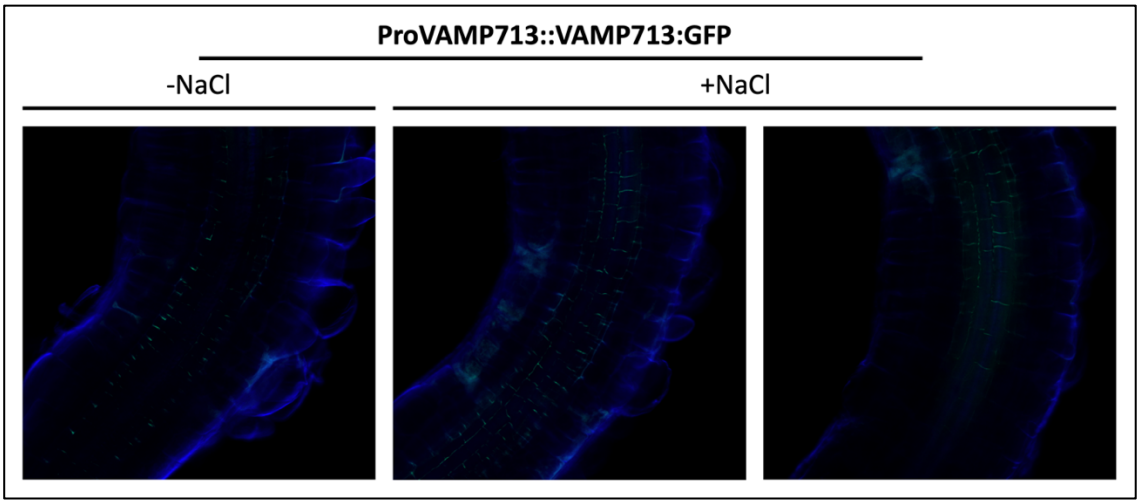

Figure 4.17: *Adjacent to the meristematic zone, VAMP713:GFP is present. Transgenic ProVAMP713::VAMP713:GFP lines were grown on ½ MS agar plates for 5 days after germination, then transferred to media containing 150 mM NaCl for 48 hours. For comparison, control seedlings were transferred to plates not containing salt. Root tips were imaged with a Zeiss LSCM 800.*

Chapter Summary

- This chapter looked at the role of the VAMP71 family members in the expression of auxin regulated genes during salt stress. Mutants like *vamp712* showed significant upregulation of auxin efflux carrier genes *PIN1* and *PIN2*, whereas *vamp711* mutants show significant downregulation of *PIN1*, *PIN2*, and auxin-induced genes *IAA1* and *IAA2* under salt stress. Moreover, in normal growth conditions the expression of the *PIN1, IAA1* and *IAA2* genes were significantly increased in *vamp711* mutants relative to the wild type control plants, suggesting the response to salt may be influenced by this higher basal expression level.
- **Auxin Degradation Pathway and GH3 Genes**: Confocal microscopy experiments revealed altered auxin abundance and localisation patterns in the *vamp712* and *vamp713* mutants, and gene expression analysis revealed to a significant upregulation of *GH3* genes under salt stress. GH3 genes, which are involved in auxin degradation, show a rapid and transient increase in expression in these mutants, peaking between three- and five-hours. This expression pattern was also observed to a lesser extent in wild type, unlike the marginal increases observed in *vamp711* mutants.
- **Root Growth Responses**: Under salt stress conditions and supplemented IAA treatment, *vamp711* mutants exhibited significantly reduced primary root growth compared to wild-type and *vamp712* mutants. The presence of NPA and salt stress results showed limited differences in inhibition to primary root growth, though significant differences in lateral root development were observed among different genotypes.
- **Ion Transporter and ROS-Related Genes**: VAMP712 and VAMP713 are essential for the normal expression levels of ion transporter genes HKT1 and NHX1. Salt stress causes significant changes in the expression of these genes and ROS detoxification genes (APX2, CAT1, and GST1), with *vamp71* mutants showing heightened sensitivity and varied responses, indicating their role in maintaining ion homeostasis and managing oxidative stress.

Chapter 5: VAMP712 and the Salt-Induced Proteome

A proteome-wide approach was used to assess whether VAMP712 has a direct function in the salt stress adaptive response of roots. This work aimed to screen the root proteome for differentially increased or decreased genes following a transfer to salt-treated media, identifying putative candidate genes whose protein product might be a direct or indirect interactor of VAMP712 and involved in the salt-stress response. It was decided that the salt-sensitive proteome of wild-type Col-0 and the *vamp712* mutant would be compared as this knockout line has a salt-sensitive root growth phenotype, a distinctive pattern of auxin-responsive gene expression; of all the VAMP71 family members, the least is known about VAMP712.

Because VAMP712 is a SNARE protein, involved is vesicle-trafficking and protein localisation to membranes likely via both anterograde and retrograde pathways, an optimised protein extraction technique for isolating a microsomal fraction highly enriched in membrane proteins by differential centrifugation was conducted. Four biological replicates of Col-0 and *vamp712* transgenic lines were grown for 8 days in normal ½ MS agar media, then transferred to media containing 150 mM NaCl and harvested after 48 hours of salt stress. The protein extraction technique described in Methods 2.5 yielded a fraction enriched with cytosolic proteins (S100) and solubilised membrane proteins (P100/ePM). For quality control, representative samples of isolated protein fractions were separated by polyacrylamide gel electrophoresis in the presence of sodium dodecyl sulphate (SDS-PAGE). The gel was then stained with Coomassie Blue, which binds to basic and hydrophobic residues of proteins, presenting a visible blue colour (Figure 5.1). Distinct bands across a range of molecular weights indicate the proteins are intact and degradation is minimal. To determine the successful separation of microsomal proteins from the soluble/cytosolic proteins, an aliquot of the S100 and P100/ePM protein samples were used for SDS-PAGE followed by immunoblot analysis (Gallagher et al., 2008) (Figure 5.2). Here, primary antibodies for known marker proteins of specific subcellular compartments were used to assess the efficacy of microsomal separation from soluble/cytosolic proteins. The microsomal fraction successfully bound antibodies against plasma membrane marker proteins: voltage-dependent anion-selective channel protein 1-5 (VDAC1-5, mitochondrial outer membrane); epsilon subunit of tonoplast H^+-ATPase (V-ATPase, tonoplast membrane); sterol methyltransferase 1 (SMT1, integral membrane protein of the ER); and ADP-ribosylation factor 1 (ARF1, Golgi membrane). An antibody

against cytosolic fructose-1,6-bisphosphatase (cFBPase) was used as a cytosolic marker. This antibody was detected in the S100 fraction and faintly detected in some of the ePM fractions, possibly due to residual supernatant left during the extraction procedure or cross-well contamination in the SDS-PAGE gel (Figure 5.2).

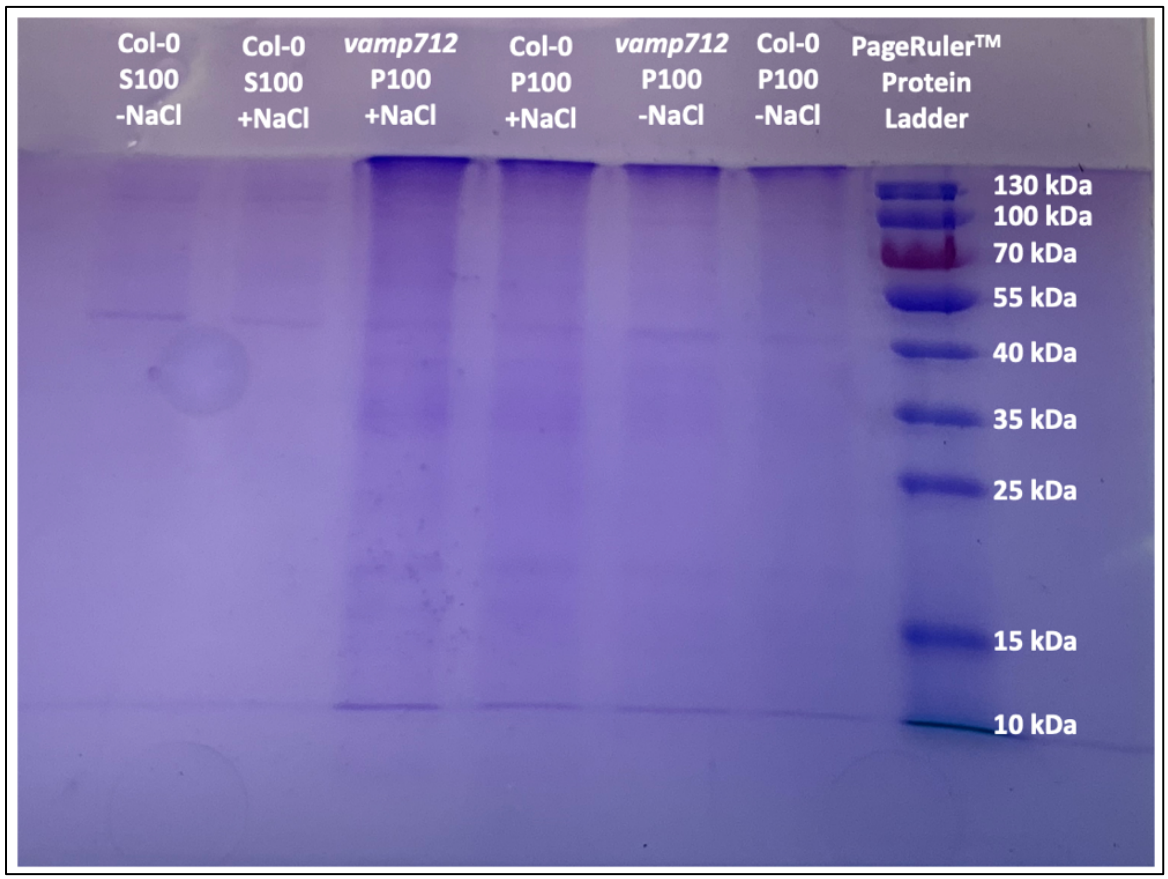

Figure 5.1 *SDS-PAGE followed by Coomassie blue staining of protein samples. Lane 1-2; wild-type Col-0 S100 without salt stress and with salt stress. Lanes 3-4; P100 fractions of vamp712 and Col-0 under salt stress. Lanes 5-6; P100 fractions of vamp712 and Col-0 under control conditions. Lane 7 contains the molecular weight standards PageRuler™ (Thermo Scientific).*

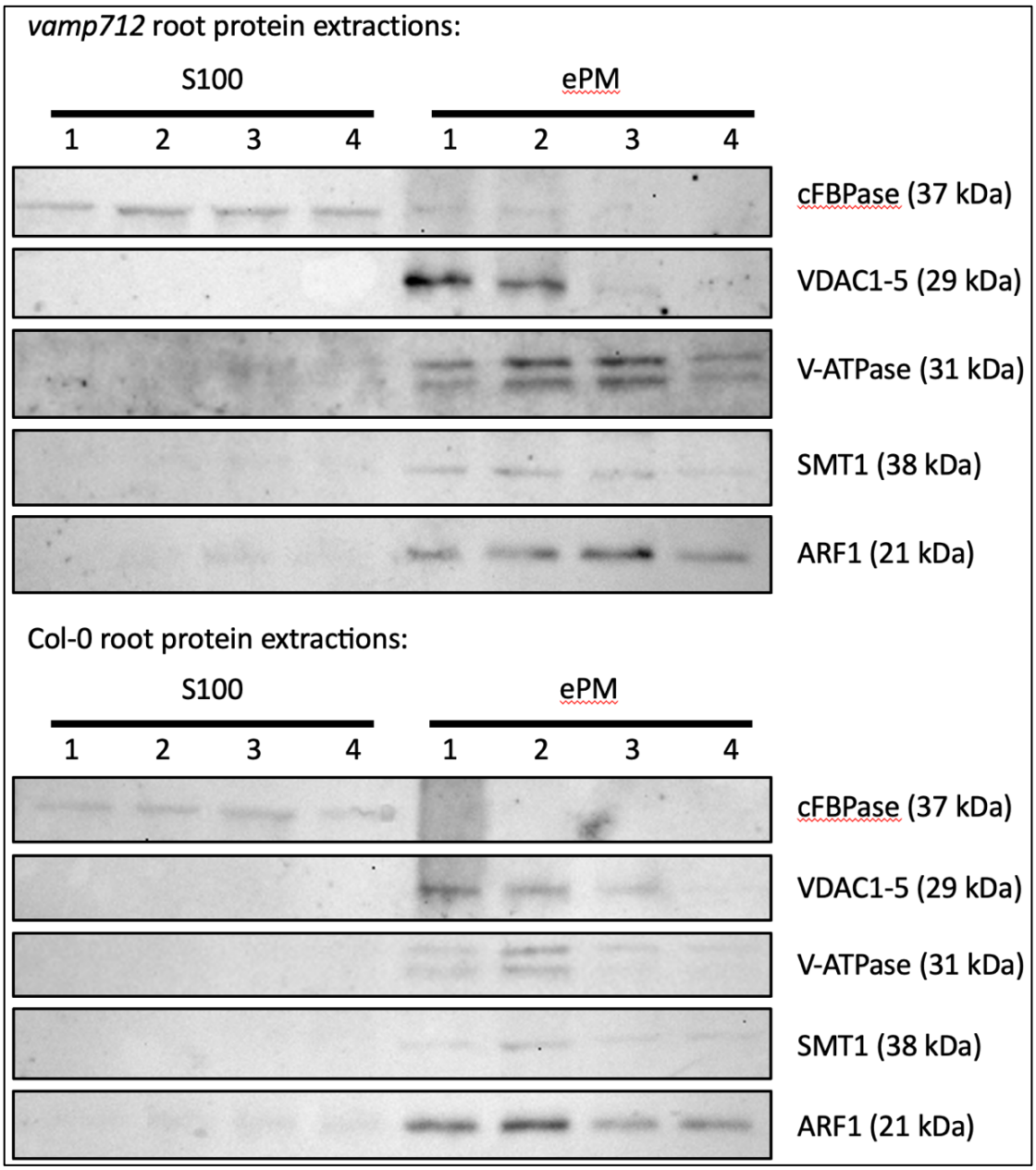

Figure 5.2: *Microsomal membrane isolation by differential centrifugation from vamp712 and Col-0 Arabidopsis roots as determined by immunoblot analysis. Primary antibody markers for different cellular compartments confirmed the successful separation of soluble cytosolic protein fraction (S100) from the membrane protein fraction (ePM). As expected, the cytosolic fructose-1,6-bisphosphatase (cFBPase) was absent from the ePM fraction but enriched in the S100 fraction. The voltage-dependent anion-selective channel protein 1-5 (VDAC1-5, mitochondrial outer membrane), epsilon subunit of tonoplast H^+ -ATPase (V-ATPase, tonoplast membrane), sterol methyltransferase 1 (SMT1, integral membrane protein of the ER), and ADP-ribosylation factor 1 (ARF1, Golgi membrane) were all absent from the S100 fraction and enriched in the ePM fraction.*

Protein identification and quantification by mass spectrometry

Following the protein quantification of isolated samples using the Bicinchoninic acid (BCA) assay (see Methods 2.5), 15 µg of the microsomal and soluble/cytosolic protein fractions were labelled using the isobaric tags for the relative and absolute quantitation (iTRAQ) method (Methods 2.5). Identification of proteins and their respective abundances were found using liquid chromatography mass spectrometry (LC-MS/MS). A total of four comparisons were made: (i) P100/ePM proteins from normal conditions versus salt-treated conditions in the Col-0 wild-type *Arabidopsis* plants; (ii) P100/ePM proteins from non-stressed conditions versus salt-treated conditions in the *vamp712* mutant lines; (iii) S100 proteins from normal conditions versus salt-treated conditions in Col-0; and (iv) S100 proteins from normal conditions versus salt-stress conditions in the *vamp712* mutant lines. Initially, only proteins with two or more sequenced peptides equal to or higher than the statistical confidence threshold ≥ 95% were regarded as a positive identification. Of the proteins that met these criteria from the P100/ePM fractions, 1300 were identified in the Col-0 comparison, compared with 1314 proteins in the *vamp712* comparison. Additionally, from the S100 fraction, 785 proteins were identified in the Col-0 comparison, and 802 proteins in the *vamp712* comparison met the criteria threshold. For comparison purposes, if this criterion was met in one of the genotypes and not the other for the corresponding protein, the result was included in the statistical analysis and is indicated as such. For each identified protein, the fold change in abundance was calculated by dividing the mean of the four salt-treated replicates by the mean of the four untreated replicates. Statistical significance was calculated using a two-tail t-test at $P<0.05$ to identify differentially expressed proteins (DEPs) (Figure 5.3). When performing many statistical tests, some proteins will have a *P-value* less than 0.05 by chance, even if all our null hypotheses are really true (McDonald, 2014). To account for this, the Benjamini-Hochberg procedure was applied to adjust the false discovery rate (FDR) with a selected FDR of 0.1 (Benjamini and Hochberg, 1995). Proteins with a *P*-value less than 0.05 but which failed the Benjamini-Hochberg test were removed from the comparison. After filtering for absolute fold changes >1.5, 29 DEPs were identified in the microsomal Col-0 comparison, of which 15 were downregulated and 14 were upregulated (Table 5.1). In the microsomal *vamp712* comparison, 25 DEPs were identified, 19 downregulated and six upregulated (Table 5.2). Of these DEPs in the microsomal comparisons, only three were common to Col-0 and *vamp712*.

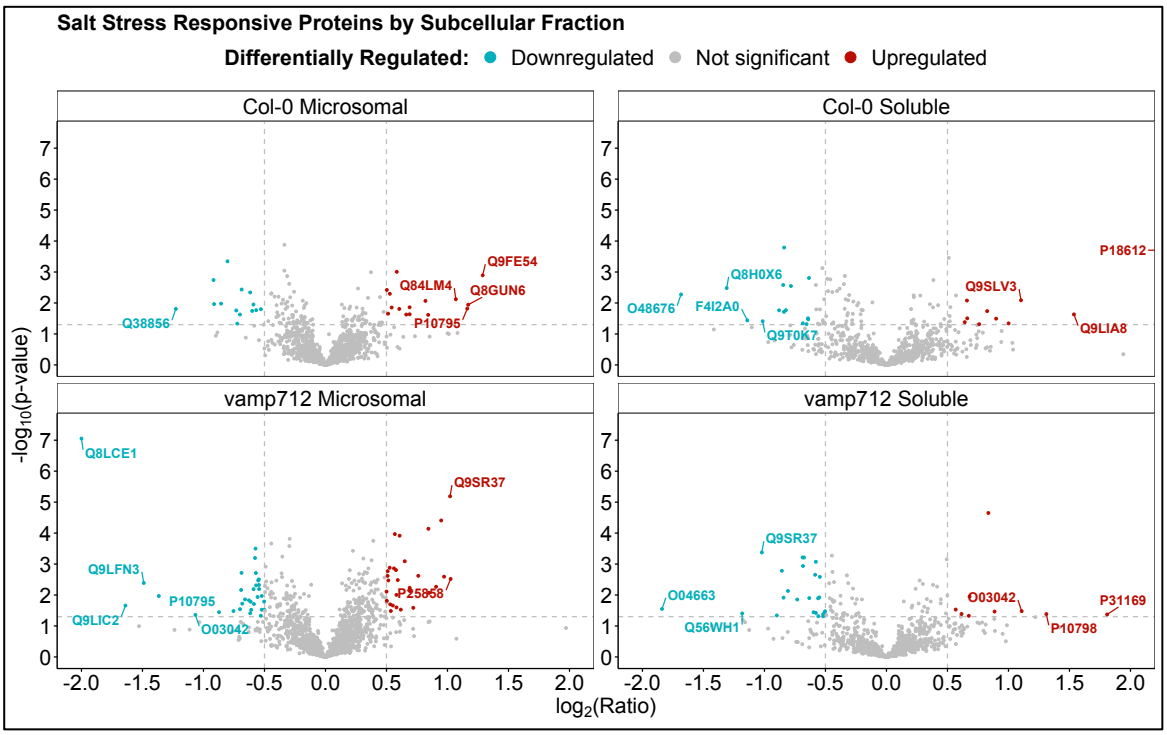

Figure 5.3: *Volcano plots of iTRAQ-labelled proteins. The volcano plot shows up-regulated differentially expressed proteins (red), unchanged proteins (grey), and down-regulated differentially expressed proteins (blue). Dashed grey-lines represent thresholds used for determining upregulated and downregulated proteins with the log_2 Fold Change (Ratio) of <-0.5 and >0.5, and the significance threshold of $-log_{10}(0.05)$.*

Table 5.1: *List of differentially expressed proteins identified in the microsomal Col-0 comparison, shown with the matched protein for pairwise comparison.*

			Col-0			*vamp712*			*vamp712*/Col-0		
LOCUS ID	**Accession[a]**	**Protein Name**	**Fold Change[b]**	**SD ratio[c]**	**P-value[d]**	**Fold Change[b]**	**SD ratio[c]**	**P-value[d]**	**Ratio[e]**	**P-value[f]**	**Sig.**
AT4G31940	Q9SZ46	Cytochrome P450	0.57	0.05	4.51E-04	0.82	0.16	1.03E-01	1.43	3.63E-02	*
AT1G52280	Q9C820	Ras-related protein RABG3d	1.50	0.12	9.86E-04	Nd	Nd	Nd	-	-	
AT1G16850	Q9FE54	F6I1.15 Uncharacterised transmembrane protein	2.44	0.45	1.28E-03	2.59*	0.86	4.00E-02	1.06	2.92E-03	**
AT1G09740	Q84TF6	Adenine nucleotide alpha hydrolases-like	0.65	0.12	4.56E-03	0.68	0.24	4.65E-02	1.05	1.93E-01	
AT3G46060	P28186	Ras-related protein RABE1c[1]	3.38	0.73	5.10E-03	Nd	Nd	Nd	-	-	
AT1G61770	Q8GUN6	Chaperone protein dnaJ 50[1]	1.99	0.20	5.95E-03	1.32*	0.31	2.24E-01	0.66	1.77E-04	***
AT4G14570	Q84LM4	Acylamino-acid-releasing enzyme	2.10	0.54	7.58E-03	0.83*	0.33	4.54E-01	0.39	4.02E-03	**
AT3G13784	Q9LIB9	Beta-fructofuranosidase, insoluble isoenzyme	1.76	0.25	8.57E-03	1.40	0.12	4.93E-03	0.80	7.73E-01	
AT2G18740	Q9ZV45	Putative small nuclear ribonucleoprotein	0.55	0.07	1.05E-02	1.22	0.56	4.50E-01	2.21	8.29E-02	
AT3G02630	Q9M879	Stearoyl-[acyl-carrier-protein] 9-desaturase 5	0.53	0.15	1.09E-02	Nd	Nd	Nd	-	-	
AT1G17860	Q9LMU2	Kunitz trypsin inhibitor 2	0.66	0.07	1.12E-02	0.81	0.11	2.40E-02	1.22	5.27E-03	**
AT4G01850	P17562	S-adenosylmethionine synthase 2	1.61	0.21	1.38E-02	0.89	0.05	2.14E-02	0.55	5.24E-03	**
AT4G19690	Q38856	Fe(2+) transport protein 1	0.43	0.18	1.55E-02	0.39*	0.10	1.23E-02	0.91	8.79E-01	
AT1G27950	Q9C7F7	Non-specific lipid transfer protein GPI-anchored 1	1.52	0.26	1.56E-02	1.47	0.04	2.22E-03	0.96	5.09E-04	***
AT5G06140	Q9FG38	Sorting nexin 1	0.67	0.18	1.70E-02	0.76	0.13	5.50E-02	1.13	1.65E-01	
AT3G16420	O04314	PYK10-binding protein 1	0.60	0.02	1.75E-02	0.52	0.04	3.91E-05	0.86	1.43E-01	
AT2G36160	Q9SIH0	40S ribosomal protein S14-1	0.66	0.15	1.81E-02	Nd	Nd	Nd	-	-	
AT1G07810	P92939	Calcium-transporting ATPase 1, ER-type	0.62	0.03	2.36E-02	Nd	Nd	Nd	-	-	
AT3G13470	Q9LJE4	Chaperonin 60 subunit beta 2	1.58	0.23	2.37E-02	0.87	0.25	1.52E-01	0.55	7.95E-01	
AT1G33850	Q9LD48	40S ribosomal protein S15	1.79	0.50	2.42E-02	Nd	Nd	Nd	-	-	
AT4G02150	O04294	Importin subunit alpha-3[1]	1.42	0.04	2.42E-02	Nd	Nd	Nd	-	-	
AT5G26280	Q93Z83	T19G15_130 TRAF-like family protein	0.61	0.10	4.64E-02	0.70	0.06	3.00E-03	1.16	1.64E-02	*
AT1G67090	P10795	Ribulose bisphosphate carboxylase small chain 1A[1]	1.78	0.44	4.76E-02	2.58	0.86	2.87E-02	1.45	1.64E-02	*

			Col-0			*vamp712*			*vamp712*/Col-0		
LOCUS ID	**Accession[a]**	**Protein Name**	**Fold Change[b]**	**SD ratio[c]**	**P-value[d]**	**Fold Change[b]**	**SD ratio[c]**	**P-value[d]**	**Ratio[e]**	**P-value[f]**	**Sig.**
AT2G30210	Q56YT0	Laccase-3[1]	0.60	0.14	5.08E-02	1.42	0.05	2.32E-01	2.36	2.18E-04	***

[a] Protein accession numbers acquired from the UniProt database searches. [b] Ratio represents the average fold-change (n = 4) in response to salt stress (150 mM NaCl) relative to the control (no salt), asterisks in the column indicate <2 peptides identified. Values less than one indicates down-regulation. [c] Standard deviation of the fold-changes (n = 4). [d] Probability value calculated with a two-tailed Student's *t-test* comparing the fold changes between the control and salt stress treatment means (n = 4). [e] Ratio of Col-0 divided by the ratio of *vamp712*. [f] Probability value obtained from a Student's *t-test* comparing the fold changes between Col-0 and *vamp712* biological replicates (n = 4). [1]Protein names with superscript 1 indicate n=3.

Table 5.2: *List of differentially expressed proteins identified in the microsomal vamp712 comparison, with the matched protein for pairwise comparison.*

			vamp712			Col-0			*vamp712*/Col-0		
LOCUS ID	**Accession[a]**	**Protein Name**	**Fold Change[b]**	**SD ratio[c]**	**P-value[d]**	**Fold Change[b]**	**SD ratio[c]**	**P-value[d]**	**Ratio[e]**	**P-value[f]**	**Sig***
AT1G66200	Q8LCE1	Glutamine synthetase cytosolic isozyme 1-2	0.25	0.03	8.83E-08	0.53	0.05	1.82E-03	2.12	9.01E-05	***
AT3G16420	O04314	PYK10-binding protein 1	0.52	0.04	3.91E-05	0.60	0.02	1.75E-02	1.16	1.43E-01	
AT3G16450	O04311	Jacalin-related lectin 33	0.56	0.02	7.24E-05	0.84	0.11	1.98E-01	1.51	6.52E-03	**
AT3G16460	O04310	Jacalin-related lectin 34	0.66	0.03	1.21E-04	0.76	0.05	1.07E-01	1.15	9.66E-01	
AT1G09200,	P59226	Histone H3.2	1.49	0.09	6.38E-04	1.35	0.19	5.11E-02	0.91	4.25E-01	
AT3G27360	Q9C901	DNA-binding enhancer protein-like protein	0.64	0.07	8.12E-04	0.86	0.12	2.88E-01	1.35	3.66E-01	
AT5G02740	A0JQ00	Ribosomal protein S24e family protein	0.67	0.09	1.56E-03	0.88	0.12	3.68E-01	1.32	1.64E-01	
AT1G09430	O80526	ATP-citrate synthase alpha chain protein 3	0.59	0.05	2.40E-03	0.83	0.12	4.01E-02	1.41	1.44E-02	*
AT1G13440	Q9FX54	Glyceraldehyde-3-phosphate dehydrogenase GAPC2	0.51	0.13	2.55E-03	0.77	0.23	1.15E-01	1.51	1.61E-01	
AT3G04120	P25858	Glyceraldehyde-3-phosphate dehydrogenase GAPC1	0.49	0.16	3.02E-03	0.76	0.13	2.58E-02	1.55	8.17E-02	
AT4G16260	Q8VZJ2	Probable glucan endo-1,3-beta-glucosidase	0.66	0.08	3.29E-03	1.02	0.26	9.13E-01	1.54	1.41E-01	
AT1G48470	Q8GXW5	Glutamine synthetase cytosolic isozyme 1-5	0.53	0.15	5.39E-03	Nd	Nd	Nd	Nd	Nd	Nd
AT3G52990	Q94KE3	Pyruvate kinase	0.62	0.07	5.85E-03	0.92	0.06	1.22E-01	1.48	2.64E-03	**

			vamp712			Col-0			*vamp712*/Col-0		
LOCUS ID	**Accession[a]**	**Protein Name**	**Fold Change[b]**	**SD ratio[c]**	**P-value[d]**	**Fold Change[b]**	**SD ratio[c]**	**P-value[d]**	**Ratio[e]**	**P-value[f]**	**Sig***
AT1G14670	Q940S0	Transmembrane 9 superfamily member 2	1.50	0.24	6.45E-03	Nd	Nd	Nd	Nd	Nd	Nd
AT5G50920	Q9FI56	Chaperone protein ClpC1	0.62	0.04	7.50E-03	1.03	0.16	7.97E-01	1.67	6.56E-04	***
AT1G09560	P94014	Germin-like protein subfamily 2 member 1	0.56	0.10	8.54E-03	0.54	0.04	8.99E-02	0.97	2.88E-03	**
AT3G57490	Q9SCM3	40S ribosomal protein S2-4	0.67	0.04	9.90E-03	Nd	Nd	Nd	Nd	Nd	Nd
AT3G44320	P46010	Nitrilase 3	1.50	0.27	1.95E-02	1.42	0.12	3.80E-03	0.94	8.09E-02	
AT3G13772	Q9LIC2	Transmembrane 9 superfamily member 7	3.12	1.33	2.18E-02	1.07*	0.32	8.24E-01	0.34	2.39E-02	*
AT4G34980	O49607	Subtilisin-like protease SBT1.6	0.67	0.16	2.51E-02	0.79*	0.23	2.30E-01	1.18	2.23E-01	
AT5G41950	Q9FHY8	Hypersensitive to Latrunculin B1	0.61	0.15	2.59E-02	0.79*	0.25	1.56E-01	1.30	6.28E-01	
AT5G65430	P48348	14-3-3-like protein GF14 kappa	0.65	0.07	2.97E-02	0.93	0.17	4.81E-01	1.42	2.76E-02	*
AT3G56430	Q9LXZ7	Uncharacterised - Import inner membrane translocase subunit	1.69	0.22	3.29E-02	1.41	0.44	1.22E-01	0.84	1.86E-04	***
AT5G23890	Q9FF91	GPI-anchored adhesin-like protein	1.53	0.40	3.89E-02	0.93	0.14	4.92E-01	0.61	1.98E-02	*

[a] Protein accession numbers acquired from the UniProt database searches. [b] Ratio represents the average fold-change (n = 4) in response to salt stress (150 mM NaCl) relative to the control (no salt), asterisks in the column indicate <2 peptides identified. Values less than one indicates down-regulation. [c] Standard deviation of the fold-changes (n = 4). [d] Probability value calculated with a two-tailed Student's *t-test* comparing the fold changes between the control and salt stress treatment means (n = 4). [e] Ratio of Col-0 divided by the ratio of *vamp712*. [f] Probability value obtained from a Student's *t-test* comparing the fold changes between Col-0 and *vamp712* biological replicates (n = 4). [1]Protein names with superscript 1 indicate n=3.

In the microsomal comparison, 21 DEPs from each genotype had significantly different fold changes compared to the matched protein in response to salt stress. Many of the identified proteins shown in Table 5.1 and Table 5.2 are not well characterised in the database, and therefore, inferences from this data for these proteins are difficult. Furthermore, only six DEPs were found to be inversely regulated in the microsomal fraction comparison.

To accompany the microsomal comparison, the same filtering procedure and statistical analysis were applied to the identified proteins from the soluble/cytosolic fraction. Here, 11 DEPs common to Col-0 and *vamp712* were found (Table 5.3). Coincidently, also identified were 11 proteins statistically significant in Col-0 and not *vamp712*, and vice-versa (Table 5.4). None of these DEPs from the soluble/cytosolic fraction showed a statistically significant inverse fold change but instead were either differentially abundant in one and unchanged in the other or regulated in the same direction to similar or different extents.

Table 5.3: *List of differentially expressed proteins identified in the soluble/cytosolic comparison common to both Col-0 and vamp712.*

			Col-0			*vamp712*			Col-0/*vamp712*		
LOCUS ID	**Accession[a]**	**Protein Name**	**Fold Change[b]**	**SD ratio[c]**	**P-value[d]**	**Fold Change[b]**	**SD ratio[c]**	**P-value[d]**	**Ratio[e]**	**P-value[f]**	**Sig***
AT5G15960	P18612	Stress-induced protein KIN1	5.13	1.03	1.97E-04	1.76	0.66	9.02E-02	0.34	8.40E-04	***
AT3G16420	O04314	PYK10-binding protein 1	0.64	0.06	1.56E-03	0.63	0.04	6.15E-04	0.97	7.59E-02	
AT2G01530	Q9ZVF2	MLP-like protein 329	0.56	0.07	2.63E-03	0.56	0.15	1.22E-02	1.00	2.69E-02	*
AT1G73260	Q8RXD5	Kunitz trypsin inhibitor 1	1.77	0.31	1.83E-02	1.52	0.20	5.02E-02	0.86	1.63E-03	**
AT5G38410	P10798	Ribulose bisphosphate carboxylase small chain 3B	1.86	0.56	3.21E-02	2.48	1.12	4.12E-02	1.33	8.13E-01	
AT4G23680	Q9SUQ9	AT4g23680/F9D16_150	2.00	0.59	4.56E-02	1.78	0.10	2.24E-05	0.89	3.89E-02	*
ATCG00490	O03042	Ribulose bisphosphate carboxylase large chain	1.69	0.50	4.86E-02	2.16	0.83	3.31E-02	1.27	2.87E-01	
AT3G51240	Q9S818	Naringenin,2-oxoglutarate 3-dioxygenase	1.67	0.78	2.28E-01	1.97	1.38	3.13E-01	1.18	3.98E-01	
AT5G19770	Q56WH1	Tubulin alpha-3 chain	0.58	0.46	2.72E-01	0.44	0.29	3.93E-02	0.76	8.35E-01	
AT5G15970	P31169	Stress-induced protein KIN2	1.57	0.99	3.13E-01	3.50	1.82	4.23E-02	2.23	4.01E-02	*
AT5G42890	Q9FMN0	Putative uncharacterized protein	2.05	1.88	3.21E-01	1.85	0.98	1.45E-01	0.90	5.24E-01	

[a] Protein accession numbers acquired from the UniProt database searches. [b] Ratio represents the average fold-change (n = 4) in response to salt stress (150 mM NaCl) relative to the control (no salt), asterisks in the column indicate <2 peptides identified. Values less than one indicates down-regulation. [c] Standard deviation of the fold-changes (n = 4). [d] Probability value calculated with a two-tailed Student's *t-test* comparing the fold changes between the control and salt stress treatment means (n = 4). [e] Ratio of Col-0 divided by the ratio of *vamp712*. [f] Probability value obtained from a Student's *t-test* comparing the fold changes between Col-0 and *vamp712* biological replicates (n = 4). [1]Protein names with superscript 1 indicate n=3.

Table 5.4: *List of differentially expressed proteins from the soluble/cytosolic comparison, unique to either Col-0 or vamp712. Matched protein shown for pairwise comparison.*

			Col-0			*vamp712*			*vamp712*/Col-0		
LOCUS ID	**Accession[a]**	**Protein Name**	**Fold Change[b]**	**SD ratio[c]**	**P-value[d]**	**Fold Change[b]**	**SD ratio[c]**	**P-value[d]**	**Ratio[e]**	**P-value[f]**	**Sig***
Unique DEGs to Col-0											
AT4G15390	O23392	HSR201 like protein (HXXXD-type acyl-transferase family)	0.56	0.07	1.62E-04	0.82	0.31	3.46E-01	1.47	3.36E-01	
AT5G04740	Q9LZ23	ACT domain-containing protein ACR12	0.58	0.11	2.84E-03	0.70	0.10	3.67E-02	1.21	4.09E-02	*
AT1G58270	Q9SLV3	ZW9 TRAF-like family protein	2.15	0.49	8.19E-03	1.22	0.53	4.43E-01	0.57	5.67E-02	
AT3G48530	Q8LBB2	SNF1-related protein kinase regulatory subunit gamma-1	0.56	0.13	1.71E-02	0.75	0.14	4.24E-02	1.33	2.45E-02	*
AT2G21045	Q8RUD6	Protein HIGH ARSENIC CONTENT 1	0.56	0.19	1.93E-02	0.74	0.16	1.95E-01	1.32	3.21E-01	
AT3G29360	Q9LIA8	UDP-glucose 6-dehydrogenase 2	2.90	1.22	2.34E-02	1.06	0.46	8.13E-01	0.37	1.55E-01	
AT4G17530	Q9SEH3	Ras-related protein RABD2c	0.64	0.16	3.13E-02	1.14	0.46	5.91E-01	1.78	8.41E-02	
AT1G20450	P42759	Dehydrin ERD10	1.58	0.41	3.14E-02	1.19	0.36	4.27E-01	0.75	7.49E-02	
AT2G07698	F4IMB5	ATPase, F1 complex, alpha subunit protein	0.64	0.18	3.37E-02	0.98	0.23	9.05E-01	1.53	2.68E-02	*
AT3G02520	Q96300	General regulatory factor 7 GRF7	1.56	0.37	4.17E-02	Nd	Nd	Nd	-	-	
AT2G31670	Q9SIP1	Stress-response A/B barrel domain-containing protein UP3	0.62	0.19	4.53E-02	1.06	0.32	7.57E-01	1.70	1.87E-01	
Unique DEGs to *vamp712*											
AT3G09260	Q9SR37	Beta-glucosidase 23	0.70	0.13	7.58E-03	0.49	0.13	4.22E-04	0.70	5.22E-02	
AT5G41670	Q9FFR3	6-phosphogluconate dehydrogenase, decarboxylating 2	0.67	0.09	1.61E-02	0.62	0.09	6.10E-04	0.92	1.99E-01	
AT1G66200	Q8LCE1	Glutamine synthetase cytosolic isozyme 1-2	0.71	0.10	1.66E-03	0.62	0.11	1.16E-03	0.87	6.05E-02	
AT3G19710	Q9LE06	Methionine aminotransferase BCAT4	0.69	0.13	1.61E-02	0.55	0.11	1.64E-03	0.81	8.54E-01	
AT4G35260	Q8LFC0	Isocitrate dehydrogenase [NAD] regulatory subunit 1	0.89	0.17	3.38E-01	0.57	0.13	7.39E-03	0.65	1.04E-01	
AT1G48830	Q9C514	40S ribosomal protein S7-1	Nd	Nd	Nd	0.64	0.13	1.25E-02	-	-	
AT2G01520	Q9ZVF3	MLP-like protein 328	0.81	0.28	3.98E-01	0.60	0.08	1.39E-02	0.74	2.15E-01	

			Col-0			*vamp712*			*vamp712*/Col-0		
LOCUS ID	**Accession[a]**	**Protein Name**	**Fold Change[b]**	**SD ratio[c]**	**P-value[d]**	**Fold Change[b]**	**SD ratio[c]**	**P-value[d]**	**Ratio[e]**	**P-value[f]**	**Sig***
AT1G07660	P59259	Histone H4	Nd	Nd	Nd	1.85	0.57	3.43E-02	-	-	
AT2G20630	Q9SIU8	Probable protein phosphatase 2C 20	0.79	0.05	7.60E-03	0.66	0.19	3.60E-02	0.83	2.80E-01	
AT1G48630	Q9C4Z6	Receptor for activated C kinase 1B	1.27	0.24	3.16E-01	1.53	0.35	4.09E-02	1.21	4.51E-03	
AT1G20620	Q42547	Catalase-3	Nd	Nd	Nd	1.60	0.37	4.69E-02	-	-	**

[a] Protein accession numbers acquired from the UniProt database searches. [b] Ratio represents the average fold-change (n = 4) in response to salt stress (150 mM NaCl) relative to the control (no salt), asterisks in the column indicate <2 peptides identified. Values less than one indicates down-regulation. [c] Standard deviation of the fold-changes (n = 4). [d] Probability value calculated with a two-tailed Student's *t-test* comparing the fold changes between the control and salt stress treatment means (n = 4). [e] Ratio of Col-0 divided by the ratio of *vamp712*. [f] Probability value obtained from a Student's *t-test* comparing the fold changes between Col-0 and *vamp712* biological replicates (n = 4). [1]Protein names with superscript 1 indicate n=3.

Since this initial unbiased screening presented candidate proteins that may be directly or indirectly regulated by the absence of *vamp712*, but the link with VAMP712 function is not apparent, this proteomic data was further analysed in a biased manner. First, a search for proteins explicitly related to salt stress was carried out. This was done by sorting the fold changes in descending order and selecting the top 160 proteins from each fraction for each genotype. Then, after collating the two protein sets and removing any duplicated proteins, those with significant enrichment for the gene ontology (GO) term *"response to salt stress"* (GO:0009651) were retrieved, and a comparison table was made for these proteins (Table 5.5).

This analysis found a total of 21 proteins that had previously been identified as related to salt stress. Four were differentially regulated in opposite directions between the Col-0 and *vamp712* comparisons. One such protein was the Ras-related protein RAB GTPase HOMOLOG G3E (RABG3e), which has a role in intracellular vesicle trafficking and protein transport and has been suggested to play a role in adaptation to salt and osmotic stress by recycling macromolecules in specific cellular compartments (Mazel et al., 2004). Plants overexpressing RABG3e exhibit accelerated endocytosis, increased tolerance to salt and osmotic stresses and reduced accumulation of reactive oxygen species during salt stress (Mazel et al., 2004). Our results found this protein was increased in abundance by 1.87-fold in Col-0 plants under salt stress, whilst in *vamp712,* it was decreased to 0.61-fold (-1.64x) treated with the same salt stress conditions. This suggests that VAMP712 is required for expression/accumulation of RABG3e in the cytosolic compartment under salt stress. According to *Student's t-test*, this ratio difference was statistically significant at $P<0.001$.

In the initial unbiased search for DEPs (Table 5.1, Table 5.4), three other Ras-related proteins closely related to RABG3e were identified. These are RABD2c, which is a regulator of membrane traffic from the Golgi apparatus towards the ER (predicted); RABG3d, involved in intracellular vesicle trafficking and protein transport (predicted); and RABE1C, involved in membrane trafficking from the Golgi to the plasma membrane (predicted). Of these genes, RABG3d and RABE1 were significantly upregulated in Col-0 exposed to salt stress 1.5- and 3.38-fold, respectively. However, these two proteins were not detected in the *vamp712* comparison, which may suggest that VAMP712 is required for their expression/accumulation in the microsomal compartment. RABD2c was detected

in both Col-0 and *vamp712* and was decreased 0.64-fold (-1.56x) in Col-0 and increased 1.14-fold in *vamp712*.

Considering VAMP712 is involved in vesicle-mediated trafficking, another biased screening approach was applied to compare the differential expression of proteins with significant enrichment for the GO term *"protein transport"* (GO:0015031). Here, 22 genes were found whose protein abundance change was ranked in the top 160 DEGs in either the soluble or microsomal fraction of Col-0 and *vamp712* (Table 5.6). As expected, almost all of these proteins were identified in the microsomal fraction, emphasising the usefulness of this extraction technique. There were six Ras-related proteins belonging to the small GTPase superfamily Rab family, three VAMPs including VAMP711, VAMP714 and VAMP721. Interestingly, the abundance of VAMP711 significantly increased 1.21-fold in Col-0 and decreased 0.71-fold (-1.27x) in *vamp712* under salt stress. This is consistent with the gene expression data gathered using RT-qPCR, which showed that the *VAMP711* transcript abundance increased in both Col-0 and *vamp712* under salt stress conditions (Figure 3.8). Though VAMP714 protein was not detected in the Col-0 comparison, an increase in abundance by 1.33-fold in *vamp712* plants under salt stress was shown (Table 5.6).

Table 5.5: *List of abundance changes of proteins with the GO term "response to salt stress" from the top 160 DEGs in both fractions and comparisons.*

			Col-0			*vamp712*			*vamp712*/Col-0		
LOCUS ID	Accession [a]	Protein Name	Fold Change[b]	SD ratio[c]	P-value[d]	Fold Change[b]	SD ratio[c]	P-value[d]	Ratio[e]	P-value[f]	Sig *
AT3G61050	Q9LEX1	Calcium-dependent lipid-binding protein	Nd	Nd	Nd	1.60	0.33	8.60E-02	-	-	-
AT3G06610	Q9C901	DNA-binding enhancer protein-like protein	0.86	0.12	2.88E-01	0.64	0.07	8.12E-04	0.74	3.66E-01	
AT1G66280	Q9C8Y9	Beta-glucosidase 22	0.99	0.04	8.79E-01	1.32	0.24	5.49E-02	1.34	1.31E-02	*
AT3G09260	Q9SR37	Beta-glucosidase 23	0.70	0.13	7.58E-03	0.49	0.13	4.22E-04	0.70	5.22E-02	
AT1G27770	Q37145	Calcium-transporting ATPase 1	0.69	0.20	1.59E-01	1.38	0.31	8.54E-02	2.01	6.13E-02	
AT4G27520	Q9T076	Early nodulin-like protein 2	1.27	0.31	3.64E-01	0.74	0.46	3.76E-01	0.58	2.77E-03	**
AT3G23830	Q9LIS2	Glycine-rich RNA-binding protein 4	1.25	0.24	1.58E-01	1.74	0.71	1.42E-01	1.39	5.55E-02	
AT5G14040	Q9FMU6	Mitochondrial phosphate carrier protein 3	1.13	0.05	2.53E-01	0.71	0.16	8.05E-03	0.63	6.24E-01	
AT1G16880	Q9FE54	F6I1.15 uncharacterised	2.44	0.45	1.28E-03	2.59	0.86	4.00E-02	1.06	2.92E-03	**
AT1G14000	Q9XI87	VH1-interacting kinase	Nd	Nd	Nd	0.55	0.45	2.47E-01	-	-	-
AT1G30580	Q9SA73	Obg-like ATPase 1	0.80	0.11	1.56E-02	1.01	0.05	9.00E-01	1.26	7.90E-02	
AT1G30580	Q9FUS8	Glutathione S-transferase U17	1.33	0.18	1.48E-01	1.22	0.23	6.14E-01	0.92	1.00E-02	**
AT3G47950	Q9SU58	ATPase 4, plasma membrane-type	1.25	0.30	1.80E-01	1.24	0.17	9.99E-02	0.99	7.21E-02	
AT2G43790	Q39026	Mitogen-activated protein kinase 6	0.69	0.54	3.72E-01	Nd	Nd	Nd	-	-	-
AT4G39090	P43296	Cysteine protease RD19A	0.80	0.09	5.61E-02	0.86	0.12	2.16E-01	1.07	3.00E-02	*
AT1G49300	Q9XI98	Ras-related protein RABG3e	1.87	0.09	5.86E-04	0.61	0.10	3.63E-04	0.33	1.01E-05	***
AT2G41380	Q9ZVC3	Putative embryo-abundant protein	0.68	0.21	4.67E-02	1.07	0.26	7.61E-01	1.59	7.50E-02	
AT5G07350	Q8VZG7	Ribonuclease TUDOR 1	1.40	0.22	6.94E-02	0.97	0.10	7.90E-01	0.69	2.84E-03	**
AT2G38750	Q9ZVJ6	Annexin D4	1.36	0.22	1.11E-01	1.26	0.09	1.31E-02	0.92	7.61E-02	
AT5G10230	Q9LX07	Annexin D7	0.66	0.45	3.22E-01	Nd	Nd	Nd	-	-	-
AT5G56030	P55737	Heat shock protein 90-2	1.63	0.37	2.05E-02	1.01	0.19	9.77E-01	0.62	5.69E-03	**

[a] Protein accession numbers acquired from the UniProt database searches. [b] Ratio represents the average fold-change (n = 4) in response to salt stress (150 mM NaCl) relative to the control (no salt), asterisks in the column indicate <2 peptides identified. Values less than one indicates down-regulation. [c] Standard deviation of the fold-changes (n = 4). [d] Probability value calculated with a two-tailed Student's *t-test* comparing the fold changes between the control and salt stress treatment means (n = 4). [e] Ratio of Col-0 divided by the ratio of *vamp712*. [f] Probability value obtained from a Student's *t-test* comparing the fold changes between Col-0 and *vamp712* biological replicates (n = 4). [1]Protein names with superscript 1 indicate n=3.

Table 5.6: *List of abundance changes of proteins with the GO term "protein transport" from the top 160 DEGs in both fractions and comparisons.*

			Col-0			*vamp712*			*vamp712*/Col-0		
LOCUS ID	**Accession[a]**	**Protein Name**	**Fold Change[b]**	**SD ratio[c]**	**P-value[d]**	**Fold Change[b]**	**SD ratio[c]**	**P-value[d]**	**Ratio[e]**	**P-value[f]**	**Sig***
AT2G43160	Q67YI9	Clathrin interactor EPSIN 2	1.31	0.35	1.91E-01	0.71	0.25	8.86E-02	0.54	1.42E-01	
AT4G17530	Q9SEH3	Ras-related protein RABD2c	0.88	0.17	3.73E-01	1.05	0.16	7.44E-01	1.19	4.70E-01	
AT1G52280	Q9C820	Ras-related protein RABG3d	1.50	0.25	9.86E-04	Nd	Nd	Nd	-	-	
AT1G49300	Q9XI98	Ras-related protein RABG3e	1.29	0.37	2.58E-01	0.62	0.48	1.47E-03	0.48	1.51E-01	
AT5G45750	Q9FK68	Ras-related protein RABA1c	1.23	0.20	1.13E-01	1.36	0.36	1.04E-01	1.10	9.67E-01	
AT4G35860	Q38922	Ras-related protein RABB1b	0.91	0.12	1.76E-01	1.34	0.44	2.00E-01	1.47	4.44E-01	
AT3G16100	Q9LW76	Ras-related protein RABG3c	0.63	0.35	1.41E-01	1.65	0.61	1.33E-01	2.60	1.99E-02	*
AT2G30050	O64740	Protein transport protein SEC13 homolog B	0.72	0.32	2.72E-01	0.90	0.21	5.79E-01	1.25	3.78E-01	
AT1G29310	Q8RWJ5	SecY protein transport family protein	1.13	0.08	3.49E-02	1.40	0.21	3.65E-03	1.24	1.17E-02	
AT5G41950	Q9FHY8	Hypersensitive to latrunculin B1	0.79	0.24	1.56E-01	0.61	0.28	2.59E-02	0.76	1.71E-01	
AT5G22770	Q8LPL6	AP-2 complex subunit alpha-1	0.77	0.18	4.32E-02	0.95	0.05	5.73E-01	1.23	1.15E-01	*
AT3G22845	Q9LIL4	Transmembrane emp24 domain-containing protein p24beta3	1.26	0.23	9.35E-02	Nd	Nd	Nd	-	-	
AT3G53230	Q9SCN8	Cell division control protein 48 homolog D	1.11	0.27	6.21E-01	1.36	0.55	4.44E-01	1.22	9.55E-01	
AT3G60860	Q9LZX8	Brefeldin A-inhibited guanine nucleotide-exchange protein 2	Nd	Nd	Nd	0.60	0.69	2.13E-01	-	-	
AT3G01610	Q9SS94	Cell division control protein 48 homolog C	Nd	Nd	Nd	0.75	0.17	6.09E-02	-	-	
AT4G11380	Q9SUS3	Beta-adaptin-like protein B	1.02	0.18	9.12E-01	1.45	0.32	1.28E-01	1.43	8.57E-01	
AT5G57870	Q93ZT6	Eukaryotic translation initiation factor isoform 4G-1	1.28	0.22	1.14E-01	0.75	0.28	2.16E-01	0.59	5.35E-01	
AT5G19760	Q9C5M0	Mitochondrial dicarboxylate/tricarboxylate transporter DTC	1.12	0.18	3.92E-01	1.39	0.23	6.08E-03	1.24	1.25E-01	
AT2G47800	Q7DM58	ABC transporter C family member 4	Nd	Nd	Nd	1.64	0.79	2.84E-01	-	-	**
AT4G32150	O49377	Vesicle-associated membrane protein 711	1.21	0.10	2.06E-02	0.79	0.15	2.08E-03	0.66	3.71E-04	***
AT5G22360	Q9FMR5	Vesicle-associated membrane protein 714	Nd	Nd	Nd	1.33	0.12	1.03E-01	-	-	
AT1G04750	Q9ZTW3	Vesicle-associated membrane protein 721	1.21	0.13	3.63E-02	1.46	0.19	3.12E-03	1.21	8.32E-03	*

[a] Protein accession numbers acquired from the UniProt database searches. [b] Ratio represents the average fold-change (n = 4) in response to salt stress (150 mM NaCl) relative to the control (no salt), asterisks in the column indicate <2 peptides identified. Values less than one indicates down-regulation. [c] Standard deviation of the fold-changes (n = 4). [d] Probability value calculated with a two-tailed Student's *t-test* comparing the fold changes between the control and salt stress treatment means (n = 4). [e] Ratio of Col-0 divided by the ratio of *vamp712*. [f] Probability value obtained from a Student's *t-test* comparing the fold changes between Col-0 and *vamp712* biological replicates (n = 4).

Gene ontology analysis

The GO enrichment analysis statistically determined which biological processes, cellular compartments or molecular functions are over- or under-represented against a background reference dataset of the total *Arabidopsis* genome. Singular Enrichment Analysis (SEA) was carried out to connect GO categories or terms that were enriched within the data. The statistically significant (*FDR adjusted P-value < 0.05*) GO terms for biological processes, cellular components and molecular functions were retrieved from the DAVID (Database for Annotation, Visualisation, and Integrated Discovery) web server. There was limited overlap in GO terms between Col-0 and *vamp712,* comparing the SEA for biological processes (Figure 5.4). The most enriched biological process term for Col-0 under salt stress was "regulation of nucleobase-containing compound metabolic process" for the microsomal comparison and "translation" for the soluble/cytosolic fraction. These two terms indicate that most of the upregulated genes are involved in changes to plant gene expression. Our GO results counted 17 genes related to these two terms combined. Response to water deprivation was also a highly enriched biological process found in the Col-0 gene list, which counted a 12 significantly enriched genes (*FDR adjusted P-value <0.05*). Comparatively, the *vamp712* upregulated genes related to various abiotic stress processes, including "response to oxidative stress", which counted 11 genes across both fractions, possibly reflecting an increased level of ROS in these plants.

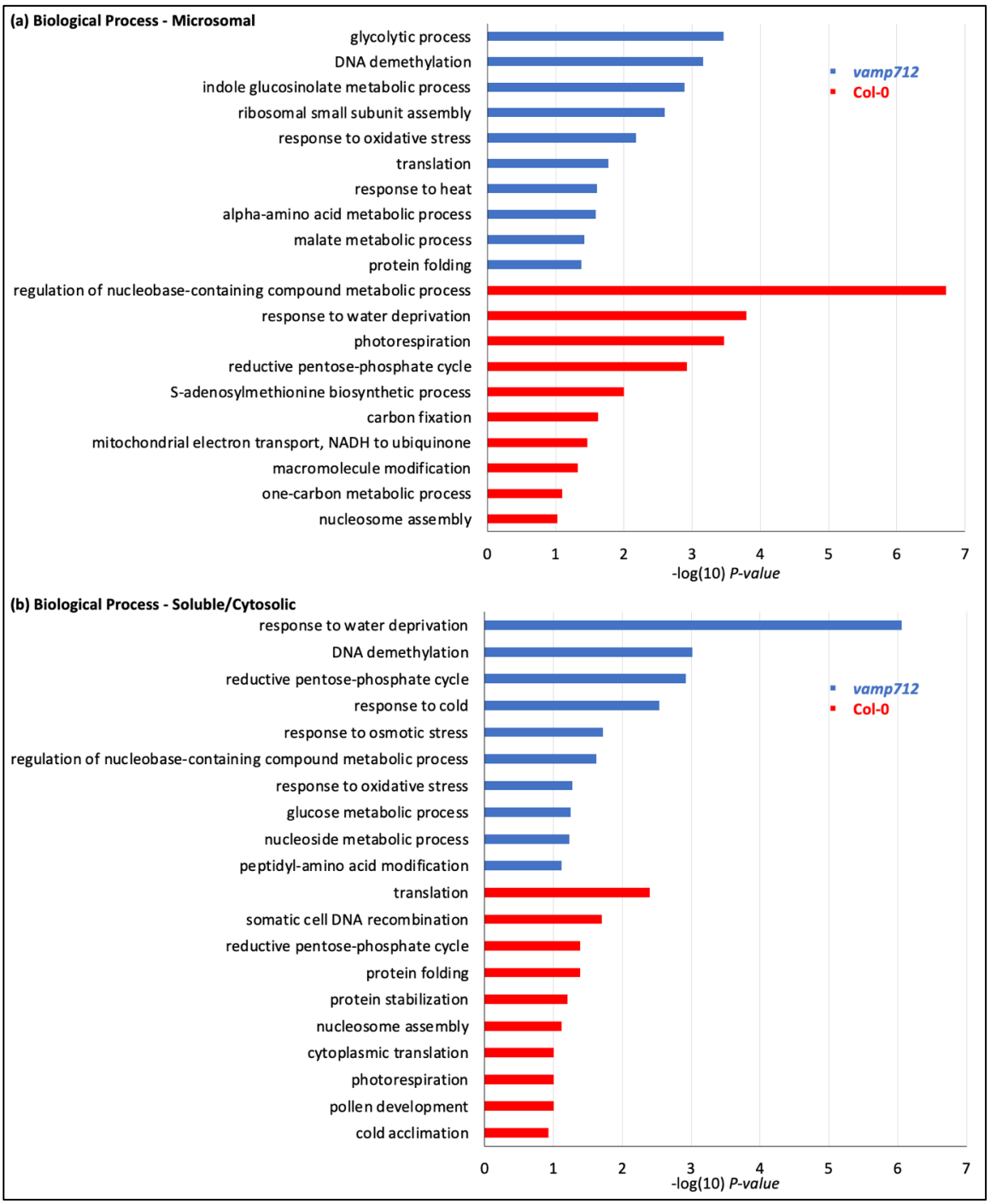

Figure 5.4: *GO enrichment analysis of vamp712 and Col-0 proteomic comparisons. The 50 highest fold-changes of upregulated genes in response to salt stress for each comparison and the two fractions separately. (a) The top 10 enriched biological processes were retrieved for vamp712 (blue bars) and Col-0 (red bars) for the top 50 upregulated gene list from the microsomal fraction comparison. (b) Likewise, from the soluble/cytosolic fraction comparison. Bars show adjusted FDR scores (-log P-value) for each GO term. The bioinformatics database DAVID (https://david.ncifcrf.gov/home.jsp) was used for GO analysis, with the threshold values: count ≥ 2, Ease = 0.25.*

Of the cellular compartments, many of the same GO terms were enriched for both Col-0 and *vamp712* loss of function mutants. Col-0 had a high enrichment for the nucleosome, which was 12-fold higher than that of *vamp712* (Figure 5.5). Interestingly, the cellular compartments, plasmodesmata, plastid, and plant-type vacuole were more enriched in *vamp712* than in Col-0. Of the DEP in *vamp712,* 18 microsomal and 13 cytosolic/soluble genes for plasmodesmata, 7 microsomal and 18 cytosolic/soluble genes for plastids, and 10 microsomal and 13 cytosolic/soluble genes for plant-type vacuole were counted in the GO enrichment analysis. In contrast, Col-0 counted 14 microsomal and 9 cytosolic for plasmodesmata, 19 microsomal and 11 cytosolic for plastids, and 15 microsomal and 4 cytosolic for plant-type vacuoles.

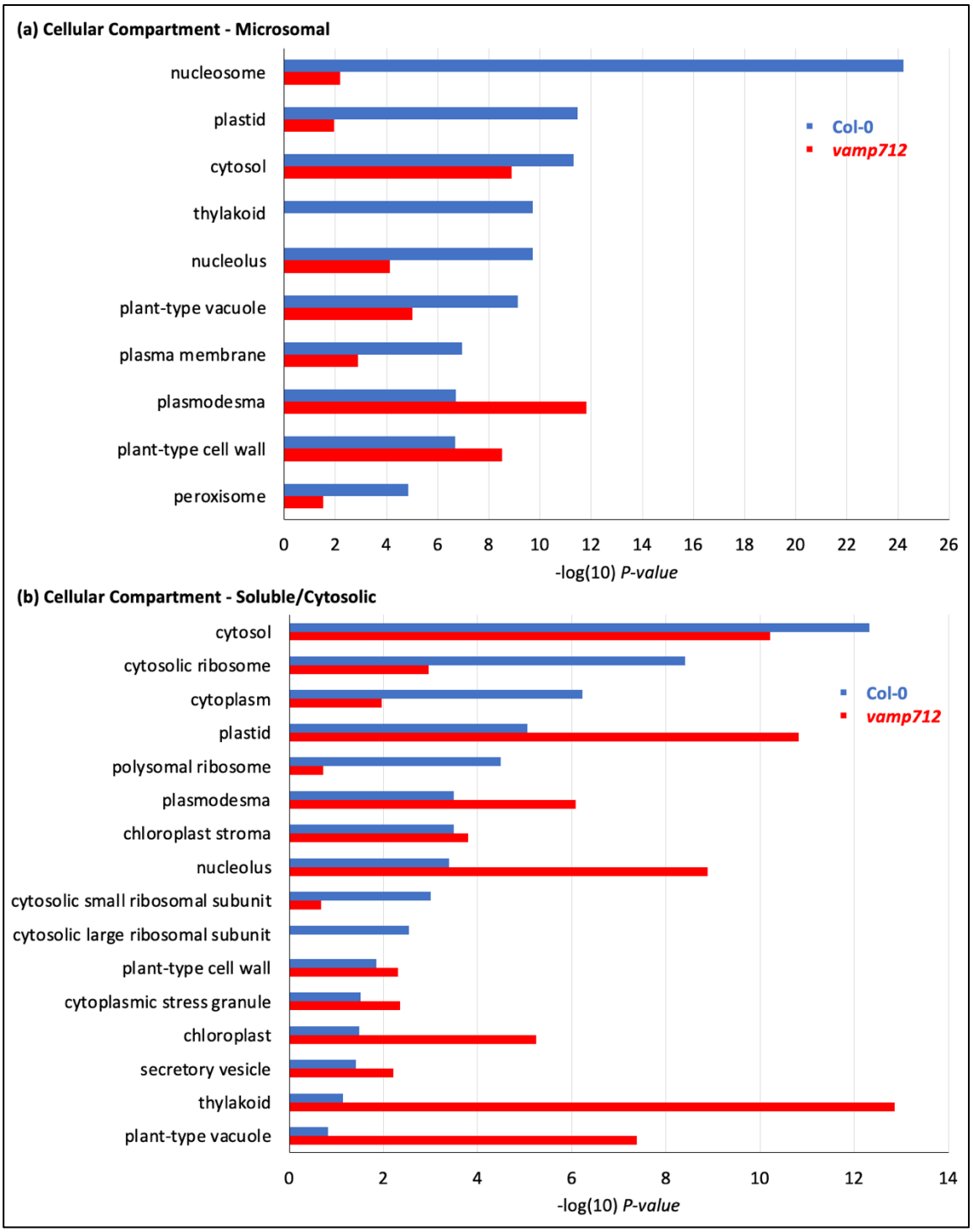

Figure 5.5: *GO enrichment analysis for cellular compartments of vamp712 and Col-0 proteomic comparisons. The 50 highest fold-changes of upregulated genes in response to salt stress for each comparison and the two fractions separately. (a) Cellular compartments for Col-0 (blue) and vamp712 (red) from proteins identified in the microsomal comparison. (b) Likewise, from the soluble/cytosolic fraction comparison. Bars show adjusted FDR scores (-log P-value) for each GO term. The bioinformatics database DAVID (https://david.ncifcrf.gov/home.jsp) was used for GO analysis, with the threshold values: count ≥ 2, Ease = 0.25.*

The GO analysis of molecular functions found five of the eight terms were common to both Col-0 and *vamp712* regarding the top 50 upregulated genes under salt stress from the microsomal protein fraction (Figure 5.6a), all with very different enrichments except for "salicylic acid binding". Protein heterodimerisation activity was the most enriched term for Col-0 in the microsomal fraction and *vamp712* in the soluble/cytosolic fraction (Figure 5.6b). This term relates to protein binding to a nonidentical protein to form a heterodimer. Therefore, the different enrichments between the two fractions could mean that more heterodimers of membrane proteins are formed in Col-0 plants, whereas more cytosolic heterodimers may be present in *vamp712* mutants. It is worth noting the absence of molecular functions relating directly to the antioxidant system, which was expected to be observed with plants exposed to salt stress and the enriched biological process "response to oxidative stress".

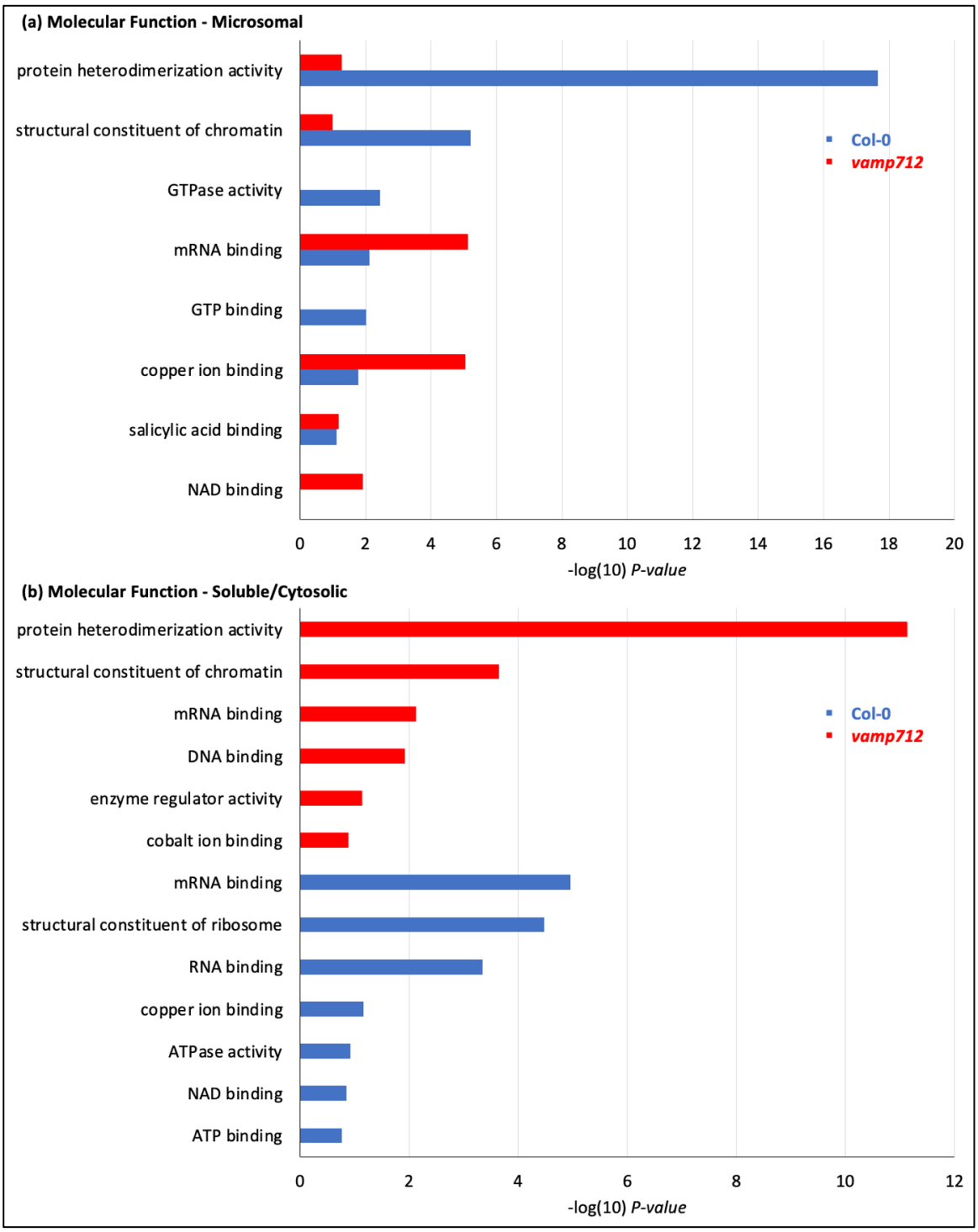

Figure 5.6: *GO enrichment analysis for molecular functions of vamp712 and Col-0 proteomic comparisons. The 50 highest fold-changes of upregulated genes in response to salt stress for each comparison and the two fractions separately. (a) Molecular functions for Col-0 (blue) and vamp712 (red) from proteins identified in the microsomal comparison. (b) Likewise, from the soluble/cytosolic fraction comparison. Bars show adjusted FDR scores (-log P-value) for each GO term. The bioinformatics database DAVID (https://david.ncifcrf.gov/home.jsp) was used for GO analysis, with the threshold values: count ≥ 2, Ease = 0.25.*

Chapter Summary:

- In this chapter, a proteome-wide approach was used to assess the role of VAMP712 in salt stress adaptation in *Arabidopsis* roots. By comparing the proteomes of wild-type Col-0 and *vamp712* mutant roots under salt stress, this chapter aimed to identify differentially expressed proteins (DEPs) and potential interactors of VAMP712.
- **Protein Extraction and Quality Control**: An optimised protein extraction technique isolated membrane-enriched microsomal fractions and cytosolic proteins. Quality control involved SDS-PAGE and immunoblot analysis using marker proteins for different cellular compartments, confirming successful separation of microsomal and cytosolic proteins.
- **Mass Spectrometry and Differential Expression**: Using iTRAQ labelling and LC-MS/MS, the study identified 1300 proteins in Col-0 and 1314 in *vamp712* from the microsomal fraction, and 785 in Col-0 and 802 in *vamp712* from the cytosolic fraction. DEPs were determined based on statistical significance and fold change, with specific filtering to ensure reliability.
- **Functional Insights and GO Analysis**: Significant changes in proteins related to salt stress and vesicle trafficking were found, including the Ras-related protein RABG3e, which showed differential regulation between Col-0 and *vamp712*. GO enrichment analysis highlighted processes like nucleobase metabolic processes and response to oxidative stress, with notable differences in cellular compartments and molecular functions between the genotypes.

Chapter 6: Discussion

Soil salinisation is increasing worldwide, contributing to a reduction in crop yields and is regarded as a significant threat to food security (FAO et al., 2018). The research presented in this thesis centred around the proposed role of three VAMP71 R-SNARE family members in root developmental changes to deepen our understanding of how plants are susceptible to the effects of soil salinity and their innate stress responses. A major negative consequence of salt stress on plants is root growth inhibition, which limits water and nutrient uptake and restricts the overall plant biomass and crop yield potential. Depending on the particular crop species, moderate soil salinity between 4 and 8 dS/m reduces yields by 50-80% (Zörb et al., 2019). To investigate whether the VAMP71 family proteins are involved in the molecular pathways that coordinate the salt-dependent inhibition of root growth, the T-DNA insertion mutants *vamp712* and *vamp713* and the novel CRISPR knockout mutant *vamp711* were used. This research provides new evidence that VAMP71 family members are induced by salt stress, and certain VAMP71 members are required more than others in mediating salt stress tolerance and root growth. This chapter will discuss the global implications of the experimental evidence in the context of the existing literature to paint a picture of how members of the *Arabidopsis* VAMP71 family regulate salt-induced root growth responses.

The absence of VAMP71 modifies the *Arabidopsis* root system architecture.

Previous work using T-DNA insertion and dominant negative mutants of the *AtVAMP714* gene showed a significantly dwarfed root phenotype compared to wild-type Col-0 at seven days post-germination on normal ½ MS agar media (Gu et al., 2021). In comparison, the results presented in this thesis show that the loss of function of the other three VAMP71 family members did not share this short-root phenotype. This is likely because of greater functional redundancy between *VAMP711*, *VAMP712* and *VAMP713*, which are more closely related to one another than to *VAMP714* according to the phylogenetic analysis (Figure 6.1) (Uemura et al., 2004). In the presence of salt stress, root phenotypic differences were however observed. Specifically, the *vamp711* and *vamp712* mutant plants had significantly inhibited primary root growth compared to wild-type and *vamp713* seedlings. The expression data of the VAMP71 gene family members of wild-type seedlings exposed to salt stress revealed that *VAMP713* was upregulated the most

(Figure 3.2). It was expected then that the *vamp713* mutant would show a significant salt-induced phenotype. This was not the case; *vamp713* seedlings had similar root growth to wild-type plants, and though shoot growth phenotypes were not recorded in this research, there were no noticeable phenotypic differences. Therefore, the upregulation of *VAMP713* may serve a different function in the salt stress result, which does not impact development.

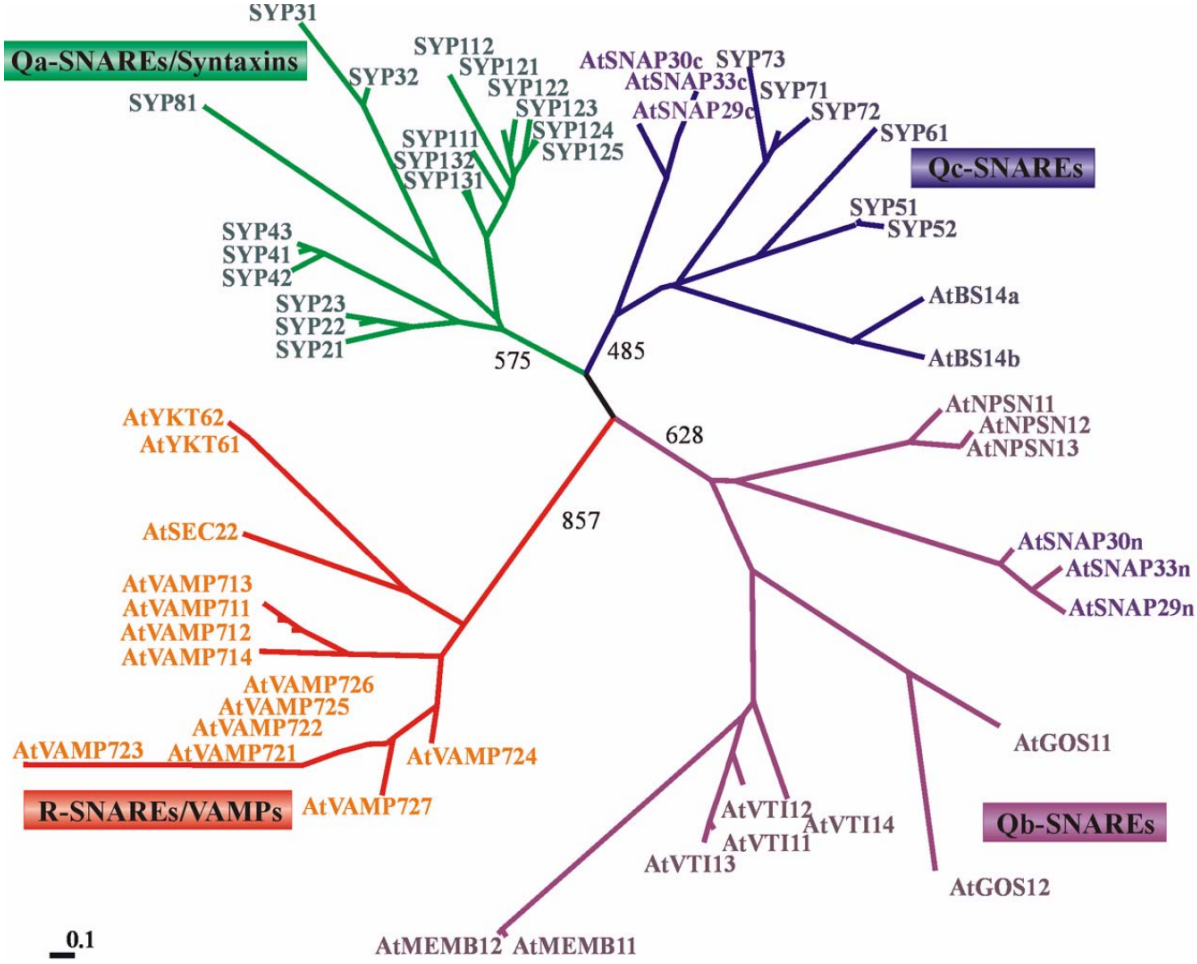

Figure 6.1: *A phylogenetic tree of the Arabidopsis SNARE family composed based on the SNARE motifs, including 67 amino acid residues. Four categories of SNAREs are shown separated by colour: green, Qa-SNARE/Syntaxin; purple, Qb-SNARE; blue, Qc-SNARE; red, R-SNARE according to the similarity of their SNARE domains. The scale bar gives the Dayhoff distance among the SNAREs. Branch numbers are bootstrap values with 1000 replications of SNARE motifs. Taken from Uemura et al. (2004).*

The VAMP71 family proteins are required for a range of correct auxin responses

The data presented here provide new information on the role of the plant R-SNARE VAMP71 family in controlling auxin-mediated responses under salinity stress. Polar auxin transport is essential to establishing functional concentration gradients of auxin that control tropic growth and cell identity and interact with other hormones to elicit specific responses

(Benjamins and Scheres, 2008). The auxin efflux carriers of the PIN protein family are key mediators of this process, some of which become localised to specific sides of the cell plasma membrane, and expression of *PIN* genes in the root meristem accurately reflects changes in auxin content indicative of a feedback regulatory system (Omelyanchuk et al., 2016). SNAREs play a crucial role in vesicle trafficking, an essential process for root growth. Specifically, the trafficking of SNAREs is vital for transporting PIN proteins in root cells (Gu et al., 2021, Shirakawa et al., 2010, Zhang et al., 2021). The localisation of PINs involves an actin-mediated recycling between the plasma membrane and endosomes, facilitating rapid changes in the placement of these transporters (Geldner et al., 2001, Kleine-Vehn et al., 2008). A model has been proposed for correctly delivering PIN proteins from the endoplasmic reticulum/Golgi to the plasma membrane mediated through a VAMP714-associated compartment (Gu et al., 2021). As a necessary precursor to endocytic recycling, this model allows dynamic control over the abundance and position of PIN protein localisation. Thus, this mechanism regulates the rate and direction of auxin efflux.

A primary aim of this thesis was to investigate the hypothesis that the other three VAMP71 proteins have the same or a similar role. The analysis of *PIN* gene expression under non-stressed conditions varied across the *vamp71* mutants, where *vamp711* mutants had significantly increased expression of *PIN1*, suggesting VAMP711 has a suppressive role (Figure 4.3). It was previously shown that the loss of function of VAMP714 resulted in decreased *PIN1* and *PIN2* gene expression (Gu et al., 2021), which was also observed in *vamp712* insertional mutants. However, in the presence of salt stress, *PIN* gene expression was significantly increased in the *vamp712* mutants, which was not the case for the wild type. Therefore, the presence of functional VAMP712 is likely not necessary for the upregulation of *PIN1* and *PIN2* expression, and there may be other mechanisms independent of VAMP712 that facilitate this change. It is possible that the increased transcript abundance of these genes does not correlate with the increased abundance of the proteins nor their correct localisation to target membranes. Therefore, if VAMP712 is required for the correct localisation of PIN1 and PIN2, then the increased *PIN1* and *PIN2* expression observed in the mutant plants may reflect a compensation mechanism. One could argue that this is the consequence of a feedback loop whereby *PIN* gene expression is increased due to defective auxin efflux. Unfortunately, the proteomic screening did not identify the PIN protein family members. Further investigations are necessary to assess the

transcript abundance of *PIN* genes quantitatively. Conducting confocal imaging with fluorescently tagged PIN1 and PIN2 in the *vamp712* mutant background would also provide insights into whether VAMP712 is essential for the proper localisation and abundance of PINs within the root tip cells.

To achieve the objective of whether VAMP712 and VAMP713 influence the abundance and distribution of auxin at the root tip, confocal imaging was done using the auxin-inducible reporter line ProDR5::GFP in both the *vamp712* and *vamp713* mutant backgrounds. The loss of function of VAMP712 and VAMP713 resulted in noticeable disruptions to the expression pattern and levels of DR5, indicating alterations in bioavailable auxin at the root tip (Figure 4.15). This observation supports our proposed model that the VAMP71 family proteins play a crucial role in various aspects of proper auxin responses, encompassing both auxin-mediated gene expression and the regulation of auxin abundance and distribution at the root tip. In contrast to the *vamp714* loss-of-function mutant, which exhibited reduced *PIN1*, *PIN2*, and *PIN4* transcription (Gu et al., 2021), the other VAMP71s showed less pronounced effects, as indicated by retained *PIN1* and *PIN2* gene expression and auxin patterning (Figure 4.1).

Auxin-induced genes regulate lateral root branching

Initiating the development of lateral roots is a significant step in establishing a root system. Lateral roots enable the plant to take up nutrients and water from a larger soil area to sustain growth. These roots initially emerge as primordia when pericycle cells of the primary root begin to divide; the cells protrude from the cortex and develop a lateral root meristem from which a root system is produced. This division depends on auxin, which induces the transcription of *AUX/IAA* gene family members (Péret et al., 2012). This gene family is known to mediate auxin-regulated developmental processes by binding to TIR/AFB (as part of the SCF complex), leading to their ubiquitination and degradation (Dharmasiri et al., 2005). The removal of Aux/IAA activates ARF transcriptional responses, thus inhibiting the auxin response (Figure 6.2) (Boer et al., 2014, Ulmasov et al., 1997).

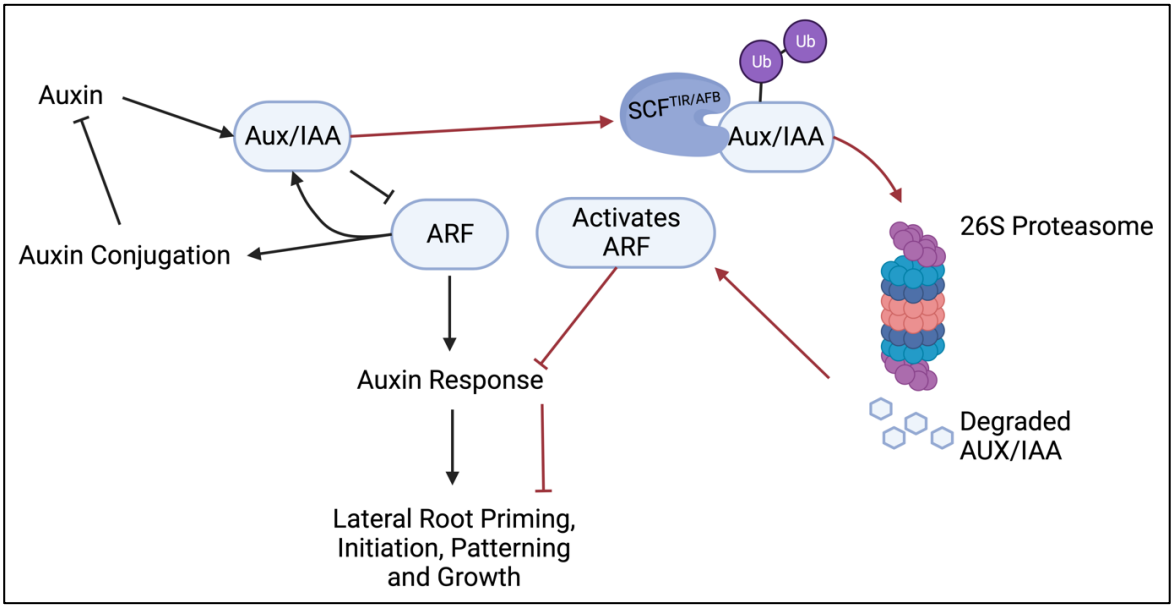

Figure 6.2: *A model of how auxin regulates lateral root initiation through Aux/IAA and ARF responses. Low auxin concentration (black arrows) activates Aux/IAA, which inhibits ARFs, leading to downstream auxin responses and lateral root formation. At high auxin concentrations (red arrows), IAA is bound by a TIR-Aux/IAA co-receptor complex, which triggers ubiquitination and subsequent degradation of the Aux/IAA repressor, thereby enabling ARF activity leading to inhibition of auxin responses. Figure created in BioRender.*

In the results presented here, there was no abnormal lateral root formation in mutants lacking the VAMP711, VAMP712, or VAMP713 expression under normal conditions. This is in contrast to *vamp714*, which exhibited reduced number and total length of lateral roots compared to wild-type (Gu et al., 2021). Under salt stress conditions, the number and total length of lateral roots in *Arabidopsis* significantly decreased, which is consistent with previous research findings (Smolko et al., 2021, Sun et al., 2007). The mutants lacking the VAMP71 proteins tended to exacerbate this trend, though *vamp711* plants had longer, less frequent lateral roots.

Gene expression analysis of auxin-induced genes *IAA1* and *IAA2* showed significant differences in *vamp711* mutants, both with and without salt stress. Additionally, *IAA1* expression was inversely regulated in *vamp712* and *vamp713* mutants compared to wild-type plants grown with and without salt stress (Figures 4.2 and 4.3). This result could be a consequence of disrupted auxin signalling, which is amplified in the presence of salt stress. If PIN1 is not correctly localised to its target membrane in the *vamp71* mutants, as is the case for *vamp714*, the polar auxin transport throughout the root will be restricted. In the context of lateral roots, polar transport of auxin acropetally toward the elongation zone and

pericycle results in arrested initiation of cell division and, thereby, abnormal lateral root development (Casimiro et al., 2001). Further work with the *vamp71* mutant lines that also express fluorescently tagged PIN1 would elucidate whether *vamp711*, *vamp712* and *vamp713* are required for correct PIN1 localisation as well as whether its abundance is significantly altered with and without salt stress.

Downstream of ARFs – the role of GH3

The auxin response downstream of ARFs can alter the homeostasis of auxin in a cell, producing other possibilities for oscillations than biosynthesis and intercellular transport. Among the key players in auxin homeostasis are the GH3 proteins, which act as integral components in the auxin degradation pathway. Through the conjugation of auxin to various amino acids, GH3 enzymes dynamically modulate intracellular free auxin levels, forming inactive IAA-aa and contributing to the fine-tuning of hormonal balance within plant cells (Chen et al., 2010, Staswick et al., 2005). In this context, the response of *GH3* genes to salt stress was investigated, aiming to unravel the intricate interplay between auxin homeostasis and the plant's adaptive mechanisms under salt stress conditions. This section examines the dynamic expression patterns of *GH3.1* and *GH3.3* in wild-type and transgenic *Arabidopsis* lines, shedding light on their potential roles in the plant's response to salinity-induced perturbations.

According to RT-qPCR, the transcript levels of *GH3.1* and *GH3.3* were reduced in *vamp712* and *vamp713* compared to wild-type and *vamp711* mutants under normal conditions (Figure 4.5). Given that high levels of auxin increase the expression of these genes, this implies that auxin levels are lower in these mutants. Supporting this, the genes *IAA1* and *IAA2*, also induced by auxin, showed the same or non-significantly reduced transcript abundance in *vamp712* and *vamp713* mutant plants compared to wild-type (Figure 4.3). Therefore, the low basal expression of these genes in *vamp712* and *vamp713* suggests altered auxin homeostasis, influencing various physiological processes regulated by auxin.

Since GH3 proteins act as negative regulators of auxin signalling by conjugating excess auxin, their reduced expression could lead to lower levels of auxin conjugation, potentially enhancing auxin signalling pathways. This would impact developmental processes, including root growth, lateral root formation, and other auxin-mediated responses. The

specific outcomes depend on the intricate interactions between auxin and other regulatory factors in the complex network governing root growth and development. As there was no observation of a significantly different root growth phenotype under non-stressed conditions, except for *vamp713* seedlings exhibiting reduced primary root growth, it is too simplistic to conclude that reduced *GH3* transcription in these mutant plants indicates increased intracellular auxin and enhanced root development. The confocal imaging of ProDR5::GFP in the *vamp712* and *vamp713* mutant backgrounds also does not support the claim that these mutants' auxin abundance is increased. The GFP signal was less intense under typical conditions in the two mutant backgrounds (Figure 4.15), suggesting less auxin abundance than wild-type. Therefore, the differential abundance of auxin-regulated genes could be due to this. To date, this evidence is only qualitative and more stringent quantitative methods of determining auxin abundance should be conducted.

The lower basal expression of *GH3* genes might still affect the plant's ability to regulate auxin levels in response to stress. Considering *GH3* genes are known to be upregulated in response to high levels of auxin (Park et al., 2007, Zou et al., 2022), the mutants may have a different baseline response to stress conditions, such as salt stress, as observed in our experimental results. When salinity stress was introduced, there was a rapid and sustained upregulation of *GH3* genes in *vamp712* and *vamp713* knockout mutants. Confocal imaging of the root tip following salt stress treatment in the *vamp712* and *vamp713* mutant backgrounds found the fluorescent cells restricted to the QC, similar to the Col-0 background, in agreement with increased *GH3* expression and their conjugation activity (Figure 4.4). This fluorescence signal was more intense than in the mutant backgrounds. Given the upregulation of *PIN1* and *PIN2* under salt stress, GH3-mediated inactivation of auxin may play a lesser role in restricting the distribution of auxin and instead, intercellular transport of auxin is responsible. There is evidence of specific localised expression of *GH3* genes crucial for meristem activity (Pierdonati et al., 2019, Zou et al., 2022). Thus, gene expression analysis of root tissues rather than whole seedlings would prove more informative.

In summary, this research has shed light on the intricate role of *VAMP71* family genes in regulating auxin-related responses under salinity stress. The observed changes in gene expression, particularly the differential regulation of *GH3*, *IAA* and *PIN* family members, suggest a nuanced interplay between vesicle trafficking mediated by some of the VAMP71

proteins and auxin homeostasis. This expression analysis of genes regulating auxin homeostasis suggests that the *vamp712* and *vamp713* mutants may have a different coping strategy, possibly involving a more prolonged or intensified auxin response. It is also possible that the upregulation of these auxin-induced genes reflects the lower basal levels, so, under salinity stress, the abundance of these proteins may not significantly differ from the other plant lines. Nevertheless, these genes in the *vamp712* and *vamp713* mutants are more sensitive to salt stress, which was necessary to induce changes in the expression of auxin-induced genes. Although the alteration observed in the RSA under normal growth conditions does not perfectly align with our expectations given these molecular insights, this analysis of auxin-regulated genes emphasises the impact of VAMP71 on plant growth under stress conditions.

Genotype-specific responses to auxin and inhibitor: Unravelling VAMP71-auxin crosstalk in *Arabidopsis* roots

Importantly, our investigation extended beyond gene expression analysis to assess the functional consequences of VAMP71-dependent altered auxin dynamics. Root measurements of seedlings treated with exogenous indole-3-acetic acid (IAA) and the polar auxin transport inhibitor N-1-naphthylphthalamic acid (NPA) unveiled genotype-specific responses. Specifically, *vamp711* knockout mutants exhibited reduced primary root growth compared to Col-0, and this effect was further pronounced under salt stress conditions (Figure 4.9).

Exogenous IAA inhibits primary root growth in *Arabidopsis* plants by altering auxin signalling pathways, leading to disruptions in cell elongation, differentiation, and overall root development (Rahman et al., 2007). This disruption is often associated with changes in the expression of vital auxin-responsive genes and the modulation of cellular processes critical for root growth regulation (True and Shaw, 2019). Given the gene expression changes in crucial auxin signalling genes observed in the *vamp71* mutants and their heightened sensitivity to salt stress, the addition of IAA is expected to exacerbate the reduction in primary root growth, particularly under salt stress conditions. The *vamp712* and *vamp713* mutants were not significantly more affected by including exogenous IAA with and without salt stress than wild-type plants (Figure 4.6). Since the *GH3* genes were induced by salt stress in these mutants, this suggests that these mutants can still respond

normally to changes in auxin homeostasis. The same cannot be said for *vamp711* mutants, where uniquely, the expression of *GH3.1* was not significantly altered by salinity stress, and *IAA1* and *IAA2* expressions were significantly decreased. The dual treatment of exogenous IAA and salt stress showed a significant reduction in primary root growth compared with the wild type (Figure 4.6). The specific alterations in the gene expression data align with the significant reduction in primary root growth observed in *vamp711* mutants, suggesting a potential link between the altered expression of these vital auxin-related genes and the observed phenotypic response. Despite the same consistency not being observed in the *vamp712* and *vamp713* mutant plants, these results highlight the need for further exploration into the specific molecular mechanisms governing the crosstalk between individual members of the VAMP71 family and auxin signalling pathways. For instance, analysing the expression of these genes on mutant seedlings treated with IAA or NPA and the combination with salt stress using RT-qPCR would provide further insight into the proposed auxin homeostasis and signalling differences.

In contrast to the observed responses to exogenous IAA, treatment with the polar auxin transport inhibitor NPA did not yield a significant difference between the mutants and wild-type plants. Additionally, the combination of NPA and salt stress did not significantly restrict the primary root growth of *vamp71* mutant seedlings (Figure 4.7). The lack of a pronounced effect in the presence of NPA raises intriguing questions about the specific mechanisms at play. The mutants may exhibit compensatory mechanisms despite alterations in auxin-related gene expression or are less affected by disruptions in polar auxin transport. Further investigations into the intricate interplay between VAMP71 family members and auxin signalling pathways, particularly under conditions involving NPA, may provide deeper insights into these mutants' regulatory dynamics governing root development.

In conclusion, this investigation into the response of *vamp71* mutants to exogenous application of IAA provides valuable preliminary insights into the intricate interplay between auxin homeostasis and stress responses. While the *vamp712* and *vamp713* mutants demonstrated resilience to the addition of IAA under both normal and salt stress conditions, the *vamp711* mutants exhibited a unique sensitivity, marked by altered expression patterns of vital auxin-related genes and a significant reduction in primary root growth. This distinctive response in *vamp711* mutants, where *GH3.1* expression remained

unaltered under salinity stress, emphasises the complexity of auxin regulation in these plants. The observed reduction in primary root growth further underscores the crucial role of VAMP71 family members in modulating auxin responses, shedding light on potential avenues for future investigations into the intricate molecular mechanisms governing plant adaptation to stress.

Deciphering the molecular symphony: Proteomic insights into VAMP712-mediated salt stress response in *Arabidopsis*

This research employed a proteomics approach to screen for potential candidate proteins involved in the VAMP712-dependent salt stress response pathway. The v-SNARE VAMP712 is classified as an R-SNARE that contains a transmembrane domain (Fasshauer et al., 1998, Gu et al., 2020). Its function involves localising to membranes and is required for the correct trafficking and positioning of membrane-bound proteins or cargo (Uemura et al., 2004). It has been suggested that R-SNAREs have a crucial role in determining specificity in vesicle budding, and one mechanism for localisation of SNAREs is interaction with vesicle coats (Figure 6.3). For instance, it has been shown that R-SNAREs could be components of the COPII vesicles that are involved in ER-Golgi transport (Springer and Schekman, 1998) and that they are packaged into COPI vesicles during retrieval from the Golgi (Rein et al., 2002).

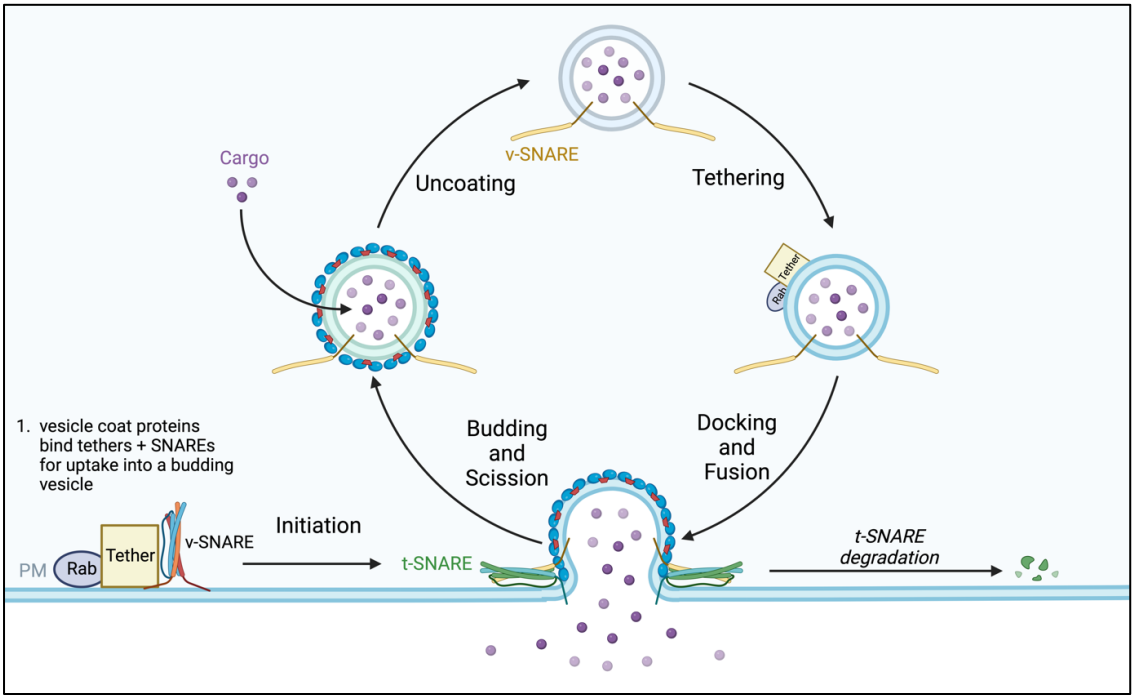

Figure 6.3: Molecular model of SNARE-mediated vesicle budding and fusion. *Initiation of coat assembly occurs when SNAREs and tethers are recruited for uptake into a budding vesicle. The coat components (blue) bind dynamin-related GTPases (red) and form a vesicle, which deforms the membrane until the vesicle is freed by scission. This vesicle contains transmembrane cargo proteins. During uncoating, the vesicle loses its coat through the inactivation of the small GTPase and the action of uncoating enzymes. The uncoated vesicles move to the acceptor compartment, typically guided by the cytoskeleton. Tethering and docking factors work in conjunction with GTP bound Rab and a tethering factor to tether the vesicle to their acceptor membrane. Docking involves the assembly of v- and t-SNAREs in a four-helix bundle. This "trans-SNARE complex" promotes the fusion of the vesicle and acceptor lipid bilayers. Cargo is transferred to the acceptor compartment, and the SNAREs are recycled.*

The connection between endocytosis and salt tolerance has been previously explored, revealing a correlation between increased salt susceptibility and defects in endocytosis (Whitacre et al., 2001). Yeast defective in vacuolar H^+-ATPase also had reduced endocytosis and higher salt stress susceptibility (Munn and Riezman, 1994). Our approach involved isolating membrane-bound proteins during the protein extraction process from wild-type and *vamp712* mutant seedlings treated with and without salt stress. This provided valuable protein abundance data related to the salt-induced vesicle trafficking process, potentially dependent on VAMP712 functionality.

Notably, the identified proteins differentially regulated between wild-type and *vamp712* belonged to the RAB GTPase family (Table 5.6). This family of small GTP-binding proteins is an essential regulator of vesicular trafficking within eukaryotic cells. They

control various steps in vesicle formation, transport, tethering, and fusion. The RAB GTPases work by switching between an active, GTP-bound form and an inactive, GDP-bound form, thereby regulating membrane trafficking events. It has been shown previously that SNARES and RAB GTPases interact functionally to promote vesicle fusion at the endosome and coordinate enhanced specificity and efficiency of membrane tethering and fusion (Ebine et al., 2011, Ohya et al., 2009). The Ras-related RAB GTPase RABG3e (formerly Rab7) was found to be abundant in wild-type and decreased in *vamp712* mutant plants treated with salt stress (Table 5.6). In all eukaryotes, the Rab7 proteins represent a critical component of the vesicle trafficking system (Zerial and McBride, 2001). Moreover, the observed changes in RABG3e abundance align with findings in other animal and yeast studies associating Rab7 with late endocytosis, which is crucial for the fusion of late endosomes to lysosomes or vacuoles (Bruckert et al., 2000, Desjardins et al., 1997).

Plants exposed to salt stress accumulate Na^+ in the shoots, and the Arabidopsis mutant *sas1* (*sodium overaccumulation in the shoot1*) has been shown to over-accumulate Na^+ here, which resulted in a severely repressed growth phenotype (Nublat et al., 2001). Overexpression lines of RABG3e also exhibit increased sodium content in the shoots but had improved growth in saline conditions over wild-type *Arabidopsis* (Mazel et al., 2004). The authors explained this to be due to the preferential accumulation of sodium in vacuoles. The increased volume of vacuoles is one mechanism of salt stress tolerance in plant cells (Mimura et al., 2003). This requires delivery of membrane material to the vacuole via intracellular vesicle trafficking, both of which involve VAMP712 and RAB3Ge. Our protein abundance data confirms that RAB3Ge is upregulated by salt stress, and this response depends on the co-expression of VAMP712. Additionally, closely related RABG3d and RABE1 were upregulated in wild-type plants under salt stress and undetected in vamp712 mutants, suggesting VAMP712 is required for their expression or accumulation in the microsomal compartment.

If VAMP712 is involved in delivering membrane material to the vacuole, we would expect to observe co-localisation with the vacuole of our GFP-tagged VAMP712 plants treated with salt stress. These lines have been created, and work is ongoing to confirm whether this is the case using confocal microscopy. It is also interesting to investigate protein-protein interactions involving VAMP712, RAB3Ge, RABG3d, and RABE1 under salt stress conditions using techniques such as co-immunoprecipitation. This would help

determine whether the expression or accumulation of RAB3Ge, RABG3d, and RABE1 depends on the presence of VAMP712. To further test whether RAB3Ge and other related RAB GTPases are linked to the expression of *VAMP712*, gene expression analysis should be conducted both in the *vamp712* knockout mutant and in overexpression lines with and without salt stress. If true, it is expected that overexpression of *VAMP712* would show an increase in expression of *RAB3Ge* and, therefore, improved tolerance to salt stress.

Changes in gene expression of ion transporter genes

The key aim of this thesis was to investigate plant responses to salinity stress and how alternative vesicle-mediated trafficking of membrane transporter proteins impacts the overall stress response. An essential mechanism plants use to counteract the effects of salinity stress is the modulation of ion homeostasis, specifically Na^+ ions. The expression of two ion transporter genes, *HKT1* and *NHX1*, were analysed in wild-type and mutant plants using a time-course experiment. The gene *HKT1* encodes a Na^+-specific ion transporter which helps recirculate Na^+ from shoots to roots, probably by mediating Na^+ loading into the phloem sap in shoots and unloading in roots, thereby lowering the amounts of Na^+ in the shoot (Mäser et al., 2002, Rus et al., 2001, Uozumi et al., 2000). The *vamp712* and *vamp713* mutant seedlings had significantly decreased expression of *HKT1* than wild-type and *vamp711* mutants under non-stressed conditions. Under salt stress conditions, the expression of *HKT1* was temporally downregulated, though this change was slower in *vamp712* and *vamp713* seedlings. This downregulation of *HKT1* in response to salt stress has also been reported by others (Dinneny et al., 2008). Increased expression of *HKT1* has been correlated with improved salinity stress tolerance (Nishiyama et al., 2012, Rus et al., 2001, Shkolnik-Inbar et al., 2013). Conversely, reduced expression of *AtHKT1;1* in roots of certain *Arabidopsis* accessions has also conferred enhanced tolerance to Na^+ (Møller et al., 2009, Rus et al., 2006). As the expression of *HKT1* in the *vamp712* and *vamp713* mutants was significantly decreased, this may have negative implications for the plant's ability to recirculate the excess Na^+ ions in the shoot following salt stress exposure and, therefore resulting in increased ion toxicity leading to premature senescence.

The application of cytokinin (CK) has been shown to repress the expression of *AtHKT1;1* in whole seedlings, resulting in increased sodium content in the shoots and reduced sodium in *Arabidopsis* roots (Mason et al., 2010). Independently, mutant plants defective in CK synthetic enzymes exhibited increased expression of *HKT1* (Nishiyama et al., 2012). Taken

together, CK appears to increase the accumulation of Na^+ in the shoots via down-regulating expression levels of *HKT1*. The expression of *HKT1* has a time-dependent and tissue-specific element, which likely optimises Na^+ flux across the plasma membrane of xylem parenchyma cells and determines the distribution of Na^+ across the plant. In the context of the *vamp71* mutants investigated here, *vamp711* mutants displayed a more rapid temporal shift in *HKT1* expression than the others. To better investigate the response of this gene in our mutant plants, future gene expression analysis experiments should be conducted in a tissue-specific manner by comparing root and shoot tissues independently in conjunction with assays that quantify the Na^+ content of these tissues.

The transcription factor ABA-INSENSITIVE 4 (ABI4) is a negative regulator of *AtHKT1;1* expression, and *abi4* loss of function mutants of *Arabidopsis* have been reported to improve salt stress tolerance with decreased Na^+ accumulation coupled with increased *HKT1* gene expression (Shkolnik-Inbar et al., 2013). The authors also found that ABI4-overexpressor plants exhibited suppressed *HKT1* expression, decreasing salt tolerance. This finding is interesting as ABA signalling has been implicated in mediating the roles of VAMP711 under stress conditions (Leshem et al., 2010). As mentioned, our *vamp711* mutants did not show dissimilar expression patterns of *HKT1* to wild-type with and without salt stress. More work is required regarding the role of VAMP71s in other plant hormone-dependent pathways, namely ABA and CK. It is also interesting to note that CK and ABA transcriptionally regulate *GH3* genes (Pierdonati et al., 2019, Zou et al., 2022); whether this is independent of the induction by auxin remains unclear. There is an antagonistic interaction between CK and auxin pathways (Ioio et al., 2007, Ioio et al., 2008), and the extent to which VAMP71s influence this relationship makes an intriguing research venture.

NHX1 – a target of vesicle trafficking under salt stress

The second ion transport gene, *NHX1*, encodes a vacuolar Na^+/H^+ antiporter involved in salt tolerance, ion homeostasis, and leaf development. Constitutive overexpression of *NHX1* confers salt stress tolerance in *Arabidopsis* by increased vacuolar sequestration of Na^+ ions (Yamaguchi et al., 2005). Further, plants with a T-DNA insertional mutant of *nhx1* were shown to be more salt-sensitive than wild-type *Arabidopsis* (Apse et al., 2003). The expression of *NHX1* in *vamp711* mutant plants showed unique patterns. Compared to the wild-type, *NHX1* expression was significantly upregulated, and following salt stress

exposure, the induced upregulation of this gene was short-lived and less intense (Figure 4.10). Interestingly, a study comparing microarray expression profiles of *Arabidopsis nhx1* mutant plants with Col-0 wild-type plants exposed to salt stress found that NHX1 influences the expression of vesicle trafficking components (Sottosanto et al., 2007). Specifically, they observed increased expression of the gene encoding RAB3Ge in the *nhx1* mutant lines. Another indication that NHX1 is linked to vesicle trafficking was the altered expression pattern of an exocyst subunit *EXO70* family member, downregulated in the *nhx1* mutant seedlings (Sottosanto et al., 2007). This family comprises a group of proteins involved in vesicle tethering during exocytosis and is essential to vesicle docking and membrane fusion (Fendrych et al., 2013). They also reported a significant downregulation of the salt-responsive myosin XI subunit (At1g08730) in *nhx1* mutants, which is required for organelle movement and polar auxin transport through the action of several vesicle-mediated processes (Holweg and Nick, 2004). Considering this indirect connection between VAMP71 and NHX1 in salinity stress tolerance pathways and polar auxin transport, a hypothesis can be made that the VAMP71s are involved in regulating the trafficking of NHX1, which our gene expression analysis supports. Therefore, NHX1 remains an exciting candidate for further investigations aimed at directly linking this important Na^+/H^+ antiporter with VAMP-mediated trafficking.

Future directions

In closing, the results of this research indicate that there may be a high degree of redundancy between the three *VAMP71* genes investigated. In contrast to previous work on *vamp714*, individual knockout mutants of *vamp711-3* do not negatively impact root development under normal growth conditions. Nevertheless, treating the mutant plants with salt stress made the phenotypic consequences of lacking individual *VAMP71* gene functions more obvious. Double- and triple-knockout mutants would be required to investigate the extent to which these R-SNARE genes are required for correct root development and the salt stress response. It will also be interesting to replicate the assays conducted here with constitutive overexpression lines of these *VAMP71* genes. Doing so will provide new insight into the feedback mechanism and whether, like *VAMP714*, there is a homeostatic balance that impacts root development.

Nevertheless, this analysis has strengthened the link between *VAMP71* family genes and auxin-mediated processes and highlights the genotype-dependent sensitivity to salt stress

and exogenous auxin. The findings have underscored the intricate nature and complexity of the plant response to salt stress. Future investigations could delve deeper into the molecular mechanisms underlying how the VAMP71 family contributes to stress-responsive auxin signalling. These include confocal microscopy to confirm the co-localisation of GFP-tagged VAMP712 with the vacuole under stress. This will provide visual evidence supporting the involvement of VAMP712 in delivering membrane material to the vacuole. Transgenic lines with altered expression levels of *GH3* genes in *vamp712* and *vamp713* mutants could be generated to confirm the hypothesis regarding the role of *GH3* genes and auxin regulation in response to stress. This could involve implementing overexpression or knockdown approaches to modulate *GH3* expression, allowing observation of the resulting impact on auxin regulation and stress responses. Similarly, genetic crosses between *vamp712*, *vamp713* mutants, and *GH3*-overexpressing lines can be done to explore complementation effects. Does the restoration of normal GH3 function rescue the observed phenotypes and auxin dynamics in the mutant backgrounds?

Following the success of the proteomics screening, several follow-up experiments should be conducted to confirm the identified differentially expressed candidates. This may include performing co-immunoprecipitation experiments under salt stress conditions to investigate protein-protein interactions involving the VAMP71 family members with the differentially expressed RAB GTPases and PIN family proteins. This will further indicate whether their expression or accumulation depends on the presence of individual or multiple VAMP71s.

This research predominantly focused on the role of VAMP71 family members in regulating the plant hormone auxin. This is because auxin has a major role in coordinating growth and development and has established links with the VAMP71 protein family. It is also possible that the VAMP71 family regulates or is regulated by other plant hormones. The phytohormone ABA is involved in the plant's response to various stresses, including salt stress (Tuteja, 2007). Xue et al. (2018) demonstrated that VAMP711 regulates ABA-mediated inhibition of PM H^+-ATPase activity and stomatal closure in response to drought stress. Quantifying the expression levels of key ABA-responsive genes in the *vamp71* mutants and wild-type under normal and salt stress conditions, as well as with the supplementation of ABA to the growth media, will indicate whether the loss or reduction of *VAMP71* expression affects the plant's sensitivity to ABA.

The gene expression analysis in this project included three critical genes involved in the antioxidant system. This found that the expression patterns following salt stress treatment tended to assimilate wild-type *Arabidopsis*, though *APX2* was exponentially increased in the *vamp71* mutants (Figure 4.11). Previously, silencing of *VAMP711* by RNAi in *Arabidopsis* disrupted the distribution of ROS and suppressed the stomatal closing under ABA treatment (Leshem et al., 2010). This indicated that VAMP711 is involved in transporting vesicles containing ROS. This result can be verified with the newly generated CRISPR knockout mutants in future work.

Finally, using salt as a stress system makes it more challenging to determine whether the observed effects on the molecular machinery are due to the associated osmotic stress, ion toxicity, or a combination of the two caused by the presence of salt. Therefore, comparing the VAMP71-mediated salt stress response with that of osmotic or drought stress is worthwhile. Exploring the potential crosstalk between the two stress response pathways may provide helpful information on known pathways or genes that interact with VAMP71 and their speculative roles in the observed phenotypes. Such insights may pave the way for innovative strategies to enhance stress tolerance in crops, ultimately contributing to sustainable agriculture practices to make saline soils more accessible. More broadly, understanding the molecular machinery mediating root development will also be helpful for improving the nutrient and water uptake of crops.

Appendices

Appendix 1: Protein sequence alignment of *Arabidopsis* VAMP71 family members.

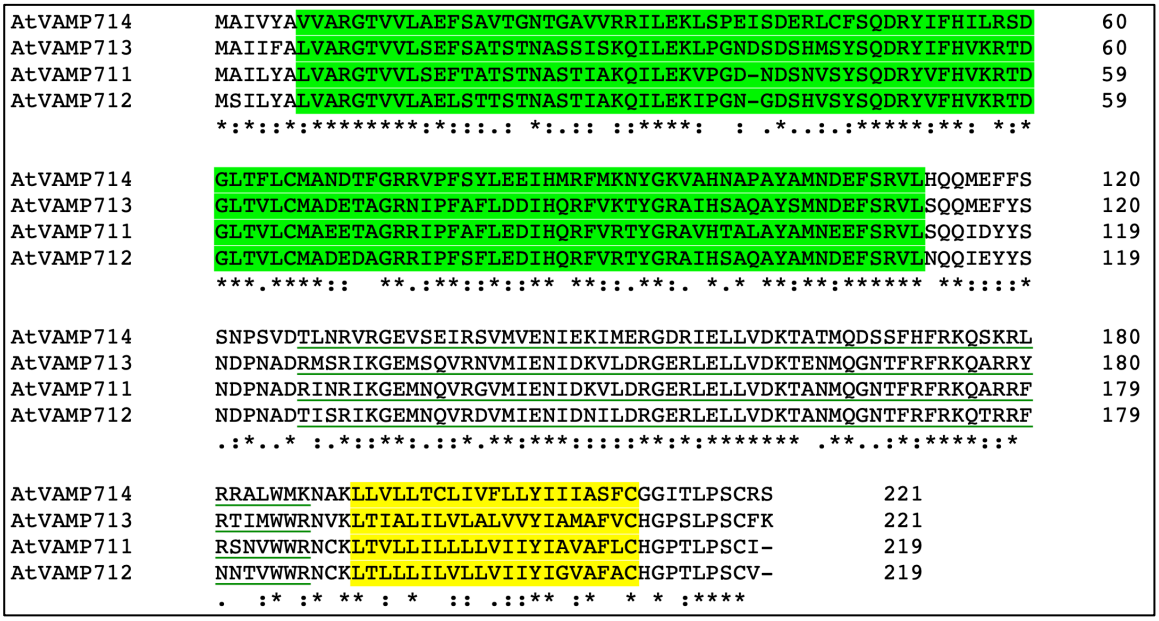

Figure S1: *CLUSTAL O(1.2.4) multiple sequence alignment of the VAMP71 group proteins showing the highly conserved protein sequence. Highlighted in green is the longin domain and highlighted in yellow is the transmembrane domain (helical; anchor for type IV membrane protein). Underlined in green represents the v-SNARE coiled-coil homology. An * (asterisk) indicates positions which have a single, fully conserved residue. A : (colon) indicates conservation between groups of strongly similar properties, whilst a . (full-stop) indicates conservation between groups of weakly similar properties.*

Appendix 2: Oligonucleotide sequences used in cloning and RT-qPCR experiments.

Table S1: Gene Oligonucleotide Sequences Used For RT-qPCR Analysis

Gene	Target Accession	Use	Forward primer	Reverse primer
IAR4	AT1G24180	qRT-PCR	AGGTGGATGGTATGGATGC	GGAAGCAAGATTCTATGGAAGT
AUX1	AT2G38120	qRT-PCR	GACGCACTTCTCGACCACTC	CCCAATCACTTTCTCCCACA
CAT1	AT1G20630	qRT-PCR	GCCCCTAAATGTGCTCACC	AAGCACTTCTCACGATTTCCA
GST1	AT1G02930	qRT-PCR	TCATCCTTCGCAACCCC	GCTATGATCGCCATGTCCTT
HKT1	AT4G10310	qRT-PCR	GAAAGGCAAAATCTACAACGTG	CCTGCAAACCCATAACTCG
NHX1	AT5G27150	qRT-PCR	GTGCTGTATCTATGGCTCTTGC	GGTAGCTTATGAGTGGTTTGGTC
SOD1	AT3G10920	qRT-PCR	GAACCTTGCTCCTTCCAGTG	TCTTCAGTTCTTTGTCTAGTCCG
APX1	AT1G07890	qRT-PCR	AAGCAATAAGCAGAAGTTGA	CAGGGTGGAAAGGAATGT
APX2	AT1G07900	qRT-PCR	CTGTCGCCACCACTCCAATC	TCTCTGCACAACGTCGCCTC
IAR3	At1g51760	qRT-PCR	GCGGTGGTGCTTTCAATGTGATTC	GCTTGCCTTGTGATAACCTGCTC
SOS1	AT2G01980	qRT-PCR	CTGGGAAGCCATATCTGTGC	GGACGCAAGAGTTTGAGAAGA
YUC5	At5g43890	qRT-PCR	TCGTCCCGGGAATTAAACGGTTCT	CCGATTTCCCTTTCCACGCGTTT
GH3.1	At2g14960	qRT-PCR	CGATCGTCGCCAGCTTCTTTAC	CCCGGCACATACAAATTCATTACG
GH3.3	At2g23170	qRT-PCR	ACCGGAGATTCAACGTATTGCC	CAG AGC TTG TGA GGA ACT CTG TG
GH3.6	At5g54510	qRT-PCR	CCTTGTTCCGTTTGATGCTT	CGTGTTACCGTTCAAGCAGA
DAO1	AT1G14130	qRT-PCR	ATCCGTTGCAAGTCCATTGA	GTTACAGAGCTCCAAACGAAA

Gene	Target Accession	Use	Forward primer	Reverse primer
DAO2	At1g14120	qRT-PCR	CCATACACACATTGCCGAACACG	GCTCCATATCGTAGCCATGTCACC
UBQ5	AT3G62250	qRT-PCR	CGTGGTGGTGCTAAGAAGAGG	GAAAGTCCCAGCTCCACAGGT
PIN 1	AT1G73590	qRT-PCR	CTTACGCCATGAACCTCCGT	GGTCGCCGGAGAAATTACCA
PIN 2	AT5G57090	qRT-PCR	TCAACAAATCTCACGGCGGA	CTTGGAGCTTTGCTTGCGTT
VAMP711	AT4G32150	qRT-PCR	GGTGGAGAAACTGCAAGCTC	ACACACTTCGCAAAGCAATG
VAMP712	AT2G25340	qRT-PCR	AAGCAAACACGTCGTTTCAA	AGGCCACACCGATGTATATG
VAMP713	AT5G11150	qRT-PCR	TTGTGAAAACATATGGCCGA	CTAGCAACTCCAAACGCTCC
VAMP714	AT5G22360	qRT-PCR	GAGATTCGATCGGTCATGGT	GGTAAAGTGATTCCTCCG
EIF4a	At3g13920	qRT-PCR	ATGAGAGGATGCTCTGCCTTCG	GCAGAGCAAACACAGCAACAG
ACT2	At3g18780	qRT-PCR	GTGGTCGTACAACCGGTATTG	TCACGTCCAGCAAGGTCAAG
IAA1	AT4G14560	qRT-PCR	GGAAGTCACCAATGGGCTTA	GAGATATGGAGCTCCGTCCA
IAA2	AT3G23030	qRT-PCR	CACCAGTGAGATCTTCCCGT	AGTCTAGAGCAGGAGCGTCG

Table S2: Oligonucleotide Sequences Used For Cloning Experiments and DNA Sequencing

Gene/Oligo Name	Target Accession	Use	Sequence
VAMP711 Pro Forward	AT4G32150	Gateway PCR Reaction	GGGGACAAGTTTGTACAAAAAAGCAGGCTAGCAAAAAAACAAAAAAAGGC
VAMP711 Pro Reverse	AT4G32150	Gateway PCR Reaction	CCACGAGGGCGTACAGAATCGCCATCGCTGATTACAAATATTTAATTTCG
VAMP712 Pro Forward	AT2G25340	Gateway PCR Reaction	GGGGACAAGTTTGTACAAAAAAGCAGGCTAATGATGAAAATTCAAGAAAGACC
VAMP712 Pro Reverse	AT2G25340	Gateway PCR Reaction	CCACCAACGCGTATAATATCGACATGAAGAAATACTAAATAAATGGTTAA
VAMP713 Pro Forward	AT5G11150	Gateway PCR Reaction	GGGGACAAGTTTGTACAAAAAAGCAGGCTAATATTATTTTTAAATACGTGTGAA
VAMP713 Pro Reverse	AT5G11150	Gateway PCR Reaction	CCACCAACGCAAATATGATCGCCATATTGAAATGATTTTGAGGAA
VAMP711 CDS Forward	AT4G32150	Gateway PCR Reaction	ATGGCGATTCTGTACGCC
VAMP711 CDS Reverse	AT4G32150	Gateway PCR Reaction	GGGGACCACTTTGTACAAGAAAGCTGGGTAAATGCAAGATGGTAGAGTAGG
VAMP712 CDS Forward	AT2G25340	Gateway PCR Reaction	ATGTCGATATTATACGCGTTGG
VAMP712 CDS Reverse	AT2G25340	Gateway PCR Reaction	GGGGACCACTTTGTACAAGAAAGCTGGGTAAACGCAAGAGGGTAGAGT
VAMP713 CDS Forward	AT5G11150	Gateway PCR Reaction	ATGGCGATCATATTTGCGTT

Gene/Oligo Name	Target Accession	Use	Sequence
VAMP713 CDS Reverse	AT5G11150	Gateway PCR Reaction	GGGGACCACTTTGTACAAGAAAGCTGGGTAAAGCAATAAGCAGAAGTTGA
DT1-BsF	AT4G32150	VAMP711 CRISPR	ATATATGGTCTCGATTGGGGTTGCTGTCGTTGTCTCCGTT
DT1-F0	AT4G32150	VAMP711 CRISPR	TGGGGTTGCTGTCGTTGTCTCCGTTTTAGAGCTAGAAATAGC
DT2-R0	AT4G32150	VAMP711 CRISPR	AACATAGGATTAATCGTATTAACAATCTCTTAGTCGACTCTAC
DT2-BsR	AT4G32150	VAMP711 CRISPR	ATTATTGGTCTCGAAACATAGGATTAATCGTATTAACAA
V711 Pro Seq F1	AT4G32150	DNA Sequencing	GAGGCCAAACAGTATCTCTAC
V711 Pro Seq F2	AT4G32150	DNA Sequencing	GCTTGGGACTAATAACAA
V711 Pro Seq F3	AT4G32150	DNA Sequencing	CGTAGGGTTTATGAAGATC
V711 Pro Seq F4	AT4G32150	DNA Sequencing	GCGTTAACCATTAATAATC
V711 CDS Seq F1	AT4G32150	DNA Sequencing	GCTCGTGGCACGGTGGTT
V711 CDS Seq F2	AT4G32150	DNA Sequencing	CGTATTAAGGGTGAAATG

Gene/Oligo Name	Target Accession	Use	Sequence
V713 Pro Seq F1	AT5G11150	DNA Sequencing	GACCCAAAATAATTGCTA
V713 Pro Seq F2	AT5G11150	DNA Sequencing	GTCCGCCTAAATGATTTCTC
V713 Pro Seq F3	AT5G11150	DNA Sequencing	GTAAATTATCTAGGTCGTGT
V713 Pro Seq F4	AT5G11150	DNA Sequencing	GCTTCATGATGGGCGATTA
V713 CDS Seq F1	AT5G11150	DNA Sequencing	GCGTTGGTGGCTCGTGGA
V713 CDS Seq F2	AT5G11150	DNA Sequencing	CCTAATGCAGACAGGATG
V712 Pro Seq F1	AT2G25340	DNA Sequencing	AAGCAAACACGTCGTTTCAA
V712 Pro Seq F2	AT2G25340	DNA Sequencing	AGGCCACACCGATGTATATG
V712 CDS Seq F1	AT2G25340	DNA Sequencing	GGAGTTAAGCACTACGTCCA
V712 CDS Seq F2	AT2G25340	DNA Sequencing	TGGAAGACGTAACGATCCTG

Appendix 3: Genomic DNA analysis of *vamp711* CRISPR mutants.

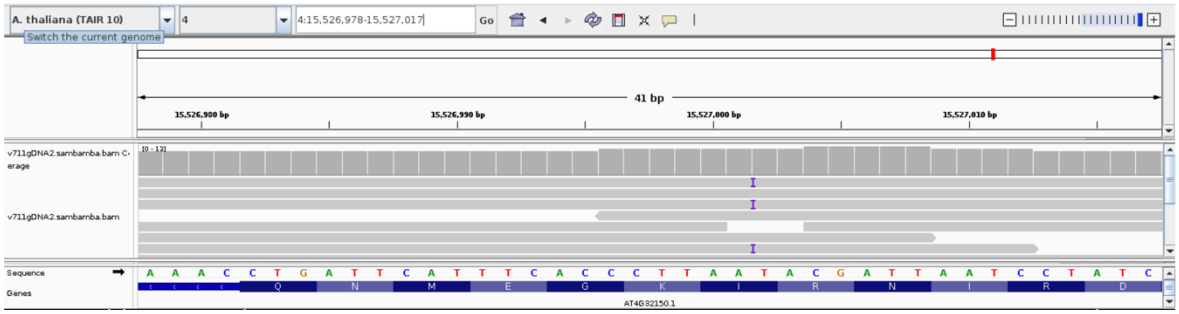

Figure S2: *Whole genome sequencing confirms the vamp711 CRISPR mutants are heterozygous for the gene mutation. Analysis shows target 2 (ATAGGATTAATCGTATTAA) in on chromosome 4: 15526998 to 15527016. The mutation identified (chr4:15527001 A->AT insertion, p.Ile130fs, frameshift) is within this region.*

References:

Adamowski, M. & Friml, J. 2015. PIN-Dependent Auxin Transport: Action, Regulation, and Evolution. *The Plant Cell,* **27,** 20-32.

Alonso, J. M., Stepanova, A. N., Leisse, T. J., Kim, C. J., Chen, H., Shinn, P., Stevenson, D. K., Zimmerman, J., Barajas, P., Cheuk, R., Gadrinab, C., Heller, C., Jeske, A., Koesema, E., Meyers, C. C., Parker, H., Prednis, L., Ansari, Y., Choy, N., Deen, H., Geralt, M., Hazari, N., Hom, E., Karnes, M., Mulholland, C., Ndubaku, R., Schmidt, I., Guzman, P., Aguilar-Henonin, L., Schmid, M., Weigel, D., Carter, D. E., Marchand, T., Risseeuw, E., Brogden, D., Zeko, A., Crosby, W. L., Berry, C. C. & Ecker, J. R. 2003. Genome-Wide Insertional Mutagenesis of Arabidopsis thaliana. *Science,* **301,** 653-657.

Apse, M. P., Sottosanto, J. B. & Blumwald, E. 2003. Vacuolar cation/H+ exchange, ion homeostasis, and leaf development are altered in a T‐DNA insertional mutant of AtNHX1, the Arabidopsis vacuolar Na+/H+ antiporter. *The plant journal,* **36,** 229-239.

Arora, N. K. 2019. Impact of climate change on agriculture production and its sustainable solutions. *Environmental Sustainability,* **2,** 95-96.

Banik, S. & Dutta, D. 2023. Membrane Proteins in Plant Salinity Stress Perception, Sensing, and Response. *The Journal of Membrane Biology,* **256,** 109-124.

Benjamini, Y. & Hochberg, Y. 1995. Controlling the False Discovery Rate: A Practical and Powerful Approach to Multiple Testing. *Journal of the Royal Statistical Society. Series B (Methodological),* **57,** 289-300.

Benjamins, R. & Scheres, B. 2008. Auxin: the looping star in plant development. *Annu. Rev. Plant Biol.,* **59,** 443-465.

Berthomieu, P., Conéjéro, G., Nublat, A., Brackenbury, W. J., Lambert, C., Savio, C., Uozumi, N., Oiki, S., Yamada, K., Cellier, F., Gosti, F., Simonneau, T., Essah, P. A., Tester, M., Véry, A. A., Sentenac, H. & Casse, F. 2003. Functional analysis of AtHKT1 in Arabidopsis shows that Na(+) recirculation by the phloem is crucial for salt tolerance. *Embo j,* **22,** 2004-14.

Bhatla, S. C. & Lal, M. A. 2018. Auxins. *Plant Physiology, Development and Metabolism.* Singapore: Springer Nature Singapore.

Boer, D. R., Freire-Rios, A., Van Den Berg, W. A., Saaki, T., Manfield, I. W., Kepinski, S., López-Vidrieo, I., Franco-Zorrilla, J. M., De Vries, S. C., Solano, R., Weijers, D. & Coll, M. 2014. Structural basis for DNA binding specificity by the auxin-dependent ARF transcription factors. *Cell,* **156,** 577-89.

Bouzroud, S., Gouiaa, S., Hu, N., Bernadac, A., Mila, I., Bendaou, N., Smouni, A., Bouzayen, M. & Zouine, M. 2018. Auxin Response Factors (ARFs) are potential mediators of auxin action in tomato response to biotic and abiotic stress (Solanum lycopersicum). *PLoS One,* **13,** e0193517.

Bruckert, F., Laurent, O. & Satre, M. 2000. Rab7, a multifaceted GTP-binding protein regulating access to degradative compartments in eukaryotic cells. *Protoplasma,* **210,** 108-116.

Cackett, L., Cannistraci, C. V., Meier, S., Ferrandi, P., Pěnčík, A., Gehring, C., Novák, O., Ingle, R. A. & Donaldson, L. 2022. Salt-Specific Gene Expression Reveals Elevated Auxin Levels in Arabidopsis thaliana Plants Grown Under Saline Conditions. *Frontiers in Plant Science,* **13**.

Calderón Villalobos, L. I., Lee, S., De Oliveira, C., Ivetac, A., Brandt, W., Armitage, L., Sheard, L. B., Tan, X., Parry, G., Mao, H., Zheng, N., Napier, R., Kepinski, S. &

Estelle, M. 2012. A combinatorial TIR1/AFB-Aux/IAA co-receptor system for differential sensing of auxin. *Nat Chem Biol,* **8,** 477-85.
Casimiro, I., Marchant, A., Bhalerao, R. P., Beeckman, T., Dhooge, S., Swarup, R., Graham, N., Inzé, D., Sandberg, G., Casero, P. J. & Bennett, M. 2001. Auxin transport promotes Arabidopsis lateral root initiation. *Plant Cell,* **13,** 843-52.
Chen, Q., Westfall, C. S., Hicks, L. M., Wang, S. & Jez, J. M. 2010. Kinetic basis for the conjugation of auxin by a GH3 family indole-acetic acid-amido synthetase. *J Biol Chem,* **285,** 29780-6.
Chen, Z., Hu, L., Han, N., Hu, J., Yang, Y., Xiang, T., Zhang, X. & Wang, L. 2015. Overexpression of a miR393-resistant form of transport inhibitor response protein 1 (mTIR1) enhances salt tolerance by increased osmoregulation and Na+ exclusion in Arabidopsis thaliana. *Plant Cell Physiol,* **56,** 73-83.
Clough, S. J. & Bent, A. F. 1998. Floral dip: a simplified method for Agrobacterium - mediated transformation of Arabidopsis thaliana. *The Plant Journal,* **16,** 735-743.
Desjardins, M., Nzala, N. N., Corsini, R. & Rondeau, C. 1997. Maturation of phagosomes is accompanied by changes in their fusion properties and size-selective acquisition of solute materials from endosomes. *J Cell Sci,* **110 (Pt 18),** 2303-14.
Dharmasiri, N., Dharmasiri, S., Weijers, D., Lechner, E., Yamada, M., Hobbie, L., Ehrismann, J. S., Jürgens, G. & Estelle, M. 2005. Plant development is regulated by a family of auxin receptor F box proteins. *Dev Cell,* **9,** 109-19.
Dimichele, W. A., Phillips, T. L. & Olmstead, R. G. 1987. Opportunistic evolution: Abiotic environmental stress and the fossil record of plants. *Review of Palaeobotany and Palynology,* **50,** 151-178.
Dinler, B. S., Antoniou, C. & Fotopoulos, V. 2014. Interplay between GST and nitric oxide in the early response of soybean (Glycine max L.) plants to salinity stress. *Journal of Plant Physiology,* **171,** 1740-1747.
Dinneny, J. R., Long, T. A., Wang, J. Y., Jung, J. W., Mace, D., Pointer, S., Barron, C., Brady, S. M., Schiefelbein, J. & Benfey, P. N. 2008. Cell Identity Mediates the Response of Arabidopsis Roots to Abiotic Stress. *Science,* **320,** 942-945.
Dolan, L., Janmaat, K., Willemsen, V., Linstead, P., Poethig, S., Roberts, K. & Scheres, B. 1993. Cellular organisation of the Arabidopsis thaliana root. *Development,* **119,** 71-84.
Du, W., Lu, Y., Li, Q., Luo, S., Shen, S., Li, N. & Chen, X. 2022. TIR1/AFB proteins: Active players in abiotic and biotic stress signaling. *Frontiers in Plant Science,* **13**.
Ebine, K., Fujimoto, M., Okatani, Y., Nishiyama, T., Goh, T., Ito, E., Dainobu, T., Nishitani, A., Uemura, T. & Sato, M. H. 2011. A membrane trafficking pathway regulated by the plant-specific RAB GTPase ARA6. *Nature cell biology,* **13,** 853-859.
Ebine, K. & Ueda, T. 2009. Unique mechanism of plant endocytic/vacuolar transport pathways. *Journal of Plant Research,* **122,** 21-30.
Edwards, K., Johnstone, C. & Thompson, C. 1991. A simple and rapid method for the preparation of plant genomic DNA for PCR analysis. *Nucleic Acids Res,* **19,** 1349.
Fao, I., Unicef & Pma, O. 2018. The state of food security and nutrition in the world 2018. *Building climate resilience for food security and nutrition***,** 222.
Fasshauer, D., Sutton, R. B., Brunger, A. T. & Jahn, R. 1998. Conserved structural features of the synaptic fusion complex: SNARE proteins reclassified as Q- and R-SNAREs. *Proc Natl Acad Sci U S A,* **95,** 15781-6.

Fendrych, M., Synek, L., Pečenková, T., Drdová, E. J., Sekereš, J., Rycke, R. D., Nowack, M. K. & Žárský, V. 2013. Visualization of the exocyst complex dynamics at the plasma membrane of Arabidopsis thaliana. *Molecular Biology of the Cell,* **24,** 510-520.

Flowers, T. J., Troke, P. F., And & Yeo, A. R. 1977. The Mechanism of Salt Tolerance in Halophytes. *Annual Review of Plant Physiology,* **28,** 89-121.

Friml, J., Vieten, A., Sauer, M., Weijers, D., Schwarz, H., Hamann, T., Offringa, R. & Jürgens, G. 2003. Efflux-dependent auxin gradients establish the apical–basal axis of Arabidopsis. *Nature,* **426,** 147-153.

Friml, J., Wiśniewska, J., Benková, E., Mendgen, K. & Palme, K. 2002. Lateral relocation of auxin efflux regulator PIN3 mediates tropism in Arabidopsis. *Nature,* **415,** 806-9.

Fu, Y., Yang, Y., Chen, S., Ning, N. & Hu, H. 2019. Arabidopsis IAR4 Modulates Primary Root Growth Under Salt Stress Through ROS-Mediated Modulation of Auxin Distribution. *Frontiers in Plant Science,* **10**.

Gallagher, S., Winston , S. E., Fuller , S. A. & Hurrell , J. G. R. 2008. Immunoblotting and Immunodetection. *Current Protocols in Molecular Biology,* **83,** 10.8.1-10.8.28.

Galvan-Ampudia, C. S., Julkowska, M. M., Darwish, E., Gandullo, J., Korver, R. A., Brunoud, G., Haring, M. A., Munnik, T., Vernoux, T. & Testerink, C. 2013. Halotropism is a response of plant roots to avoid a saline environment. *Curr Biol,* **23,** 2044-50.

Geisler, M. M. 2021. A Retro-Perspective on Auxin Transport. *Front Plant Sci,* **12,** 756968.

Geldner, N., Friml, J., Stierhof, Y.-D., Jürgens, G. & Palme, K. 2001. Auxin transport inhibitors block PIN1 cycling and vesicle trafficking. *Nature,* **413,** 425-428.

Gu, X., Brennan, A., Wei, W., Guo, G. & Lindsey, K. 2020. Vesicle Transport in Plants: A Revised Phylogeny of SNARE Proteins. *Evol Bioinform Online,* **16,** 1176934320956575.

Gu, X., Fonseka, K., Agneessens, J., Casson, S. A., Smertenko, A., Guo, G., Topping, J. F., Hussey, P. J. & Lindsey, K. 2021. The Arabidopsis R‐SNARE VAMP714 is essential for polarisation of PIN proteins and auxin responses. *New Phytologist,* **230,** 550-566.

Ha, C. V., Le, D. T., Nishiyama, R., Watanabe, Y., Sulieman, S., Tran, U. T., Mochida, K., Dong, N. V., Yamaguchi-Shinozaki, K., Shinozaki, K. & Tran, L. S. 2013. The auxin response factor transcription factor family in soybean: genome-wide identification and expression analyses during development and water stress. *DNA Res,* **20,** 511-24.

Hasanuzzaman, M. & Fujita, M. 2022. Plant Responses and Tolerance to Salt Stress: Physiological and Molecular Interventions. *Int J Mol Sci,* **23**.

He, X. J., Mu, R. L., Cao, W. H., Zhang, Z. G., Zhang, J. S. & Chen, S. Y. 2005. AtNAC2, a transcription factor downstream of ethylene and auxin signaling pathways, is involved in salt stress response and lateral root development. *Plant J,* **44,** 903-16.

Healey, A., Furtado, A., Cooper, T. & Henry, R. J. 2014. Protocol: a simple method for extracting next-generation sequencing quality genomic DNA from recalcitrant plant species. *Plant Methods,* **10,** 21.

Herth, W. & Schnepf, E. 1980. The fluorochrome, calcofluor white, binds oriented to structural polysaccharide fibrils. *Protoplasma,* **105,** 129-133.

Hofgen, R. & Willmitzer, L. 1988. Storage of competent cells for Agrobacterium transformation. *Nucleic Acids Research,* **16,** 9877-9877.

Holweg, C. & Nick, P. 2004. Arabidopsis myosin XI mutant is defective in organelle movement and polar auxin transport. *Proceedings of the National Academy of Sciences,* **101,** 10488-10493.

Hong, S. H., Tripathi, B. N., Chung, M.-S., Cho, C., Lee, S., Kim, J.-H., Bai, H.-W., Bae, H.-J., Cho, J.-Y., Chung, B. Y. & Lee, S. S. 2018. Functional switching of ascorbate peroxidase 2 of rice (OsAPX2) between peroxidase and molecular chaperone. *Scientific Reports,* **8,** 9171.

Iglesias, M. J., Terrile, M. C., Bartoli, C. G., D'ippólito, S. & Casalongué, C. A. 2010. Auxin signaling participates in the adaptative response against oxidative stress and salinity by interacting with redox metabolism in Arabidopsis. *Plant Mol Biol,* **74,** 215-22.

Iglesias, M. J., Terrile, M. C., Windels, D., Lombardo, M. C., Bartoli, C. G., Vazquez, F., Estelle, M. & Casalongué, C. A. 2014. MiR393 Regulation of Auxin Signaling and Redox-Related Components during Acclimation to Salinity in Arabidopsis. *PLOS ONE,* **9,** e107678.

Ioio, R. D., Linhares, F. S., Scacchi, E., Casamitjana-Martinez, E., Heidstra, R., Costantino, P. & Sabatini, S. 2007. Cytokinins determine Arabidopsis root-meristem size by controlling cell differentiation. *Current biology,* **17,** 678-682.

Ioio, R. D., Nakamura, K., Moubayidin, L., Perilli, S., Taniguchi, M., Morita, M. T., Aoyama, T., Costantino, P. & Sabatini, S. 2008. A genetic framework for the control of cell division and differentiation in the root meristem. *Science,* **322,** 1380-1384.

Jahn, R. & Scheller, R. H. 2006. SNAREs--engines for membrane fusion. *Nat Rev Mol Cell Biol,* **7,** 631-43.

Kleine-Vehn, J., Dhonukshe, P., Sauer, M., Brewer, P. B., Wiśniewska, J., Paciorek, T., Benková, E. & Friml, J. 2008. ARF GEF-dependent transcytosis and polar delivery of PIN auxin carriers in Arabidopsis. *Current biology,* **18,** 526-531.

Kong, X., Luo, Z., Dong, H., Eneji, A. E. & Li, W. 2011. Effects of non-uniform root zone salinity on water use, Na+ recirculation, and Na+ and H+ flux in cotton. *Journal of Experimental Botany,* **63,** 2105-2116.

Korver, R. A., Koevoets, I. T. & Testerink, C. 2018. Out of Shape During Stress: A Key Role for Auxin. *Trends in Plant Science,* **23,** 783-793.

Kurihara, D., Mizuta, Y., Sato, Y. & Higashiyama, T. 2015. ClearSee: a rapid optical clearing reagent for whole-plant fluorescence imaging. *Development,* **142,** 4168-4179.

Laemmli, U. K. 1970. Cleavage of structural proteins during the assembly of the head of bacteriophage T4. *Nature,* **227,** 680-5.

Larkin, M. A., Blackshields, G., Brown, N. P., Chenna, R., Mcgettigan, P. A., Mcwilliam, H., Valentin, F., Wallace, I. M., Wilm, A., Lopez, R., Thompson, J. D., Gibson, T. J. & Higgins, D. G. 2007. Clustal W and Clustal X version 2.0. *Bioinformatics,* **23,** 2947-8.

Leshem, Y., Golani, Y., Kaye, Y. & Levine, A. 2010. Reduced expression of the v-SNAREs AtVAMP71/AtVAMP7C gene family in Arabidopsis reduces drought tolerance by suppression of abscisic acid-dependent stomatal closure. *J Exp Bot,* **61,** 2615-22.

Leshem, Y., Melamed-Book, N., Cagnac, O., Ronen, G., Nishri, Y., Solomon, M., Cohen, G. & Levine, A. 2006. Suppression of *Arabidopsis* vesicle-SNARE expression inhibited fusion of H_2O_2 containing vesicles with tonoplast and increased salt tolerance. *Proceedings of the National Academy of Sciences,* **103,** 18008-18013.

Liu, W., Li, R.-J., Han, T.-T., Cai, W., Fu, Z.-W. & Lu, Y.-T. 2015. Salt Stress Reduces Root Meristem Size by Nitric Oxide-Mediated Modulation of Auxin Accumulation and Signaling in Arabidopsis *Plant Physiology,* **168,** 343-356.

Löfke, C., Zwiewka, M., Heilmann, I., Van Montagu, M. C. E., Teichmann, T. & Friml, J. 2013. Asymmetric gibberellin signaling regulates vacuolar trafficking of PIN auxin transporters during root gravitropism. *Proceedings of the National Academy of Sciences,* **110,** 3627-3632.

Luo, J., Zhou, J. J. & Zhang, J. Z. 2018. Aux/IAA Gene Family in Plants: Molecular Structure, Regulation, and Function. *Int J Mol Sci,* **19**.

Maraschin Fdos, S., Memelink, J. & Offringa, R. 2009. Auxin-induced, SCF(TIR1)-mediated poly-ubiquitination marks AUX/IAA proteins for degradation. *Plant J,* **59,** 100-9.

Martinez-Zapater, J. M. & Salinas, J. 1998. Arabidopsis Protocols. . *The Quarterly Review of Biology,* **73,** 345-345.

Mäser, P., Eckelman, B., Vaidyanathan, R., Horie, T., Fairbairn, D. J., Kubo, M., Yamagami, M., Yamaguchi, K., Nishimura, M., Uozumi, N., Robertson, W., Sussman, M. R. & Schroeder, J. I. 2002. Altered shoot/root Na+ distribution and bifurcating salt sensitivity in Arabidopsis by genetic disruption of the Na+ transporter AtHKT1. *FEBS Lett,* **531,** 157-61.

Mason, M. G., Jha, D., Salt, D. E., Tester, M., Hill, K., Kieber, J. J. & Eric Schaller, G. 2010. Type‐B response regulators ARR1 and ARR12 regulate expression of AtHKT1; 1 and accumulation of sodium in Arabidopsis shoots. *The Plant Journal,* **64,** 753-763.

Matanis, T., Akhmanova, A., Wulf, P., Del Nery, E., Weide, T., Stepanova, T., Galjart, N., Grosveld, F., Goud, B., De Zeeuw, C. I., Barnekow, A. & Hoogenraad, C. C. 2002. Bicaudal-D regulates COPI-independent Golgi-ER transport by recruiting the dynein-dynactin motor complex. *Nat Cell Biol,* **4,** 986-92.

Mazel, A., Leshem, Y., Tiwari, B. S. & Levine, A. 2004. Induction of salt and osmotic stress tolerance by overexpression of an intracellular vesicle trafficking protein AtRab7 (AtRabG3e). *Plant Physiol,* **134,** 118-28.

Mcdonald, J. H. 2014. *Handbook of biolological statistics*, New York•.

Mellor, N., Bennett, M. J. & King, J. R. 2016. GH3-Mediated Auxin Conjugation Can Result in Either Transient or Oscillatory Transcriptional Auxin Responses. *Bull Math Biol,* **78,** 210-34.

Meyerowitz, E. M. 1989. Arabidopsis, a useful weed. *Cell,* **56,** 263-9.

Mimura, T., Kura-Hotta, M., Tsujimura, T., Ohnishi, M., Miura, M., Okazaki, Y., Mimura, M., Maeshima, M. & Washitani-Nemoto, S. 2003. Rapid increase of vacuolar volume in response to salt stress. *Planta,* **216,** 397-402.

Møller, I. S., Gilliham, M., Jha, D., Mayo, G. M., Roy, S. J., Coates, J. C., Haseloff, J. & Tester, M. 2009. Shoot Na+ exclusion and increased salinity tolerance engineered by cell type–specific alteration of Na+ transport in Arabidopsis. *The Plant Cell,* **21,** 2163-2178.

Mravec, J., Kubes, M., Bielach, A., Gaykova, V., Petrásek, J., Skůpa, P., Chand, S., Benková, E., Zazímalová, E. & Friml, J. 2008. Interaction of PIN and PGP transport mechanisms in auxin distribution-dependent development. *Development,* **135,** 3345-54.

Müller, A., Guan, C., Gälweiler, L., Tänzler, P., Huijser, P., Marchant, A., Parry, G., Bennett, M., Wisman, E. & Palme, K. 1998. AtPIN2 defines a locus of Arabidopsis for root gravitropism control. *The EMBO Journal,* **17,** 6903-6911.

Munn, A. L. & Riezman, H. 1994. Endocytosis is required for the growth of vacuolar H(+)-ATPase-defective yeast: identification of six new END genes. *J Cell Biol,* **127,** 373-86.

Munns, R. 1993. Physiological processes limiting plant growth in saline soils: some dogmas and hypotheses. *Plant, Cell & Environment,* **16,** 15-24.

Munns, R. 2002. Comparative physiology of salt and water stress. *Plant Cell Environ,* **25,** 239-250.

Nakayama, N., Smith, R. S., Mandel, T., Robinson, S., Kimura, S., Boudaoud, A. & Kuhlemeier, C. 2012. Mechanical regulation of auxin-mediated growth. *Curr Biol,* **22,** 1468-76.

Nishiyama, R., Le, D. T., Watanabe, Y., Matsui, A., Tanaka, M., Seki, M., Yamaguchi-Shinozaki, K., Shinozaki, K. & Tran, L.-S. P. 2012. Transcriptome Analyses of a Salt-Tolerant Cytokinin-Deficient Mutant Reveal Differential Regulation of Salt Stress Response by Cytokinin Deficiency. *PLOS ONE,* **7,** e32124.

Nublat, A., Desplans, J., Casse, F. & Berthomieu, P. 2001. sas1, an Arabidopsis mutant overaccumulating sodium in the shoot, shows deficiency in the control of the root radial transport of sodium. *Plant Cell,* **13,** 125-37.

Ohya, T., Miaczynska, M., Coskun, Ü., Lommer, B., Runge, A., Drechsel, D., Kalaidzidis, Y. & Zerial, M. 2009. Reconstitution of Rab-and SNARE-dependent membrane fusion by synthetic endosomes. *Nature,* **459,** 1091-1097.

Omelyanchuk, N., Kovrizhnykh, V., Oshchepkova, E., Pasternak, T., Palme, K. & Mironova, V. 2016. A detailed expression map of the PIN1 auxin transporter in Arabidopsis thaliana root. *BMC plant biology,* **16,** 1-12.

Park, J. E., Park, J. Y., Kim, Y. S., Staswick, P. E., Jeon, J., Yun, J., Kim, S. Y., Kim, J., Lee, Y. H. & Park, C. M. 2007. GH3-mediated auxin homeostasis links growth regulation with stress adaptation response in Arabidopsis. *J Biol Chem,* **282,** 10036-10046.

Parry, G., Calderon-Villalobos, L. I., Prigge, M., Peret, B., Dharmasiri, S., Itoh, H., Lechner, E., Gray, W. M., Bennett, M. & Estelle, M. 2009. Complex regulation of the TIR1/AFB family of auxin receptors. *Proceedings of the National Academy of Sciences,* **106,** 22540-22545.

Parry, G. & Estelle, M. 2006. Auxin receptors: a new role for F-box proteins. *Current Opinion in Cell Biology,* **18,** 152-156.

Péret, B., Swarup, K., Ferguson, A., Seth, M., Yang, Y., Dhondt, S., James, N., Casimiro, I., Perry, P., Syed, A., Yang, H., Reemmer, J., Venison, E., Howells, C., Perez-Amador, M. A., Yun, J., Alonso, J., Beemster, G. T., Laplaze, L., Murphy, A., Bennett, M. J., Nielsen, E. & Swarup, R. 2012. AUX/LAX genes encode a family of auxin influx transporters that perform distinct functions during Arabidopsis development. *Plant Cell,* **24,** 2874-85.

Perilli, S., Di Mambro, R. & Sabatini, S. 2012. Growth and development of the root apical meristem. *Current Opinion in Plant Biology,* **15,** 17-23.

Petersson, S. V., Johansson, A. I., Kowalczyk, M., Makoveychuk, A., Wang, J. Y., Moritz, T., Grebe, M., Benfey, P. N., Sandberg, G. R. & Ljung, K. 2009. An Auxin Gradient and Maximum in the Arabidopsis Root Apex Shown by High-Resolution Cell-Specific Analysis of IAA Distribution and Synthesis. *The Plant Cell,* **21,** 1659-1668.

Pfaffl, M. W., Horgan, G. W. & Dempfle, L. 2002. Relative expression software tool (REST©) for group-wise comparison and statistical analysis of relative expression results in real-time PCR. *Nucleic Acids Research,* **30,** e36-e36.

Pierdonati, E., Unterholzner, S. J., Salvi, E., Svolacchia, N., Bertolotti, G., Dello Ioio, R., Sabatini, S. & Di Mambro, R. 2019. Cytokinin-Dependent Control of GH3 Group II Family Genes in the Arabidopsis Root. *Plants (Basel),* **8**.

Prigge, M. J., Platre, M., Kadakia, N., Zhang, Y., Greenham, K., Szutu, W., Pandey, B. K., Bhosale, R. A., Bennett, M. J., Busch, W. & Estelle, M. 2020. Genetic analysis of the Arabidopsis TIR1/AFB auxin receptors reveals both overlapping and specialized functions. *eLife,* **9,** e54740.

Rahman, A., Bannigan, A., Sulaman, W., Pechter, P., Blancaflor, E. B. & Baskin, T. I. 2007. Auxin, actin and growth of the Arabidopsis thaliana primary root. *Plant J,* **50,** 514-28.

Raja, V., Majeed, U., Kang, H., Andrabi, K. I. & John, R. 2017. Abiotic stress: Interplay between ROS, hormones and MAPKs. *Environmental and Experimental Botany,* **137,** 142-157.

Rehman, R. U. & Di Sansebastiano, G.-P. 2014. SNARE Proteins as Signaling Elements. *In:* HAKEEM, K. R., REHMAN, R. U. & TAHIR, I. (eds.) *Plant signaling: Understanding the molecular crosstalk.* New Delhi: Springer India.

Rein, U., Andag, U., Duden, R., Schmitt, H. D. & Spang, A. 2002. ARF-GAP–mediated interaction between the ER-Golgi v-SNAREs and the COPI coat. *The Journal of cell biology,* **157,** 395-404.

Reinhardt, D., Pesce, E. R., Stieger, P., Mandel, T., Baltensperger, K., Bennett, M., Traas, J., Friml, J. & Kuhlemeier, C. 2003. Regulation of phyllotaxis by polar auxin transport. *Nature,* **426,** 255-60.

Rosso, M. G., Li, Y., Strizhov, N., Reiss, B., Dekker, K. & Weisshaar, B. 2003. An Arabidopsis thaliana T-DNA mutagenized population (GABI-Kat) for flanking sequence tag-based reverse genetics. *Plant Molecular Biology,* **53,** 247-259.

Rubery, P. H. & Sheldrake, A. R. 1974. Carrier-mediated auxin transport. *Planta,* **118,** 101-21.

Rus, A., Baxter, I., Muthukumar, B., Gustin, J., Lahner, B., Yakubova, E. & Salt, D. E. 2006. Natural variants of At HKT1 enhance Na+ accumulation in two wild populations of Arabidopsis. *PLoS genetics,* **2,** e210.

Rus, A., Yokoi, S., Sharkhuu, A., Reddy, M., Lee, B. H., Matsumoto, T. K., Koiwa, H., Zhu, J. K., Bressan, R. A. & Hasegawa, P. M. 2001. AtHKT1 is a salt tolerance determinant that controls Na(+) entry into plant roots. *Proc Natl Acad Sci U S A,* **98,** 14150-5.

Sabatini, S., Beis, D., Wolkenfelt, H., Murfett, J., Guilfoyle, T., Malamy, J., Benfey, P., Leyser, O., Bechtold, N., Weisbeek, P. & Scheres, B. 1999. An auxin-dependent distal organizer of pattern and polarity in the Arabidopsis root. *Cell,* **99,** 463-72.

Salehin, M., Bagchi, R. & Estelle, M. 2015. SCFTIR1/AFB-based auxin perception: mechanism and role in plant growth and development. *Plant Cell,* **27,** 9-19.

Shen, C., Bai, Y., Wang, S., Zhang, S., Wu, Y., Chen, M., Jiang, D. & Qi, Y. 2010. Expression profile of PIN, AUX/LAX and PGP auxin transporter gene families in Sorghum bicolor under phytohormone and abiotic stress. *The FEBS Journal,* **277,** 2954-2969.

Shi, H., Liu, W., Wei, Y. & Ye, T. 2017. Integration of auxin/indole-3-acetic acid 17 and RGA-LIKE3 confers salt stress resistance through stabilization by nitric oxide in Arabidopsis. *Journal of Experimental Botany,* **68,** 1239-1249.

Shi, H. & Zhu, J.-K. 2002. Regulation of expression of the vacuolar Na+/H+ antiporter gene AtNHX1 by salt stress and abscisic acid. *Plant Molecular Biology,* **50,** 543-550.

Shirakawa, M., Ueda, H., Shimada, T., Koumoto, Y., Shimada, T. L., Kondo, M., Takahashi, T., Okuyama, Y., Nishimura, M. & Hara-Nishimura, I. 2010.

Arabidopsis Qa-SNARE SYP2 proteins localized to different subcellular regions function redundantly in vacuolar protein sorting and plant development. *The Plant Journal,* **64,** 924-935.
Shkolnik-Inbar, D., Adler, G. & Bar-Zvi, D. 2013. ABI4 downregulates expression of the sodium transporter HKT1;1 in Arabidopsis roots and affects salt tolerance. *Plant J,* **73,** 993-1005.
Shorter, J., Beard, M. B., Seemann, J., Dirac-Svejstrup, A. B. & Warren, G. 2002. Sequential tethering of Golgins and catalysis of SNAREpin assembly by the vesicle-tethering protein p115. *J Cell Biol,* **157,** 45-62.
Smolko, A., Bauer, N., Pavlović, I., Pěnčík, A., Novák, O. & Salopek-Sondi, B. 2021. Altered Root Growth, Auxin Metabolism and Distribution in Arabidopsis thaliana Exposed to Salt and Osmotic Stress. *Int J Mol Sci,* **22**.
Söllner, T., Whiteheart, S. W., Brunner, M., Erdjument-Bromage, H., Geromanos, S., Tempst, P. & Rothman, J. E. 1993. SNAP receptors implicated in vesicle targeting and fusion. *Nature,* **362,** 318-324.
Song, S., Hao, L., Zhao, P., Xu, Y., Zhong, N., Zhang, H. & Liu, N. 2019. Genome-wide Identification, Expression Profiling and Evolutionary Analysis of Auxin Response Factor Gene Family in Potato (Solanum tuberosum Group Phureja). *Sci Rep,* **9,** 1755.
Sottosanto, J. B., Saranga, Y. & Blumwald, E. 2007. Impact of AtNHX1, a vacuolar Na+/H+ antiporter, upon gene expression during short- and long-term salt stress in Arabidopsis thaliana. *BMC Plant Biology,* **7,** 18.
Sozzani, R. & Iyer-Pascuzzi, A. 2014. Postembryonic control of root meristem growth and development. *Current Opinion in Plant Biology,* **17,** 7-12.
Springer, S. & Schekman, R. 1998. Nucleation of COPII vesicular coat complex by endoplasmic reticulum to Golgi vesicle SNAREs. *Science,* **281,** 698-700.
Staswick, P. E., Serban, B., Rowe, M., Tiryaki, I., Maldonado, M. T., Maldonado, M. C. & Suza, W. 2005. Characterization of an Arabidopsis enzyme family that conjugates amino acids to indole-3-acetic acid. *Plant Cell,* **17,** 616-27.
Sun, F., Zhang, W., Hu, H., Li, B., Wang, Y., Zhao, Y., Li, K., Liu, M. & Li, X. 2007. Salt Modulates Gravity Signaling Pathway to Regulate Growth Direction of Primary Roots in Arabidopsis. *Plant Physiology,* **146,** 178-188.
Swarup, R., Friml, J., Marchant, A., Ljung, K., Sandberg, G., Palme, K. & Bennett, M. 2001. Localization of the auxin permease AUX1 suggests two functionally distinct hormone transport pathways operate in the Arabidopsis root apex. *Genes Dev,* **15,** 2648-53.
The Arabidopsis Genome, I. 2000. Analysis of the genome sequence of the flowering plant Arabidopsis thaliana. *Nature,* **408,** 796-815.
Tiwari, S. B., Hagen, G. & Guilfoyle, T. J. 2004. Aux/IAA proteins contain a potent transcriptional repression domain. *Plant Cell,* **16,** 533-43.
True, J. H. & Shaw, S. L. 2019. Exogenous Auxin Induces Transverse Microtubule Arrays Through TRANSPORT INHIBITOR RESPONSE1/AUXIN SIGNALING F-BOX Receptors1. *Plant Physiology,* **182,** 892-907.
Tuteja, N. 2007. Abscisic Acid and abiotic stress signaling. *Plant Signal Behav,* **2,** 135-8.
Uemura, T., Ueda, T., Ohniwa, R. L., Nakano, A., Takeyasu, K. & Sato, M. H. 2004. Systematic Analysis of SNARE Molecules in *Arabidopsis*: Dissection of the post-Golgi Network in Plant Cells. *Cell Structure and Function,* **29,** 49-65.
Ulmasov, T., Murfett, J., Hagen, G. & Guilfoyle, T. J. 1997. Aux/IAA proteins repress expression of reporter genes containing natural and highly active synthetic auxin response elements. *Plant Cell,* **9,** 1963-71.

Uozumi, N., Kim, E. J., Rubio, F., Yamaguchi, T., Muto, S., Tsuboi, A., Bakker, E. P., Nakamura, T. & Schroeder, J. I. 2000. The Arabidopsis HKT1 gene homolog mediates inward Na(+) currents in xenopus laevis oocytes and Na(+) uptake in Saccharomyces cerevisiae. *Plant Physiol,* **122,** 1249-59.

Ursache, R., Andersen, T. G., Marhavý, P. & Geldner, N. 2018. A protocol for combining fluorescent proteins with histological stains for diverse cell wall components. *Plant J,* **93,** 399-412.

Vaseva, Ii, Mishev, K., Depaepe, T., Vassileva, V. & Van Der Straeten, D. 2021. The Diverse Salt-Stress Response of Arabidopsis ctr1-1 and ein2-1Ethylene Signaling Mutants Is Linked to Altered Root Auxin Homeostasis. *Plants (Basel),* **10**.

Verma, S., Negi, N. P., Pareek, S., Mudgal, G. & Kumar, D. 2022. Auxin response factors in plant adaptation to drought and salinity stress. *Physiol Plant,* **174,** e13714.

Wang, Y., Li, K. & Li, X. 2009. Auxin redistribution modulates plastic development of root system architecture under salt stress in Arabidopsis thaliana. *J Plant Physiol,* **166,** 1637-45.

Whitacre, J., Davis, D., Toenjes, K., Brower, S. & Adams, A. 2001. Generation of an isogenic collection of yeast actin mutants and identification of three interrelated phenotypes. *Genetics,* **157,** 533-43.

Wisniewska, J., Xu, J., Seifertová, D., Brewer, P. B., Ruzicka, K., Blilou, I., Rouquié, D., Benková, E., Scheres, B. & Friml, J. 2006. Polar PIN localization directs auxin flow in plants. *Science,* **312,** 883.

Xing, H.-L., Dong, L., Wang, Z.-P., Zhang, H.-Y., Han, C.-Y., Liu, B., Wang, X.-C. & Chen, Q.-J. 2014. A CRISPR/Cas9 toolkit for multiplex genome editing in plants. *BMC plant biology,* **14,** 1-12.

Xue, Y., Yang, Y., Yang, Z., Wang, X. & Guo, Y. 2018. VAMP711 Is Required for Abscisic Acid-Mediated Inhibition of Plasma Membrane H(+)-ATPase Activity. *Plant Physiol,* **178,** 1332-1343.

Yamaguchi, T., Aharon, G. S., Sottosanto, J. B. & Blumwald, E. 2005. Vacuolar Na+/H+ antiporter cation selectivity is regulated by calmodulin from within the vacuole in a Ca2+-and pH-dependent manner. *Proceedings of the National Academy of Sciences,* **102,** 16107-16112.

Zerial, M. & Mcbride, H. 2001. Rab proteins as membrane organizers. *Nat Rev Mol Cell Biol,* **2,** 107-17.

Zhang, B., Karnik, R., Wang, Y., Wallmeroth, N., Blatt, M. R. & Grefen, C. 2015. The Arabidopsis R-SNARE VAMP721 Interacts with KAT1 and KC1 K+ Channels to Moderate K+ Current at the Plasma Membrane. *The Plant Cell,* **27,** 1697-1717.

Zhang, L., Ma, J., Liu, H., Yi, Q., Wang, Y., Xing, J., Zhang, P., Ji, S., Li, M., Li, J., Shen, J. & Lin, J. 2021. SNARE proteins VAMP721 and VAMP722 mediate the post-Golgi trafficking required for auxin-mediated development in Arabidopsis. *The Plant Journal,* **108,** 426-440.

Zhao, S., Zhang, Q., Liu, M., Zhou, H., Ma, C. & Wang, P. 2021. Regulation of Plant Responses to Salt Stress. *International Journal of Molecular Sciences,* **22,** 4609.

Zhu, J.-K. 2007. Plant Salt Stress. *Encyclopedia of Life Sciences.*

Zörb, C., Geilfus, C. M. & Dietz, K. J. 2019. Salinity and crop yield. *Plant biology,* **21,** 31-38.

Zou, W., Lin, P., Zhao, Z., Wang, D., Qin, L., Xu, F., Su, Y., Wu, Q. & Que, Y. 2022. Genome-Wide Identification of Auxin-Responsive GH3 Gene Family in

Saccharum and the Expression of ScGH3-1 in Stress Response. *Int J Mol Sci,* **23**.